



Universität  
Bremen

---

**Comparative study of Miro1 and Miro2 proteins  
through tagging of the endogenous genes**

---

**Dissertation**

in fulfillment of the requirements for the degree of  
Doctor of Natural Sciences (Dr. rer. nat)

at the Faculty 02 – Biology and Chemistry  
of the University of Bremen, Germany

Mona Khazaei, M.Sc.

Bremen, September 2023



This cumulative dissertation summarizes the work conducted at the Mitochondrial Dynamic group, Department 2 Biology/Chemistry at University of Bremen, Germany, between June 2020 and June 2023 and was funded by the U Bremen Excellence Chairs.



**Thesis Reviewers**

**Thomas L. Schwarz, Prof. Dr.**

**Markus Schwarzländer, Prof. Dr.**

Dissertation defense: 27.10.2023 at 10.00, Room: C0300

## Versicherung an Eides Statt

Ich, Mona Khazaei

versichere an Eides Statt durch meine Unterschrift, dass ich die vorstehende Arbeit selbständig und ohne fremde Hilfe angefertigt und alle Stellen, die ich wörtlich dem Sinne nach aus Veröffentlichungen entnommen habe, als solche kenntlich gemacht habe, mich auch keiner anderen als der angegebenen Literatur oder sonstiger Hilfsmittel bedient habe.

Ich versichere an Eides Statt, dass ich die vorgenannten Angaben nach bestem Wissen und Gewissen gemacht habe und dass die Angaben der Wahrheit entsprechen und ich nichts verschwiegen habe.

Die Strafbarkeit einer falschen eidesstattlichen Versicherung ist mir bekannt, namentlich die Strafandrohung gem. § 156 StGB bis zu drei Jahren Freiheitsstrafe oder Geldstrafe bei vorsätzlicher Begehung der Tat bzw. gem. § 161 Abs. 1 StGB bis zu einem Jahr Freiheitsstrafe oder Geldstrafe bei fahrlässiger Begehung.

Bremen, 15.11.2023, Mona Khazaei

Ort, Datum, Unterschrift



## **Acknowledgment**

I would like to extend my heartfelt gratitude to my PhD supervisor, Professor Thomas L. Schwarz, for granting me the opportunity to pursue my doctoral studies under his guidance. It has been a great honor and source of pride for me working under your supervision Tom. You are an exceptional supportive and kind mentor. Despite the geographical distance, you provided unwavering support not only in resolving project-related issues but also in addressing personal challenges I encountered during my journey. Your reassuring phrase at the end of our weekly meetings, "you know where to find me if you need," was a constant source of comfort, and you consistently made yourself available whenever I needed assistance. I owe much of my project's success to your guidance. You have a wealth of knowledge, not only in the scientific realm but also in life, and I have always been fascinated by your perspectives and your patient approach to various situations and individuals. You are an extraordinarily generous and caring person. I will always remember how you tried to help me when my family fell ill due to COVID-19 in Iran. I have gained invaluable insights from you, and you have prompted me to perceive things from a different perspective. Thank you so much.

I would like to express my sincere thanks to Professor Markus Schwarzländer, the second reviewer of my thesis, for dedicating his valuable time to review my work.

I am deeply grateful to Dr. Kathrin Maedler for allowing me to work in her lab, affording me the opportunity to participate in two intriguing projects, introducing me to Tom, granting me access to her lab facilities for my PhD experiments, and consistently providing support. I also thank her for serving as one of the examiners of my PhD defense.

I extend my sincerest gratitude to Professor Rita Groß-Hardt, the initiator of the MitoDive consortium, who invited Tom to Bremen and made my PhD work possible. Her unwavering support and willingness to engage in discussions were reassuring, and her presence was a source of strength. I extend special thanks to you for granting me access to your facilities when I required them. I also appreciate your presence as the head of the committee during my defense.

My sincere appreciation goes out to the U Bremen Excellence Chair, the founder of my PhD project. With their support, I never had to worry about obtaining the resources I needed, and I am deeply grateful for that.

I would like to thank Douglas Bruno Kagambo and Karam Botrous, the student

representatives in my committee.

A special thanks goes to Amin, who connected me with Kathrin and made my dream of working on mammalian system became true and helped me a lot, even when it was not his responsibility.

I am thankful to Katrischa Hennekens for her assistance and technical support in the laboratory throughout these years.

I also extend my heartfelt thanks to all the members of Rita's lab for their technical and scientific support. Special thanks to Yanbo Mao, Isil Erbasol Serbes, Saurabh Joshi, Hanna Marie Becker, Dawit Tekleyohans, Anja Hoffmann, and René Kristall.

I express my gratitude to Mr. Ingo Neumann for his kind administrative support.

I sincerely thank former and current members of Tom's lab in Boston for their generous support and scientific advice throughout my entire PhD project, both while I was working in Germany and during my stay in Boston. Himanish Basu, Kayla Davis, Ismael Izquierdo-Villalba, Guoli Zhao, Sindhuja Gowrisankaran, Jill Falk, Whitney Gibbs, Chen Ding, Lala Mkhitarian, and Papa Ndiaye – thank you all!

I also appreciate Dr. Mark Simone for assisting me with imaging work in Boston and Dr. Annette Petter for her help with imaging work in Bremen.

I extend my heartfelt thanks to all my dear PhD colleagues, friends, and students I have had the privilege of working with or meeting during my PhD journey: Kshitija, my dear colleague, we navigated all the challenges together, Shirin, my kind-hearted and supportive friend, Huan, my cherished and kind friend, Blaz, Murali, Heena, Gabi, Amal, Karthika, Ausilia, David Gotti, David Bund, Karthik, Saheri, Suderson, Nick, Solomon, Esein, Mikyta, Mehrshid, Anusha, Harshika – thank you all. It was my pleasure to get to know you and work with you.

I would like to express special thanks and heartfelt gratitude to my dear mother, who has always been a pillar of support even from afar. You are the main reason for all the success I have achieved in my life. God bless you, my dearest. Thanks to my dear father, brothers, and sisters for their support from a distance. I love you all.

I express my heartfelt gratitude to my dear friends Hale, Claas, and my beloved Theo for their unwavering support and for standing by me like family. I am incredibly fortunate to have you in my life.

Last but not least, I sincerely thank my best friend and husband, Pouria. Thank you for your unwavering support, love, and kindness, for traveling long distances every weekend to visit me, and for being the driving force behind my achievements. Without

you, I couldn't have made it.

## 1 Abstract

Mitochondria, known as powerhouse of the cells, are highly dynamic organelles capable of traversing long distances within neurons to supply energy to remote regions such as synaptic terminals. Research has shown that mitochondria show a diversity in their motility behavior. This diversity caused by factors such as directionality of their movement, stop and run time and so on. Kinesin/Dynein microtubule motor proteins and TRAK adaptor proteins are involved in long range mitochondrial movement. Mitochondrial Rho GTPases (Miro) protein as an outer mitochondrial membrane protein link the motor /adaptor protein complex to the mitochondria to facilitate mitochondrial trafficking. Miro1 and Miro2 are the two known Miro isoforms in mammalian cells. Miro protein not only play a key role in mitochondrial movement but also involves in shaping mitochondrial morphology, generating energy, mitophagy and more. Although many studies have discovered a diversity in expression level of Miro1 and Miro2 in different cell types, the functional significance of Miro1 and Miro2 is still not clear.

Therefore, to gain deeper understanding of Miro1 and Miro2 functional differences in the context of mitochondrial trafficking, the objectives of this study were set as follows: first, to determine whether Miro1 and Miro2 are equally distributed across the entire mitochondrial population. Second, to study whether the Miro isoforms interact with distinct protein complexes, or do they share common binding partners and present in same protein complex as heterodimers.

To achieve these goals, I generated stable cell lines using Crispr Cas9 technology: Flag-GFP-Miro1 knock-in SH-SY5Y cells, MYC-mRFP-Miro2 knock-in HeLa cells, and a double knock-in of Miro1 and Miro2 HeLa cells. These cell lines enable the study of not only the localization and distribution of endogenous Miro1 and Miro2 among different mitochondrial populations but also their biochemical characteristics using mass spectrometry analysis. Preliminary data showed that Miro1 and Miro2 were not only localized on mitochondria using immunocytochemistry but some of them were also found in close proximity to each other, as demonstrated by the Proximity Ligation Assay (PLA). Additionally, immunoprecipitation analysis did not detect any interactions between Miro2, Kinesin, MYO19, and TRAK proteins, indicating that miro2 may not interact with motor-adaptor complex at the endogenous level. Immunoprecipitation studies related to Miro1's interaction with the motor-adaptor complex protein are still

ongoing, and further protocol optimization is necessary. There are two main experiments in the list for future. First, to immunoprecipitate Miro1 and Miro2 and send sample for mass spectrometry analysis in order to identify their binding partners. Second, to isolate mitochondria containing each isoform separately and subject them to proteomic and lipidomic analyses. This investigation aims to determine whether labeling a subset of mitochondria with Miro1 or Miro2 leads to alterations in the proteome and lipidome composition of that subset or not.

The results of this research are expected to provide insights into about functional differences between Miro1 and Miro2 proteins and how these differences affect mitochondrial movement-related characteristics. Considering that mitochondrial motility impairment is associated with the onset and progression of some neurodegenerative diseases such as Alzheimer's and Parkinson's and given the important role of Miro proteins in mitochondrial transport, we hope that these findings can be useful in the discovery of a novel therapeutic approach for neurodegenerative diseases.

## 2 Zusammenfassung

Mitochondrien, bekannt als Kraftwerke der Zellen, sind hochdynamische Organellen, die in der Lage sind, weite Strecken innerhalb von Neuronen zurückzulegen, um Energie in entfernte Bereiche wie synaptische Enden zu liefern. Forschungsergebnisse haben gezeigt, dass Mitochondrien eine Vielfalt in ihrem Bewegungsverhalten aufweisen. Diese Vielfalt wird durch Faktoren wie die Richtung ihrer Bewegung, Stopp- und Laufzeiten und so weiter verursacht. Kinesin/Dynein-Mikrotubulus-Motorproteine und TRAK-Adapterproteine sind an der langstreckigen Bewegung der Mitochondrien beteiligt. Das mitochondriale Rho-GTPase (Miro) Protein als äußeres Mitochondrienmembranprotein verknüpft das Motor-/Adapter-Protein-Komplex mit den Mitochondrien, um den Transport der Mitochondrien zu erleichtern. Miro1 und Miro2 sind die beiden bekannten Miro-Isoformen in Säugetierzellen. Miro-Proteine spielen nicht nur eine Schlüsselrolle in der Bewegung der Mitochondrien, sondern sind auch an der Gestaltung der mitochondrialen Morphologie, der Energieerzeugung, der Mitophagie und vielem mehr beteiligt. Obwohl viele Studien eine Vielfalt im Expressionsniveau von Miro1 und Miro2 in verschiedenen Zelltypen entdeckt haben, ist die funktionelle Bedeutung von Miro1 und Miro2 noch nicht geklärt.

Daher wurden die Ziele dieser Studie wie folgt festgelegt, um ein besseres Verständnis der funktionellen Unterschiede zwischen Miro1 und Miro2 im Zusammenhang mit dem mitochondrialen Transport zu erlangen: Erstens, um festzustellen, ob Miro1 und Miro2 gleichmäßig in der gesamten mitochondrialen Population verteilt sind. Zweitens, um zu untersuchen, ob die Miro-Isoformen mit unterschiedlichen Protein-Komplexen interagieren oder ob sie gemeinsame Bindungspartner haben und als Heterodimere im selben Protein-Komplex präsent sind.

Um diese Ziele zu erreichen, wurden stabile Zelllinien mithilfe der CRISPR-Cas9-Technologie generiert: Flag-GFP-Miro1-Knock-in in SH-SY5Y-Zellen, MYC-mRFP-Miro2-Knock-in in HeLa-Zellen und ein doppelter Knock-in von Miro1 und Miro2 in HeLa-Zellen. Diese Zelllinien ermöglichen nicht nur die Untersuchung der Lokalisation und Verteilung von endogenem Miro1 und Miro2 in verschiedenen mitochondrialen Populationen, sondern auch die Untersuchung ihrer biochemischen Eigenschaften mittels Massenspektrometrie-Analyse. Vorläufige Daten zeigten, dass Miro1 und

Miro2 nicht nur mithilfe der Immunzytochemie auf Mitochondrien lokalisiert wurden, sondern dass einige von ihnen auch in unmittelbarer Nähe zueinander gefunden wurden, wie durch den Proximity Ligation Assay (PLA) gezeigt wurde. Darüber hinaus zeigte die Immunpräzipitation keine Wechselwirkungen zwischen Miro2, Kinesin, MYO19 und TRAK-Proteinen, was darauf hindeutet, dass Miro2 möglicherweise nicht auf endogener Ebene mit dem Motor-Adapter-Komplex interagiert. Die Immunpräzipitationsstudien zur Wechselwirkung von Miro1 mit dem Motor-Adapter-Komplex-Protein sind noch im Gange, und eine weitere Protokolloptimierung ist erforderlich.

In der Liste für zukünftige Experimente gibt es zwei Hauptexperimente. Erstens, Miro1 und Miro2 immunpräzipitieren und Proben zur Massenspektrometrie-Analyse senden, um ihre Bindungspartner zu identifizieren. Zweitens, Mitochondrien isolieren, die jede Isoform separat enthält, und sie proteomischen und lipidomischen Analysen unterziehen. Die Ergebnisse dieser Forschung sollen Einblicke in die funktionellen Unterschiede zwischen Miro1 und Miro2-Proteinen und wie diese Unterschiede die mit der mitochondrialen Bewegung zusammenhängenden Eigenschaften beeinflussen, bieten. Angesichts dessen, dass Beeinträchtigungen und Dysregulationen der mitochondrialen Motilität mit dem Auftreten und Fortschreiten einiger neurodegenerativer Erkrankungen wie Alzheimer und Parkinson in Verbindung stehen und angesichts der wichtigen Rolle der Miro-Proteine im mitochondrialen Transport hoffen wir, dass diese Ergebnisse nützlich bei der Entdeckung eines neuen therapeutischen Ansatzes für neurodegenerative Erkrankungen sein können.



## Table of Contents

1	Abstract .....	i
2	Zusammenfassung .....	iii
3	Introduction .....	1
3.1	Mitochondria play a key role in neuronal health and survival.....	1
3.2	Mitochondria are highly dynamic organelles with different motility behaviours 2	
3.3	Fission and fusion are necessary for mitochondrial turnover .....	3
3.4	The Motor-Adaptor protein complex mediates the long-range mitochondrial trafficking .....	4
3.5	Microtubule's motor protein .....	6
3.5.1	Kinesin and Dynein .....	6
3.5.2	Trafficking kinesin protein-TRAK1 and TRAK2 .....	8
3.6	Miro proteins.....	9
3.7	Crisper cas-9 knock-in technology is a reliable approach to analyze miro1 and miro2 expression and localization in living cells .....	16
3.8	Mass spectrometry helps in to functional study of proteome and lipidome of Miro1 or Miro2-containing mitochondrial populations .....	18
3.9	SH-SY5Y a human cell line with neuronal-like characteristics and morphology.....	19
3.10	HeLa cell line an easy cell line for making Crispr knock-in stable cell line ..	20
3.11	Objectives of the Study .....	20
4	Material and method .....	24
4.1	Cell culturing and maintenance .....	24
4.2	GuidRNA (gRNA) design and cloning .....	24
4.3	Homology directed repair template design and cloning.....	27
4.4	Co-transfection, puromycin selection and single colony expansion.....	29
4.5	Knock-in validation- PCR genotyping.....	30
4.5.1	DNA isolation.....	30
4.5.2	Primer design and standard PCR.....	30
4.5.3	Sequencing.....	32
4.5.4	Knock-in validation- Western Blot analysis .....	32
4.6	Immunocytochemistry (ICC) .....	33
4.7	Co-Immunoprecipitation (CoIP).....	34
4.8	Formaldehyde cross linking .....	36
4.9	Duolink ® Proximity Ligation assay (PLA) .....	36
4.10	SH-SY5Y differentiation.....	38
4.11	Immunocytochemistry (ICC) of differentiated SH-SY5Y .....	40

4.12	Expansion microscopy .....	41
5	Result .....	45
5.1	Utilizing the CRISPR-Cas knock-in technology, we aimed to add epitope and fluorescent tags in N-terminus of endogenous Miro1 and Miro2 proteins.....	45
5.2	Sanger sequencing confirmed gRNA cloning into CRISPR/ Cas9 vector ...	46
5.3	Screening for recombinant clones. Strategy 1. Screening for fluorescent cells did not succeed in identifying either FLAG-eGFP-Miro1 or MYC-mRFP-Miro2 Knock-in SH-SY5Y cells. ....	48
5.4	Screening for recombinant clones. Strategy 2. The FLAG-eGFP-Miro1 but not MYC-mRFP-Miro2 Knock-in SH-SY5Y cell was successfully identified by direct PCR screening of clones. ....	53
5.5	The combination of using HeLa cells and the second strategy resulted in the successful establishment of stable MYC-mRFP-Miro2 Knock-in cells.....	60
5.6	Double Miro1/Miro2 Knock-in cells were successfully generated in the background of MYC-mRFP-Miro2 Knock-in HeLa cells.....	66
5.7	The Immunoprecipitation (IP) of either FLAG-eGFP-Miro1 or MYC-mRFP-Miro2 was successful in terms of pulling down the bait proteins, but it did not result in the convincing capture of the prey proteins. ....	69
5.8	Proximity ligation assay (PLA) confirmed Miro1 and Miro2 are in close proximity on mitochondria, although it cannot be concluded that they form heterodimerize.....	79
5.9	Although MYC-mRFP-Miro2 signal is vary from cell to cell, there is co-localization of the MYC-mRFP-Miro2 signal and HSP60 signals in most of the cells in DMKI cells. ....	82
5.10	The FLAG-eGFP-Miro1 fusion protein showed partial co-localization with mitochondria in differentiated KI SH-SY5Y cells.....	85
6	Discussion:.....	88
7	Summarizing Remarks and future perspectives.....	98
8	References.....	100
9	list of figures.....	110
10	list of tables.....	112
11	Appendices.....	113



### **3 Introduction**

#### **3.1 Mitochondria play a key role in neuronal health and survival**

It has been assumed that mitochondria are present in all the nucleated eukaryotic cells and account for at least one fifth of the cell volume, underscoring their importance. (Simcox & Reeve, 2016). Energy requirement of cells determines the number of existing mitochondria in those cells. Cells with high energy needs such as Muscles, cardiomyocytes and neurons contain more mitochondria compare to the cells with low energy demand (Genova & Lenaz, 2014). Mitochondria are well-known due to their vital role in energy production via oxidative phosphorylation. However, they are involved in many other cellular processes e.g., protein synthesis, amino acid and nucleotide metabolism, fatty-acid catabolism, lipid, quinone and steroid biosynthesis, iron-Sulphur (Fe/S) cluster biogenesis, apoptosis, ion homeostasis, stress response, cell signaling, and ROS production which are all crucial for proper functioning of the cells (Nahacka et al., 2021a; Roger et al., 2017; Simcox & Reeve, 2016). Mitochondria play a key role in maintaining calcium homeostasis during neurotransmission and short-term plasticity in neurons (Emptage et al., 2001; MacAskill et al., 2009; Mattson et al., 2008; Mochida et al., 2008; Schwarz, 2013; Wang & Schwarz, 2009). Mitochondria are highly motile organelles that undergo fission and fusion in order to make interconnected network and travel short and long distances to meet physiological needs of the cells. These functions are necessary in order to preserve mitochondrial network structure and function as a crucial element for cellular health, as abnormal mitochondrial structures have been observed in many pathological states and neurodegenerative diseases (Engelhart & Hoppins, 2019; Scott & Youle, 2010). Proper neuronal growth, survival and function, as high energy demand cells, is depend on continues supply of ATP (Nicholls & Budd, 2000). Synapses, where neurotransmitters are transported to subsequent neurons and can be meters away from cell body, are the main sites of energy consumption. The most of the required energy is produced by mitochondria (about 93%) and the rest through glycolysis. (Harris et al., 2012). In this situation, neurons have to adapt a specific mechanism to keep proper energy hemostasis. In addition, in axon and synapses, mitochondrial distribution undergoes changes due to axonal and synaptic plasticity and constant activity remodeling. Thus, in order to maintain energy homeostasis mitochondrial movement and tethering has to be regulated on a swift timeframe. In this way

mitochondrial recruitment and redistribution can happen easily based on changes on metabolic needs (Hollenbeck, 1996; Hollenbeck & Saxton, n.d.; Sheng, 2014). It has been reported that impairment in mitochondrial functions and trafficking are linked with neurological diseases, and are probably take part in or exacerbate some physiological and pathophysiological processes (Nahacka et al., 2021b).

### **3.2 Mitochondria are highly dynamic organelles with different motility behaviors**

Mitochondria are highly dynamic organelles and proper regulation of mitochondrial movement, broadcasting and clearance is crucial to maintain cellular energy hemostasis. Mitochondrial dynamic is crucial for cellular health, survival and proper functions especially in neurons due to their special morphology. While most cells are between micrometers to tens of micrometers in size, neuronal axons and dendrites in human peripheral nerves or corticospinal tracts can be over a meter long. Therefore, mitochondrial movement has to be well regulated to provide energy to far cellular regions such as active growth cones, nodes of Ranvier and synaptic terminals which need high level of energy for their proper function (Cheng et al., 2010; Schwarz, 2013; Zinsmaier et al., 2009). Live imaging of neuronal mitochondria targeted fluorescent dyes or genetically encoded mitochondrial proteins could depict this fact that mitochondria are different in their motility behavior. At the same time some mitochondria undergo fission and fusion, some are moving towards cell periphery or nucleus, others stop for short time and start running again, and some stop moving constantly or change their movement directions (Schwarz, 2013). Mitochondria can immediately stop moving for short time and then continue to move or stay immobile and stationary where they stay longer. (Gutnick et al., 2019; Hollenbeck, 1996; Hollenbeck & Saxton, 2005; Ligon & Steward, 2000; Morris & Hollenbeck, 1995.) In mature neurons, approximately one-third of axonal mitochondria are in motion (Chen & Sheng, 2013; Kang et al., 2008.), about 15% shortly pause or anchor at synapses and ~14% motile mitochondria actively travel through presynaptic terminals. A stationary mitochondrion in the presynaptic region supplies a constant source of energy (Shanmughapriya et al., 2020). Mitochondria form highly organized reticular structures in non-neuronal cells and they travel to the cell periphery to meet their energy demands (Cunniff et al., 2016). Mitochondrial trafficking is very important for axonal growth and branching, preserving action potentials, and facilitating synaptic

transmission. It has been reported that disruption in mitochondrial trafficking is linked with axonal degeneration, dysregulation of synaptic transmission and, particularly, to the pathologies of Alzheimer's disease, amyotrophic lateral sclerosis (ALS), and Parkinson's disease (Canty et al., 2023; Hardy, 2010; Li et al., 2015; Mórotz et al., 2012; Nguyen et al., 2014; Zhang et al., 2015). These investigations have discovered the significance of proper mitochondrial trafficking regulation for cellular health.

### **3.3 Fission and fusion are necessary for mitochondrial turnover**

Mitochondria undergo fission and fusion continuously in many different cell types. Mitochondria are different in shape, length, size and number which are controlled by fusion and fission. Mitochondrial fission and fusion regulate sharing organelle content, mitochondrial division and broadcasting and boost the secretion of intermembrane space proteins during apoptosis. Numerous specialized proteins are involved in active process of fission and fusion from mechanical enzymes responsible for physical alteration of mitochondrial membranes, and adaptor proteins that mediate tethering of the mechanical proteins with mitochondria (Figure 3-1) (Detmer & Chan, 2007b; Engelhart & Hoppins, 2019; Scott & Youle, 2010). Large dynamin-related GTPases play an important role in mitochondrial fusion and fission. Within this group, mitofusin1/mitofusin2 (MFN1/MFN2) and optic atrophy protein1(OPA1) are the main elements of mitochondrial fusion. MFN1/MFN2 mediates the mitochondrial outer-membrane fusion, whereas mitochondrial inner-membrane fusion is facilitated by optic atrophy 1 (Opa1). Mutations in either OPA1 or MFN2 cause in dominant optic atrophy or Charcot-Marie-Tooth neuropathy type 2A (Ding et al., 2016). Despite Mfn1 and Mfn2 show high degree of sequence similarity, they diverge in terms of their functions and mechanistic characteristics. Heterozygous point mutations of Mfn2 itself causes peripheral neuropathy Charcot–Marie–Tooth syndrome type 2A (CMT2A), which leads to a continues loss of function and sensation in the hands and feet. Moreover, lack of Mfn1 and Mfn2 in mouse embryonic fibroblasts (MEFs) caused mitochondrial fragmentation, whereas in wild type cells mitochondria formed a reticular and connected network. Overexpression of Mfn1<sup>wt</sup>-Flag in Mfn1 null cells or Mfn2<sup>wt</sup>-Flag in Mfn2 null cells reshaped the mitochondrial reticular networks but transducing the cells with empty vector did not have the same impact. On the other hand, it has been reported that Mfn1 and Mfn2 do heterodimerize and this heterodimerization is the most effective form of complex for mitochondrial fusion. Mfn1 or Mfn2 homodimerization is

also reported, however, fusion activity of homodimerized either Mfn1 or Mfn2 is relatively low emphasizing on the important role of both Mfn1 and Mfn2 in making joined mitochondrial network. (Ban et al., 2017; Detmer & Chan, 2007a; Hoppins et al., 2011; J Ford et al., 2019; Stuppia et al., 2015). GTPase dynamin-related protein 1 (DRP1; encoded by *DNM1L*) play a key role in mitochondrial fission by wrapping around outer mitochondrial membrane and cutting it. Dysfunctional DRP1 induces hyper-fusion of mitochondrial network, emphasizing the essential role of DRP1 in mitochondrial fission. Drp1 is also involved in not only mitochondrial but also peroxisomal proliferation through fission of pre- existing organelles. It is reported that general DRP1 knockout is embryonic lethal in mouse and mitochondrial network hyper-fusion and reduction in the number of single mitochondria in each specific area was observed by silencing of DRP1 in WT cells as well as in dynamin triple-knockout fibroblasts (Fonseca et al., 2019; Ishihara et al., 2009; Robertson et al., 2023; Wakabayashi et al., 2009). *DNM1L* and *DRP1* heterozygous *de novo* missense mutations defects mitochondrial and peroxisomal fission and ended to encephalopathy (EMPF1) which is a destructive neurodevelopmental disorder with no efficient cure. The majority of patients carrying DRP1 mutations do not live beyond childhood or early adolescence (Ryan et al., 2018).

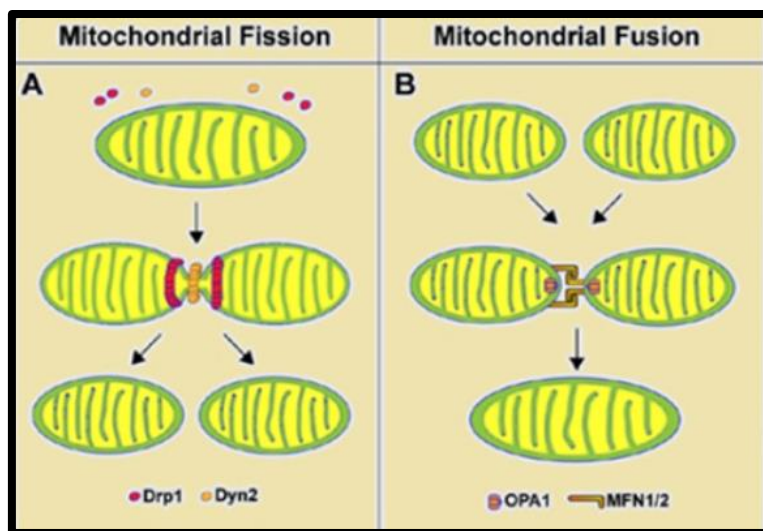


**Figure 3-1 Schematic of mitochondrial fission and fusion.**

A) Drp1 and Dyn2 proteins mediate mitochondrial fission by condensing mitochondrial membrane. B) homodimerized or heterodimerized MFN1 and MFN2 are involved in outer mitochondrial membrane fusion, however, OPA1 is required for mitochondrial inner membrane fusion. (Picture is reproduced from Çelen, 2018).

### **3.4 The Motor-Adaptor protein complex mediates the long-range**

## mitochondrial trafficking

Mitochondria dynamically move to the area of the cell where they need energy or calcium homeostasis is disrupted (Nahacka et al., 2021b). Anterograde movement of mitochondria mediated by kinesin-1 microtubule motor protein, whereas mitochondrial retrograde movement is happened through mitochondria interaction with dynein-dynactin complex (Y. Chen & Sheng, 2013). Trafficking Kinesin Protein (TRAK, also called Milton or TRAK1/OIP106, TRAK2/GRIF1), adaptor protein tethers microtubule motor proteins to mitochondria through Rho-like GTPase (Miro) protein, a mitochondrial outer membrane protein (figure 3-2)(Glater et al., 2006; Stowers et al., 2002; van Spronsen et al., 2013). Altogether, all the members of motor-adaptor complex are important for proper mitochondrial movement. Kinesin-1 motor protein is autoinhibited and not able to move along microtubule tracks in the absence of TRAK adaptor protein. TRAK1 increases the ability of kinesin-1 to runs long distances and enhances its performance to tackle obstacles on microtubules (Henrichs et al., 2020). The importance of Miro and TRAK adaptor proteins for mitochondrial movement was first discovered in *Drosophila* neurons. In neurons, loss of either dMiro or Milton, TRAK's homologue in *Drosophila*, defects synaptic transmission, disturbs mitochondrial distribution and causes early mortality(Guo et al., 2005; Stowers et al., 2002). These results highlight the importance of having a proper understanding about motor-adaptor complex interaction pattern to gain a comprehensive knowledge about mitochondrial trafficking.

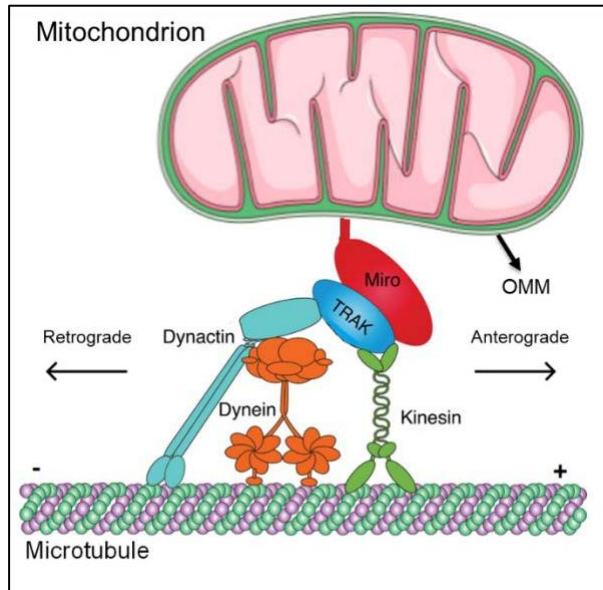


**Figure 3-2 Schematic of Mitochondrial motor-adaptor complex.**

Mitochondrial motility toward plus or minus end of microtubule tracks is regulated by motor-adaptor complex. From one hand motor-adaptor complex is tethered to the outer mitochondria membrane via C-terminus transmembrane domain of Miro protein and from other hand they bind to Miro protein through TRAK adaptor protein. Kinesin motor protein is involved in anterograde movement of mitochondria to the plus (+) end of microtubule, while Dynein-Dynactin motor protein mediates retrograde movement of mitochondria towards minus (-) end of microtubule tracks. (Picture is reproduced with slight modification from Zinsmaier, 2021).

### **3.5 Microtubule's motor protein**

#### **3.5.1 Kinesin and Dynein**

Eukaryotic cells have various motor proteins that differ in terms of binding to cytoskeletal tracks (either actin or microtubules), direction of their runs and the payloads they transport. (Alberts B et al., 2002). Short-range trafficking of mitochondria is mediated by and long-range movement of mitochondria is mediated by actin-based motor proteins, whereas microtubule-based motor proteins are involved in long-range movement of mitochondrial (Hollenbeck & Saxton, 2005). Kinesin is a microtubule-based motor protein that can move anterogradely and retrogradely. However, Dynein which is also microtubule-dependent motor protein only involves in retrograde trafficking toward minus end of microtubule tracks. (Hollenbeck & Saxton, 2005; Pilling et al., 2006). The mechanical forces that kinesin and dynein require to transport cargo along microtubule tracks is provided by ATP hydrolysis. Fourteen kinesin families, Kinesin1- to Kinesin-14, form the big kinesin superfamily (KIF) (Abraham et al., 2018). Most kinesin families contain two light chains, two heavy chains, and alpha-helical neck *domains* that form a *coiled coil* stalk

domain. They all have the same motor domain at the N-terminus; however, they differ in their Carboxy-terminal tails because they are specialized to carry different cargos such as organelles, vesicles and chromosomes along microtubule tracks. (Cooper GM & Adams K., 2022.; Abraham et al., 2018; Schliwa, 2003). Kinesin1 have three heavy chain variants (KIF5B expressed in various cell types, and KIF5A and KIF5C predominantly expressed in neurons), known as the main motor protein in charge of mammalian mitochondrial anterograde trafficking. (Cooper GM, 2000. Kruppa & Buss, 2021). Beside various light and intermediate chains, dynein has two or three heavy chains. Dynein's motor domain is a member of the AAA+ protein family (ATPases Associated with diverse cellular Activities) and is the globular head domain of the heavy chains (Gleave et al., 2014). The lower part of dynein, containing the intermediate and light chains, is believed to bind to other subcellular component, like organelles and vesicles. There are different types of axonemal dyneins, present in cilia and flagella, and cytoplasmic dyneins as well. All the dynein family members involved in retrograde trafficking, although cytoplasmic dyneins differ based on the different payload they transport. Typical kinesin and members of kinesin family which are involved in plus end-movement of cargos, runs toward the cell periphery, while cytoplasmic dyneins and the kinesins involved in minus end-movement of payloads, carry the cargos toward nucleus, where is the microtubule organizing center (Cooper GM., 2000b, 2000a)). Although dynein is the essential motor protein mediates mitochondrial retrograde movement, it needs kinesin-1, that delivers freshly produced dynein from the cell body to the synapse( Drerup et al., 2017; Twelvetrees et al., 2016). Most of dynein's mutations linked with disease change overall dynein-dependent retrograde movement, while loss of function mutation in the dynactin subunit ACTR10 specifically defects dynein binding to mitochondria in zebrafish(Drerup et al., 2017). Despite Kinesin and dynein are both motor proteins, they are not similar. Dynein is larger than kinesin and it can take a larger step which make it faster than kinesin. However, kinesin carry and transfer bigger cargos. The dynein family is limited in terms of the number of members and the diversity of the tasks it does, kinesin superfamily contains a broad range of motor proteins with higher diversity in task. Inside the cell, dynein needs to interact with dynactin to be activated, while TRAK1 and kinesin-1 interaction is necessary for kinesin activation and taking long runs specially in case of kinesin-1-dependent mitochondrial long-range transport in the crowded cytosol, while dynactin interaction is needed for dynein activation (Henrichs et al., 2020).

### 3.5.2 Trafficking kinesin protein-TRAK1 and TRAK2

TRAK1 and TRAK2, the mammalian homologues of the *Drosophila* Milton protein, share 58% similarity in their sequence. There are also homologs of Milton/TRAK proteins or TRAK protein-like ancestors in *C. elegans*, Zebra fish and non-mammalian vertebrates, marsupials and eutherian mammals (Lumsden et al., 2016; Nahacka et al., 2021c). Both TRAKs known as adaptors that link kinesin/dynein motor to mitochondria via their interaction with Miro1/Miro2 in different tissues. TRAK1/2 directly interacts with kinesin heavy chain non motor domain through their N-terminal coiled-coil domain, and dynein-dynactin, via C-terminal cargo binding domain and they bind to Miro through their c-terminal domain (Brickley & Stephenson, 2011; Canty et al., 2023; Stowers et al., 2002). TRAK and its orthologs are responsible for performing the same function in different species ranging from *Drosophila* to mammals. In mouse embryonic fibroblasts, TRAK1 overexpression enhances anterograde movement of mitochondria, while TRAK2 overexpression increases retrograde mitochondrial trafficking (Fenton et al., 2021). When kinesin-1 binds to TRAK1, it becomes active and its run length extends, thereby enhancing the long-distance transportation of mitochondria through kinesin-1 in the crowded cytosol (Henrichs et al., 2020). Co-expression of TRAK1, TRAK2, or Milton with kinesin heavy chain enhances mitochondrial redistribution and mitochondria colocalize with TRAK1, TRAK2, Milton, and kinesin heavy chains at the cellular periphery (Brickley & Stephenson, 2011). TRAK1 which is localized mainly axons of neurons and needed for proper axon protrusion, however TRAK2 extensively present in dendrites and is required for dendritic development. In Addition, TRAK1 interacts with both kinesin and dynein/dynactin in neurons, whereas, TRAK2 mostly bind to dynein/dynactin, suggesting that TRAK1 and TRAK2 play a distinct role in mitochondrial movement. (Canty et al., 2023; Glater et al., 2006; MacAskill et al., 2009; van Spronsen et al., 2013). In contrast, when TRAK1 and TRAK2 were co-expressed together with peroxisomal labelled (PEX) active GTP-bound state (P13V) Miro1 in Cos7 cells, they both co-localized with Kinesin (KIF5C) on peroxisomes. However, the assembly of the truncated version of Dynein/Dynactin complex, P135, on peroxisomes was dependent on the presence of TRAK1. On the other hand, neither TRAK1 nor TRAK2 co-assembled with KIF5C when co-expressed along with PEX Miro2 (Davis et al., 2023). This lack of co-assembly might be attributed to the absence of other proteins that facilitate the assembly of motor-adaptor proteins on mitochondria, which were not

present on peroxisomes.

### **3.6 Miro proteins**

Despite being initially classified as a member of the Rho GTPase family, the Miro (mitochondrial Rho-like) GTPase protein was later reclassified under the small GTPases subfamily due to the absence of the characteristic 'Rho' insert typically found in Rho GTPases (Reis et al., 2009; Wennerberg & Der, 2004). Miro is conserved evolutionarily from yeast to mammals. Yeast (Miro homolog Gem1) and some of the lower metazoans (dMiro in *Drosophila melanogaster*) have one Miro, whereas some of the higher metazoans have two Miro, i.e., Miro1 and Miro2 in mammals (Beljan et al., 2020; Boureux et al., 2007; Frederick et al., 2004; X. Li et al., 2015; Nahacka et al., 2022; Vlahou et al., 2011). In mammals, Miro1 is encoded by the RHOT1 gene located on chromosome 17, while Miro2 is encoded by the RHOT2 gene located on chromosome 16. Both proteins contain 620 amino acid residues that are 60% identical (Nahacka et al., 2021b; Reis et al., 2009). They are composed of two GTPase domains that are linked together through two EF-hands domains. The EF-hand motif has a helix-loop-helix structure with a canonical Ca<sup>2+</sup> binding motifs (Klosowiak et al., 2013) Miro is tethered to the outer mitochondrial membrane through the C-terminus transmembrane domain (Figure 3-3). Miro1 and Miro2 have been considered as essential factors regulating mitochondrial transport (Canty et al., 2023; van Spronsen et al., 2013). Long-range mitochondrial movement is made by Miro's interaction with kinesin and dynein microtubule motor protein, and their adaptor proteins, TRAK1/2 (Nangaku et al., 2009; Susalka and Pfister, 2000; Kittler, 2015; López-Doménech et al., 2018; Henrichs et al., 2020), whereas local, short-range, trafficking is mediated by the assembly of mitochondria with actin and its motor protein myosin (Modi et al., 2018; Oeding et al., 2018; Bocanegra et al., 2020).

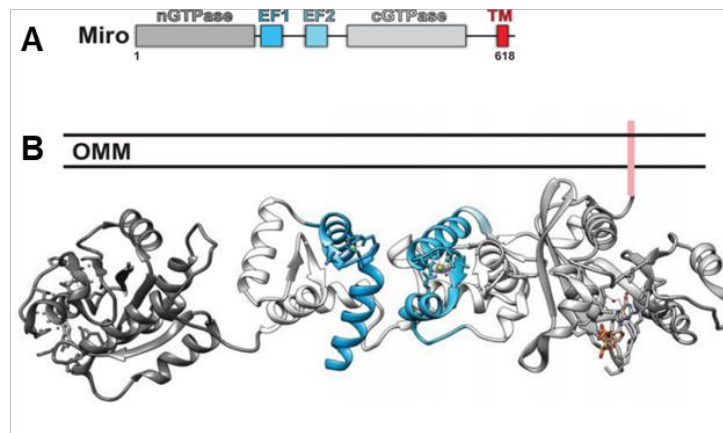


**Figure 3-3 Structural features of Miro.**

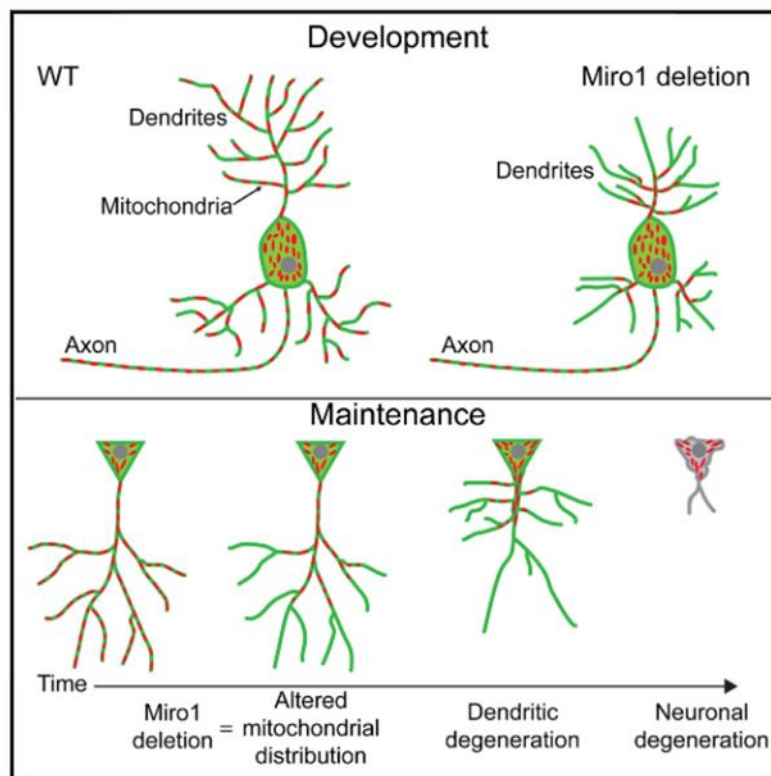
(a) Domain organization: Miro has two GTPase domain, nGTPase and cGTPase, linked together through two EF-hand linkers EF1 and EF2. C-terminus transmembrane domain tethered Miro to the outer mitochondria domain (OMM). (b) Miro structure' Model: nGTPase (dark grey, PDB: 6D71), EF-hands (blue) and C-terminus (PDB: 5KSZ) with cGTPase (light grey) and transmembrane domain (red) (Picture is reproduced from Eberhardt et al., 2020).

As previously stated, Mammalian Miro isoforms exhibit a high degree of sequence similarity, suggesting potential compensatory functions they may share in certain aspects. It has been shown that Miro1 and Miro2 are necessary for proper mitochondrial cristae architecture and Endoplasmic Reticulum-Mitochondria Contacts Sites (ERMCS). Genetic deletion of Miro1 and Miro2 in mouse embryonic fibroblasts (MEF) caused a reduction in ERMCS and disturbed mitochondrial cristae organization. Expression of mitochondrial matrix-targeted GFP (mtRoGFP) in Miro1/2 double-knockout (DKO) cells exhibited fragmented GFP signal with high abundant hollow regions. This was along with presence of shorter mitochondria beside enlarged and more spherical segments, as well as a non-uniform arrangement of mitochondrial cristae. In opposite, in wild-type (WT) cells, elongated and thin mitochondria beside individual mitochondria showing continuous GFP staining were dominant (Kruppa & Buss, 2021; Modi et al., 2019). Overexpression of Miro1 or Miro2 in DKO cells could re-create mitochondrial matrix continuity indicating the crucial role of Miro proteins in matrix structure maintenance. Furthermore, biochemical studies have confirmed that the interaction between Miro1 and Miro2 with Sam50 and MICOS facilitates the coupling of the MIB/MICOS complex, bridging the inner and outer mitochondrial membranes to the TRAKs adaptor (Modi et al., 2019). In addition, it has been reported that Miro1 and Miro2 are responsive to calcium stress and play a role in mediating

mitophagy to maintain the homeostasis of the mitochondrial network, primarily through their  $\text{Ca}^{2+}$ -sensing EF-Hand domain. The EF-hand motifs of Miro1 sense the increase in mitochondrial  $\text{Ca}^{2+}$  levels, resulting in the inhibition of Mitofusin (MFN) by Miro1 and the cessation of mitochondrial fusion. Subsequently, mitochondrial fission, mediated by Drp1, segregates unhealthy mitochondria. This process is followed by the recruitment of Parkin, initiating mitophagy to remove the damaged mitochondria and thereby maintaining the homeostasis of the mitochondrial network, particularly in high  $\text{Ca}^{2+}$  conditions (Fatiga et al., 2021). López-Doménech and co-workers 2018 have shown that Miro is critical for recruiting and stabilizing Myosin19 (Myo19) on the OMM for coupling mitochondria to the actin cytoskeleton to mediate short-range mitochondrial movement. Using indirect immunofluorescence labelling they confirmed that Myo19 protein quantity associated with mitochondria is dependent on Miro1/Miro2 expression level. In the HeLa cells transfected with Miro1/Miro2 siRNA, the Myo19 mitochondrial signals were notably reduced which could be rescued by overexpression of Miro2 (López-Doménech et al., 2018). Despite playing cooperative roles in various cellular processes, as mentioned earlier, Miro1 and Miro2 surprisingly exhibit distinct functions in terms of mitochondrial movement along microtubule tracks. (Eberhardt et al., 2020; Modi et al., 2019). In the organisms with only one isoform of Miro, lack of Miro has a severe effect not only in mitochondrial movement but also in mitochondrial morphology. Null mutations in dMiro, the most closely related human Miro1 isoform in *Drosophila*, result in disrupted axonal and dendritic transport of mitochondria and notable mitochondrial accumulation in the neuronal cell body compare to WT control. In mutant larval neurons, mitochondria exhibit a pronounced clustering towards the soma, while distal neuronal structures such as neuromuscular junctions lack mitochondria. The mutations in Miro1 and Miro2 result in noticeable phenotypic effects characterized by slim body morphology, abnormally small muscle size, and progressive locomotive defects. These manifestations ultimately lead to mortality during the larval or early pupal stages. However, the adverse phenotype is rescued by WT dMiro expression specifically in neurons, emphasizing the crucial role of dMiro in neuronal function and survival (Guo et al., 2005; Wang et al., 2011). In yeast one of the key components needed for maintenance of mitochondrial normal tubular network and mitochondrial inheritance is Gem1p, a Miro homolog. Mutation in Gem1p disturbs mitochondrial movement and morphology. In Gem1p mutants, most of mitochondria were round showing a non-uniform membrane shape beside some

formed grape-like shape or were collapsed which did not detect in WT cells(Frederick et al., 2004). Despite the high degree of sequence similarity among mammalian Miro isoforms, their functional differences in terms of mitochondrial motility regulation and their specific interaction partners in the motor-adaptor complex remain unclear. Miro1's role in mitochondrial trafficking has long been studied, whereas Miro2's function is not well defined. Numerous studies have focused on the importance of Miro1 in mitochondrial motility and cellular health. Studies have suggested that Miro1 plays a critical role in the development of upper motor neurons and the retrograde transport of axonal mitochondria. A neuron-specific Miro1 KO mouse model shows physical symptoms of neurological and upper motor neuron disease and increasing death rate after approximately four weeks (Nguyen et al., 2014). Proper mitochondrial distribution in a neuron is crucial for development and maintenance of dendritic trees and disruption of mitochondrial spreading in mature neurons is linked with neurodegeneration. Using Miro1 and Miro2 knockout mouse models researchers have reported that Miro1-dependent mitochondrial movement is not only important for dendritic tree development but also for maintenance of dendritic complexity. In Miro1 knockout (Miro1<sup>KO</sup>) embryonic neurons, a depletion of mitochondria in distal dendrites and a reduction in dendritic complexity were observed. Conversely, the dendritic architecture in Miro2 knockout (Miro2<sup>KO</sup>) neurons was similar to wild-type (WT) control, indicating that the presence of Miro1, but not Miro2, is necessary for proper dendritic development. Moreover, Miro1<sup>KO</sup> mature neurons showed fast degeneration of distal dendrites and eventual cell death (Figure 3-4). Furthermore, a significant reduction in anterograde and retrograde mitochondrial movement in dendrites (85%) and axons (65%) has been seen in Miro1<sup>KO</sup> mouse hippocampal neuronal cultures, while no significant impact on mitochondrial motility was reported in Miro2<sup>KO</sup> neurons. Interestingly, in double knockout (Miro<sup>DKO</sup>) mouse embryonic fibroblasts (MEFs), there was a significant decrease in microtubule-dependent mitochondrial motility compared to wild-type (WT) cells. However, no significant difference in mitochondrial motility was observed compared to Miro1<sup>KO</sup> cells. The restoration of mitochondrial motility was observed upon the expression of Miro1, indicating that Miro1 can fully recover the motility. However, when Miro2 was expressed, only partial recovery of mitochondrial motility was observed, suggesting that Miro2 may not be the primary regulator of mitochondrial trafficking. This observation suggests that Miro1 has the ability to compensate for the function of Miro2 in regulating mitochondrial motility.(López-

Doménech et al., 2016; Norkett et al., 2018).



The disturbance of mitochondrial spreading in mature neurons results in the reduction of dendritic complexity, leading the occurrence of neurodegeneration (Picture is reproduced from López-Doménech et al., 2016).

On the other hand, the knock-out of Miro1 in mouse embryos was found to be lethal, indicating its crucial role in embryonic development. This knock-out also led to a significant reduction in mitochondrial movement in mouse embryonic cells (MEFs) compared to wild-type (WT) cells. In contrast, Miro2 knock-out mice reached adulthood without any observable problems, and there was no significant difference in mitochondrial motility between the knock-out and wild-type cells. In addition, the specific knock-out of Miro1 in neurons has been shown to have a preferential impact on retrograde mitochondrial distribution and run length in cortical axons. This finding suggests that Miro1 and Miro2 play an unequal role in regulating the back-and-forth movement of mitochondria in neurons (Nguyen et al., 2014). Furthermore, it has been revealed that the presence of Miro1 is necessary for the late stage of mouse embryo development and this function cannot be compensated by Miro2, whereas Miro2 plays a role in embryo development at the earliest stage that can be compensated by Miro1 in the absence of Miro2 if both copies of Miro1 are present but only until specific developmental time point (E12.5). Mitochondria were concentrated in the prenuclear region in Miro1KO MEF cells compare to either Miro2<sup>KO</sup> or WT MEF cells. Interestingly,

mitochondrial accumulation in the proximal regions were higher in Miro<sup>DKO</sup> MEFs compare to Miro1<sup>KO</sup> cells, which could imply a non-redundant and important role of Miro2 in mitochondrial trafficking regulation. The functional difference of Miro1 and Miro2's GTPase domains in relation to mitochondrial trafficking is less known, despite several studies have investigated this subject by manipulating the GTPase domains through the overexpression of mutated forms. It has been revealed that overexpressing a constitutively active GTP-bound state (P13V) leads to changes in mitochondrial distribution. Conversely, overexpression of Miro1 N-GTPase constitutively inactive GDP-bound state (T18N) mutation reduces mitochondrial trafficking and disrupts their normal distribution. (MacAskill et al., 2009; Saotome et al., 2008; Wang & Schwarz, 2009). Moreover, by misdirecting of Miro protein to peroxisome through replacing of the Miro outer mitochondrial membrane domain with PEX3 peroxisomal membrane domain, Davis et., al 2022 have investigated the GTPase domain of Miro1 and Miro2 functional differences in terms motor-adaptor recruitment. It has been shown only Miro1 n-GTPase locked in the active GTP-state recruited TRAK1/2, kinesin, or P135 on the peroxisomes and significantly induced the peroxisomal movement towards growth cones. However, Miro1 nGTPase locked in the GDP-stat expression did not recruit motor-adaptor complex on peroxisome and peroxisomes remained in cell body. Surprisingly, co-expression of PEX-Miro2, regardless of its GTPase domains state, with motor-adaptor complex did not result in co-assembly of the complex on peroxisome and peroxisomal movement, despite it is generally accepted that Miro2 supports mitochondrial motility (Davis et al., 2022). In terms of the Miro proteins roles in mitochondrial segregation during mitosis, it has been observed that in Miro<sup>DKO</sup> cells lacking both Miro1 and Miro2, there is an unequal distribution of mitochondria between daughter cells. Additionally, these DKO cells exhibit a lower rate of cell division compared to cells with intact Miro proteins. Overexpression of Myo19 in Miro<sup>DKO</sup> cells partially recovered unequal mitochondrial segregation indicating that Miro protein but not Myo19 is the main moderator of appropriate and accurate mitochondrial segregation, either through adjusting the mitochondrial related activity of Myo19 or by regulation of short-range mitochondrial movement with Myo19 alongside long-range microtubule dependent movement of mitochondria through kinesin and dynein motor complexes (Norkett et al., 2018). Unexpectedly, in purified mitochondrial fractions from all different cell types wild type to M1<sup>KO</sup>, M2<sup>KO</sup> and MiroDKO MEFs, both TRAK1 and TRAK2, kinesin heavy chain,

P150/Glued and the dynein intermediate chain were found with the same quantity. Moreover, upon overexpression of tagged TRAK1/TRAK2, they were localized on the mitochondria even when Miro protein was not present in the cells. This data suggests that there might be additional TRAK adaptors like Mitofusin1/2 that mediate TRAKs anchoring to the mitochondria and make mitochondrial microtubule dependent trafficking (Norkett et al., 2018). Moreover, when Miro1 and Miro2 are overexpressed in mammalian cells, they exhibit co-distribution and co-immunoprecipitation with Milton, TRAK1, or TRAK2. Additionally, Miro1 co-immunoprecipitated with TRAK2 in brain extracts. In hippocampal neurons, overexpression of fluorescently tagged TRAK2 or Miro1 constructs leads to an increase in the transportation of mitochondria to the outer regions of the neurons (Brickley & Stephenson, 2011). Despite the observed differences in mitochondrial motility behavior, the functional significance of each Miro isoform as a key mediator of mitochondrial trafficking and how they contribute to this diversity remain unclear. Moreover, Miro2 is less studied than Miro1, and there is not enough information to support Miro2 role long-range mitochondrial motility. It is also not known how the presence or absence of Miro proteins, as well as their preference for binding to specific motor-adaptor proteins, contribute to the diversity of mitochondrial trafficking. To address these questions, several intriguing inquiries need to be answered. One of the primary questions pertains to the distribution pattern of Miro1 and Miro2 across different mitochondrial populations, which is currently not well understood. Therefore, the first question to address is whether Miro proteins selectively mark distinct mitochondrial populations or if they are ubiquitously present in all mitochondria. Furthermore, the localization patterns of Miro proteins on mitochondria remain poorly understood. It is unclear whether they are localized in the same regions or if there is heterogeneity in their distribution. If there is heterogeneity, this raises questions about the potential influence of a specific Miro isoform on mitochondrial motility behavior diversity. How does this heterogeneity impact various parameters of mitochondrial trafficking, such as velocity, direction, speed, run and pause times, and others? Additionally, how does it affect the stoichiometry of the motor-protein complex that interacts with Miro isoforms? For instance, it is possible that Miro and TRAK form dimers, but information regarding the interaction preferences of Miro1 and Miro2, whether they predominantly form homodimers or heterodimers, is currently lacking. Moreover, the heterogeneity in Miro isoforms may also contribute to heterogeneity in the proteome and lipidome composition of the labelled mitochondria.

These questions extend to the role of Miro isoforms in organelle-organelle interaction, does each isoform preferentially involved in interaction of special organelles or they both are needed as a general tool for all the interaction between different organelles. As it has been shown that Miros is involved not only in mitochondrial movement but also in cell division, mitophagy, ER-mitochondria connections, and other processes. Therefore, it is crucial to continue studying Miro proteins at the molecular and biochemical levels to gain a better understanding of how their functional differences influences mitochondrial motility, which is very important for proper cell function and survival especially for neurons.

### **3.7 Crisper cas-9 knock-in technology is a reliable approach to analyze miro1 and miro2 expression and localization in living cells**

Having precise information about protein localization is a good way to gain better understanding about protein function, since protein localization and function are closely related. Protein labelling is one of the most well-known approaches to study protein localization (Matsuda & Oinuma, 2019a). Although Immunohistochemical (IHC) and Immunocytochemical (ICC) analysis using antibodies has been widely used for this purpose, but it is most of the time associated with problems related to the sensitivity and specificity of antibodies. Additionally, cells have to be fixed and permeabilized in IHC and ICC which is not suitable for live imaging studies. On the other hand, transient overexpression of an epitope-tagged protein in cells is another alternative method to study subcellular localization of proteins. While, protein overexpression often leads to protein artificial mis-localizations or disturb proper cellular functions (Willems et al., 2020). Genome engineering is a powerful technique for studying protein functions and localization. CRISPR/Cas9 genome editing technology has been widely used in as a biology tool to study gene expression and imaging (B. Chen et al., 2013; Qi et al., 2013). Protein localization has been studied through generation of endogenous gene knock-in or knock-out cell lines using CRISPR-Cas9. Researchers can interrupt the gene by random insertions or deletions through non-homologous end joining (NHEJ) to make a knock-out or to insert the DNA sequence with a homologous template through homology-directed repair (HDR) to knock-in tags or fluorescent proteins. These changes make the direct imaging of the protein of interest and its subcellular distribution in neurons in vitro and in vivo (Figure 3-5)(Matsuda & Oinuma, 2019b; Nelles et al., 2016; Wiedenheft et al., 2012).

Additionally, knock-out a gene using Crispr Cas 9 helps the researcher to investigate the effect of gene and protein loss on cellular processes which is valuable in order to gain insight about specific genes and proteins roles (Shalem et al., 2014). Additionally, make point mutation in genes using CRISPR-Cas9 enables the researchers to especially focus on the functional importance of specific amino acid changes(Levi et al., 2020). On the other hand, the advent of CRISPR-Cas9 screening techniques, such as CRISPR interference (CRISPRi) and CRISPR activation (CRISPRa) is widely used as a screening technique for activation or suppression of gene in order to study gene expression and understand gene function in eukaryotic models. With these techniques researchers could identify main genes involved in particular cellular processes or signaling pathways(Gilbert et al., 2013; Y. Liu et al., 2019). CRISPR/Cas9 knock-in is a famous method to insert epitope tag at the genomic loci of gene of interest to avoid the limitations of antibody-based techniques and transient protein overexpression for protein localization studies. In addition, it is compatible with live imaging and increases specificity and sensitivity and resulting in more precise and biologically relevant information of protein localization within cells(Willems et al., 2020). Therefore, due to the limitations mentioned above, we used Crisper Cas9 knock-in to tag endogenous Miro1 and Miro2 for further analysis. By this way we can not only study their localization and distribution in live cells but also to purify the subpopulations enriched for each Miro isoforms and to compare the proteomes and lipidomes of these different pools.

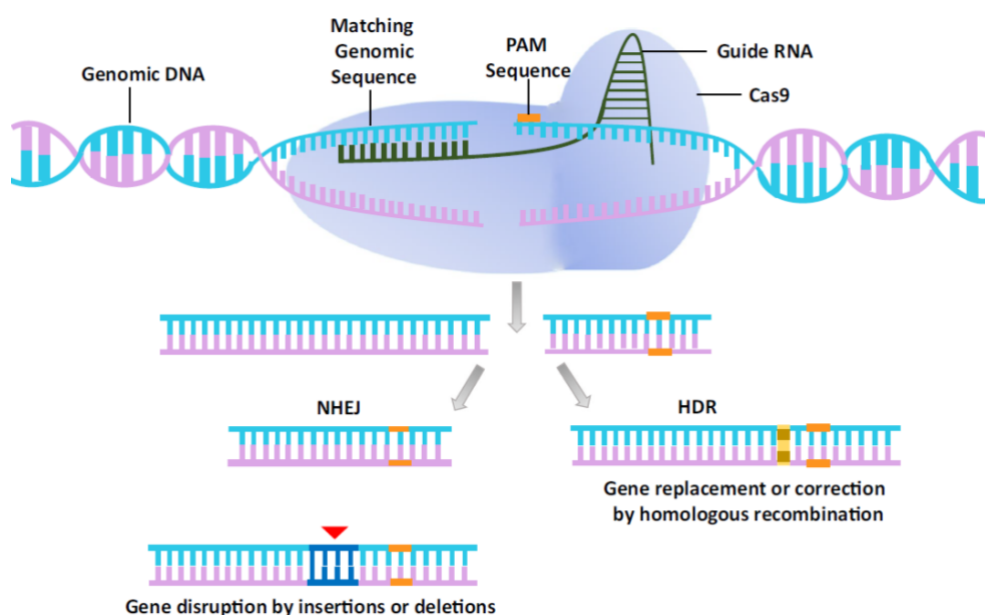


### **Figure 3-4 Schematic representation of CRISPR-Cas9-mediated genome editing process.**

This approach utilizes the RNA-programmable DNA endonuclease derived from the *Streptococcus pyogenes* CRISPR-Cas9 system. The targeting of specific DNA sequences is achieved through a single guide RNA (sgRNA) sequence, which pairs with a 20-nucleotide DNA sequence upstream of the protospacer-associated motif (PAM). This binding results in a double-strand break (DSB) occurring 3 base pairs upstream of the NGG sequence. Subsequently, the DSBs can be repaired by either non-homologous end joining (NHEJ) or homology-directed repair (HDR). Repair via NHEJ, which is prone to errors, often leads to the insertion or deletion of nucleotides (Indels) that can potentially cause genome instability. On the other hand, if an exogenous donor DNA template is present, the DSB can be accurately repaired through the error-free HDR pathway, allowing for precise modifications to be engineered into the DNA (Picture is reproduced from Ghosh et al., 2019).

### **3.8 Mass spectrometry helps in to functional study of proteome and lipidome of Miro1 or Miro2-containing mitochondrial populations**

Mass spectrometry (MS) has rapidly developed during the past 20 years and since then it has expanded from analyzing small inorganic components to biological macromolecules like proteins and lipids, practically with no mass limitations within the life and health sciences (Köfeler et al., 2012). MS has gained popularity amongst the technique can be used for large scale protein investigations due to its ability to manage the complexities associated with the proteome. Two-dimensional gel electrophoresis (2DE), two-hybrid analysis, and protein microarrays cannot reach the depth of instructive proteome analysis achieved by mass spectrometry. MS can be used for different purposes such as classifying protein expression, elucidation of protein interactions, and identification of protein modification site (Han et al., 2008). MS is also a common technique to assay lipid content of an organism, organelle or a cell. Lipids have gained attention in the bio-medical community by passing the years not only due to their in-energy storage but also their critical role in various cellular regulation cycles and thus attain rising interest. Due to the sensitivity and selectivity of MS, this method is a famous alternative for qualitative and quantitative lipidomics analysis (Köfeler et al., 2012). It has been shown that the energy demand of axon and dendrite are different. This diversity raises the intriguing question of whether mitochondria have developed distinct molecular characteristics to meet their required needs or not. To address this question, we would perform purification of mitochondrial communities expressing tagged Miro1 and Miro2, followed by comparative analysis of their proteome and lipidome pools using mass spectrometry. Additionally, we have

employed the Co-Immunoprecipitation (CoIP) technique with tag-specific conjugated magnetic agarose beads to specifically capture Miro1 and Miro2 proteins in knock-in cells. This approach allowed us to investigate the stoichiometry of isolated isoforms in two ways: First, utilizing SDS-PAGE and specific antibodies against potential interacting partners, we determined whether they form the same protein complex and explored the possibility of homodimerization or heterodimerization. Second, by subjecting the pulled-down samples to mass spectrometry analysis, we obtained a comprehensive list of potential interactors, shedding light on the distinct protein interactions of Miro1 and Miro2. Understanding the diversity in these interactions will provide valuable insights into the functional differences between Miro1 and Miro2.

### **3.9 SH-SY5Y a human cell line with neuronal-like characteristics and morphology**

The SH-SY5Y neuroblast-like cell line is a subclone derived from the SK-N-SH parental neuroblastoma cell line. The parental cell line, established in 1970 from a bone marrow biopsy containing neuroblast-like and epithelial-like cells, serves as the origin of SH-SY5Y cells (Biedler et al., 1973.). SH-SY5Y cells possess a stable karyotype comprising 47 chromosomes and can undergo differentiation from a neuroblast-like state to mature human neurons using various methods, including retinoic acid (RA), phorbol esters, and specific neurotrophins like brain-derived neurotrophic factor (BDNF) (Figure 3-6). Previous research indicates that differentiating methods can favor the development of distinct neuron subtypes, such as adrenergic, cholinergic, and dopaminergic neurons (Phhlman et al., 1984; Xie et al., 2010). This versatility makes SH-SY5Y cells highly valuable for numerous neurobiology experiments. Notably, significant differences have been observed between undifferentiated and differentiated states of SH-SY5Y cells. In their undifferentiated state, these cells exhibit rapid proliferation, non-polarized morphology with few short processes, clumping growth pattern, and expression of markers associated with immature neurons (Kovalevich & Langford, 2013; P&lman et al., 1995). Upon differentiation, the cells extend long, branched processes, reduce proliferation, and in some cases, exhibit polarization (Shiple et al., 2016). SH-SY5Y is widely used as in vitro models of neuronal function and differentiation. Moreover, it is a well-known model to study neurodegenerative diseases, where mitochondrial dysfunction is considered as a key component in pathophysiology of

neurodegenerative disorders (Evinova et al., 2020). Since, the final aim of our study was to study functional differences of Miro1 and Miro2 in mitochondrial trafficking in neurons, SH-SY5Y was a good model to set up the experiments in a neuronal like environment due to its human origin, ability to be differentiated to neurons, expresses neuronal morphology and markers.

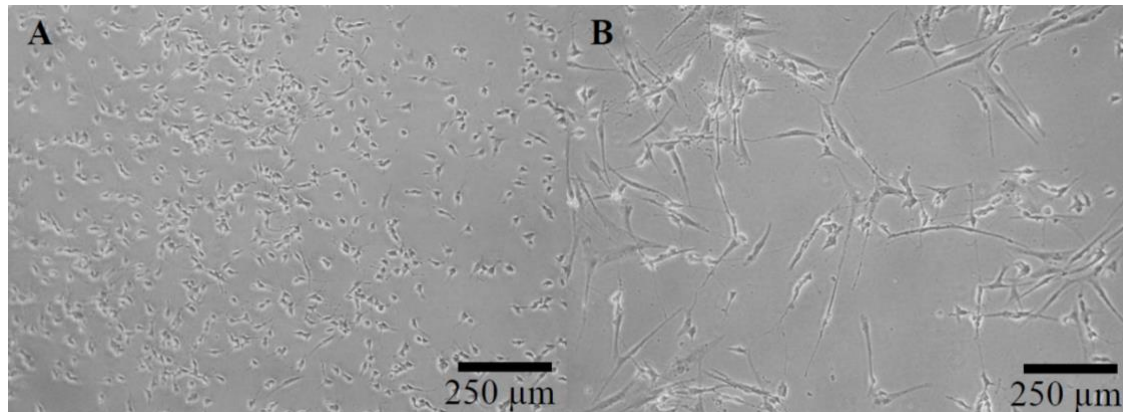


**Figure 3-5 Exemplary picture of non-differentiated control.**

(A) and differentiated SH-SY5Y(B) cells after 14 days of treatment by retinoic acid (RA) cultured in RPMI-based media (Picture is reproduced from Shipley et al., 2016).

### **3.10 HeLa cell line an easy cell line for making Crispr knock-in stable cell line**

HeLa cell line is the first developed human cell line taken from aggressive cervical cancer cells in 1950s from Henrietta Lacks, a 30-year-old woman. HeLa cells growth rate is high, can be kept in culture for a long time, easy to get, handle and transfect. Therefore, HeLa cells have been widely used as an experimental model for studying diverse cellular processes, including cell cycle regulation, cancer biology, drug screening, gene expression, and viral replication (Rahbari et al., 2009; Scherer et al., 1953; Wikipedia). Consequently, considering the challenges associated with low transfection efficiency and growth rate in SH-SY5Y cells, we transitioned to the HeLa cell line to establish a Crispr protocol. Subsequently, we employed this protocol to generate stable SH-SY5Y knock-in cell lines expressing Miro1 and Miro2.

### **3.11 Objectives of the Study**

As discussed previously, maintaining proper mitochondrial dynamics is crucial for cellular health and survival especially for neurons. It has been shown that mitochondria are different in terms of not only shape and morphology but also their motility behavior. However, the molecular mechanisms underlying such a diversity in mitochondrial motility and how it is correlated with pathology of neurodegenerative disorders are not

fully understood. Miro proteins have emerged as key regulators of mitochondrial movement, but the functional implications of differential expression of Miro1 and Miro2 in various cell types remain unclear. Additionally, the influence of this heterogeneity on mitochondrial motility and its impact on the protein and lipid composition within individual mitochondrion and cells have yet to be elucidated.

In my project, we aimed to investigate endogenous Miro1 and Miro2 proteins with respect to their localization and distribution on mitochondria, it's effect on mitochondrial motility parameters, their interaction patterns with each other, and their associations with protein complexes such as the motor-adaptor complex protein. Additionally, we sought to understand the differences in the lipidome and proteome profiles of mitochondria containing these isoforms to gain a better understanding of their functional distinctions and how they impact mitochondrial trafficking.

The objectives can be categorized into three parts: those that have already been achieved, those that have been initiated but require further optimization, and those that have not been addressed yet.

- 1- To establish stable cell lines expressing endogenous Miro1 and Miro2 fusion proteins as an experimental model for my experiment. To achieve this, we employed Crispr Cas9 technology to fuse affinity and fluorescent tags to the N-termini of the corresponding endogenous Miro1 and Miro2 genes. We successfully established three stable cell lines: Flag-GFP-Miro1 knock-in stable SH-SY5Y, MYC-mRFP-Miro2 knock-in stable HeLa, and the double Flag-GFP-Miro1/MYC-mRFP-Miro2 knock-in stable HeLa cell line, referred to as Miro DK1.
- 2- To investigate the localization and distribution patterns of Flag-GFP-Miro1 and MYC-mRFP-Miro2 proteins across different mitochondrial populations. We aimed to determine whether Flag-GFP-Miro1 and MYC-mRFP-Miro2 proteins are evenly distributed among all mitochondria or if specific mitochondria selectively expressed either Flag-GFP-Miro1 and MYC-mRFP-Miro2 proteins. Immunocytochemistry staining against Flag-GFP-Miro1 or MYC-mRFP-Miro2 revealed variability in the colocalization of each protein with mitochondrial markers, although further repetitions are needed for a conclusive analysis. Additionally, co-staining Flag-GFP-Miro1 and MYC-mRFP-Miro2 proteins with mitochondrial markers has to be done as it allows us to compare the localization and distribution of Miro fusion proteins on mitochondria.

- 3- To figure out whether Miro fusion proteins interact with distinct protein complexes or share common binding partners within the same complex as heterodimers. To address this, we employed a Co-immunoprecipitation (CoIP) protocol to pull down Flag-GFP-Miro1 or MYC-mRFP-Miro2 and examine their interactions with each other and with motor-adaptor complex proteins such as TRAK1/2, Kinesin, and MYO19. Despite trying various IP conditions, we did not detect co-precipitation of Flag-GFP-Miro1 and MYC-mRFP-Miro2 proteins with the potential binding partner together. In addition to CoIP, we explored Miro1-Miro2 interaction using a Proximity Labeling Assay (PLA), which preliminarily indicated that Miro1 and Miro2 are located on the same mitochondria, in a distance of less than 40 nanometers, but are not directly interacting with each other. Given the substantial evidence indicating the importance of Miro proteins, especially Miro1, in mitochondrial movement by anchoring motor-adaptor complex proteins to mitochondria, we plan to optimize the IP protocol by exploring different detergents and crosslinking methods to preserve interactions. This will enable us to pull down Miro proteins and their interactors and submit the samples for mass spectrometry analysis, providing insights into their endogenous interaction partners, which has not been done before. The outcome of this experiment would discover the potential variations in the interaction patterns of Flag-GFP-Miro1 and MYC-mRFP-Miro2 proteins and how these patterns correlate with their functional differences.
- 4- To assess how the presence or absence of Miro1 and Miro2 on mitochondria affects mitochondrial motility and trafficking parameters. This goal necessitated live imaging; however, due to the weak fluorescent signals from Flag-GFP-Miro1 and MYC-mRFP-Miro2, we were unable to successfully attain this objective. To examine whether mitochondria containing Miro1 or Miro2 exhibit distinct proteome and lipidome profiles, and if these profiles differ from each other. This objective remains as a part of our future plans and to it mitochondria containing each Miro isoform need to be isolated and sent for lipidomics and proteomics analysis. Establishing an efficient mitochondrial isolation protocol is the first step in achieving this goal.
- 5- Additionally, I intend to work on imaging protocols, particularly expansion microscopy, to capture higher resolution images for studying Miro1 and Miro2 localization and distribution patterns on mitochondria. Repeating the PLA

experiment with more biological replicates to generate publishable data is also on my agenda.

- 6- Finally, I plan to acquire the necessary skills to accurately quantify the acquired images and statistical analysis.

## **4 Material and method**

### **4.1 Cell culturing and maintenance**

SH-SY5Y cell line (DSMZ, ACC 209, P6) kindly provided by Dr. Kirsten Wissel, Hannover Medical School, Germany, P6 and HeLa- CCL-2 cell line purchased from ATTC. SH-SY5Y and HeLa cells were cultured in RPMI media (#A10491-01, Thermo Fisher Scientific, Waltham, MA, USA) and RPMI media (# R8758, Sigma-Aldrich, Steinheim, Germany) enriched with 10% FBS and 1% PenStrep respectively. The cells were cultured in 10 cm culture dish and kept in culture incubator in controlled condition at 37°C and in 5% CO<sub>2</sub>. HeLa cells were subcultured two or three times per week and SH-SY5Y once or twice a week depending on the splitting ratio. For splitting cells were washed by RT (23-25°C) warm PBS, subsequently detached by a treatment with 1 mL 1% trypsin/EDTA (#L11-003, PAA, Pasching, Austria) in PBS either at 37°C for 1 minute or at RT for 3 minutes. Afterwards the trypsin was deactivated and reaction was stopped by adding pre-warmed full culture media to the dish. Splitting ratio was between 1:3 or 1:4 depending on how often you want to split the cells. Cells were growing in 10 cm culture dish with maximum volume of 10 mL of full culture media.

### **4.2 GuidRNA (gRNA) design and cloning**

In Mammals Miro1 and Miro2 are encoded by RHOT1 and RHOT2 genes respectively. It is important to highlight that during our work at the genomic level, we designated the product using gene names, while at the protein level, we adopted the nomenclature Miro1 and Miro2 for naming the respective products. In order to make a Crispr knock-in stable cell line, the first step was to design a gRNA that targets the first exon of RHOT1 and RHOT2 genes close to the start codon where we were interested in inserting our tags. Therefore, we designed gRNAs on the website benchling.com that bind to the first exon of each gene at a minimum distance from the editing site. For each gene two gRNAs were selected based on the off-target score ranging between 0 to 100, Higher is better (Table 4-1).

Gene	gRNA sequence	PAM site	Off-target score	Distance to editing site(bp)	Size(bp)
RHOT1-gRNA1	Forward: <b>CACCG</b> ACTCACGTTCTCCCACCAGC Reverse: <b>AAACG</b> CTGGTGGGAGAACGTGAGTC	AGG	67.4	22	20
RHOT1-gRNA2	Forward: <b>CACCG</b> CCGACATGAAGAAAGACGTG Reverse: <b>AAACG</b> CACGTCTTTCTTCATGTCGGC	CGG	23	9	20
RHOT2-gRNA1	Forward: <b>CACCG</b> CCGGGCGGCAGCTATGAGGC Reverse: <b>AAACG</b> CCTCATAGCTGCCGCCCGGC	GGG	75.3	1	20
RHOT2-gRNA2	Forward: <b>CACCG</b> GGCTCCGGGCGGCAGCTATG Reverse: <b>AAAC</b> CATAGCTGCCGCCCGGAGCCC	AGG	77.2	0	20

**Table 4-1 gRNA list designed for Knock-in experiment with a recognition site for BbsI restriction enzyme highlighted in red.**

The gRNAs were cloned into a PX459 vector (Addgene plasmid #62988; <http://n2t.net/addgene:62988>; RRID: Addgene\_62988) (Figure 4-1). In addition to the cloning site for gRNA, the vector has expression cassette for Cas9 as well as puromycin as selection marker for subsequent selection of transfected cells.

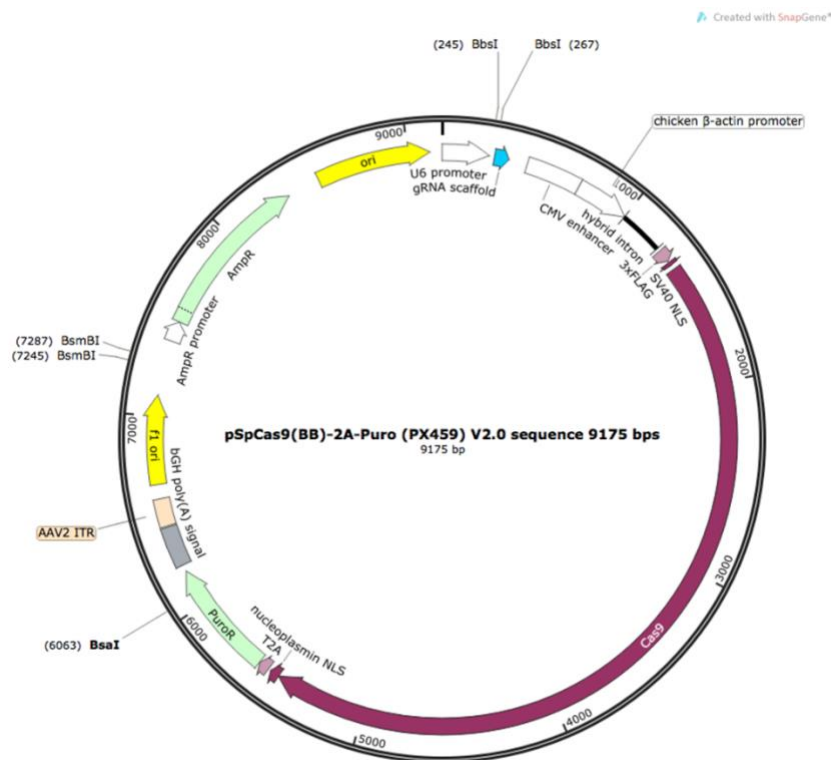


**Figure 4-1 Vector maps of Addgene PX459 backbone**

The vector contains the sequence for Cas9 (purple), Puromycin (light green) as a selection marker, U6 promoter (blue), which indicates the gRNA insert position as well as several enzymes cut sites (Picture is reproduced from Addgene.com).

The vector cloning protocol was provided by Dr. Yanbo Mao from the University of Bremen, Germany. The following steps were followed:

1. Linearization of Vectors: The vectors were digested with BbsI enzyme in a 1.5 mL reaction tube. The digested samples were then purified using the Plasmid EasyPure kit from Macherey-Nagel (#740727.5, Macherey-Nagel, Düren, Germany). The final elution was performed with 70°C ddH<sub>2</sub>O, and the digested vector samples were stored at -20°C.
2. Annealing of gRNA Oligonucleotides: The sense and antisense gRNA oligonucleotides were mixed in equal concentrations and heated at 95°C for 5 minutes. Afterward, they were incubated at room temperature (RT) for 1 hour.
3. Ligation: The annealed gRNAs were added to a T4-ligation mix in a PCR reaction tube and incubated overnight at RT in a dark place. Previously frozen components were thawed on ice and vortexed before use.
4. Transformation: The ligated constructs were transformed into chemically competent *E. coli* (#K4575J10, Thermo Fisher Scientific, Waltham, MA, USA) using a heat shock method. The transformed *E. coli* was plated on an LB agar plate (#4508.2, Carl Roth, Karlsruhe, Germany) supplemented with ampicillin and sealed with parafilm. The plate was incubated upside down overnight at 37°C to allow colony growth.
5. Colony PCR: Ten colonies were selected for colony PCR to confirm the success of the transformation. The PCR products were analyzed by electrophoresis in a 1.5% agarose gel. Five positive colonies and a negative control were inoculated in LB media (#X964.4, Carl Roth, Karlsruhe, Germany) with ampicillin for incubation on a shaker overnight at 37°C.
6. Plasmid Isolation: The plasmids from the selected colonies were isolated using the Plasmid EasyPure kit (#740727.5, Macherey-Nagel, Düren, Germany). The final elution was performed with 70°C ddH<sub>2</sub>O.
7. Sequencing: To confirm the successful generation of the CRISPR/Cas9 knock-in constructs, two samples per construct were sent for sequencing to LGC genomics. The sequencing results were analyzed using the CLC Sequence Viewer 8 software.



GGAGATTCCCTTATCACTGCCAGGCAGGTGCTGGAATAAGCAGACTGACCAATAGGGATTGCGTGAACCCGGCTCCCGGGGAAGCTGGGGG  
 AGGGGTGCAGAATACTCGACTTGTGGCAAGGTCAGGTTTCTGCATTTTTTGGCACTCGCAGTCTTCACTCTCTATGTATTGACATTA  
 GATATGAGTAGTGGAAAGGGCCGATCCTTTTAGCAGTACTTGTACTTTGCATTGGACTAACTCCTCGTACTCGAGATATTTTCATCAAAAATT  
 TTTACTCAACTCGAGTTATGCAAGCGCTCAATGAATTAGAATTATCTGGGGAGGGTCCAATTGTTGTTACCCTAAAGCGTAATCTTTGCC

**RHOT2HDR:**

Left homology arm: 800 base pairs sequence shown in dark purple.

Insert sequence: MYC and mRFP tags shown in orange and red respectively. PAM sit mutation shown in yellow highlighted red letters and glycine linkers shown in yellow small letters.

Right homology arm: 800 base pairs sequence shown in dark purple.

CCCTGGCCACCTGCACCGTCTACCCACAGAGTGCATGCTGAGGCTGGTAGACTGTGCCATGGGGACTGCCCAAGACTTTGCCGGCCACG  
 ACAACGCAGTGCACCTGTGCAGGTTTACACCGTCCGCCAGGCTGCTTTACCGCCGCCCGCAACGAGATCCTTGTGTTGGAGGTCCCGG  
 GCCTCTGAGATGCAGCAGGGACTGTGGTGGTGGGCATCACGCTGGTATGCCAGGCACCTGGACACAGGCTTGGCAGAGGCGCCAGGT  
 GTCATGGCCTCATGCTGGGACAGGCCAGGATTACGTAATCGCTGGAGCAAGCTGTTGTAATTTGGCGCCCTGTGAATACTTTCATAC  
 CTGTTGCCCTTTTGCCTAAGAAATCTTTAATGTTTCTATCTTGAATAAACATGGGCATTTATTGCATTATTGCTGCATTGTTGCACTGGCTGTC  
 TCTGGTCACTCCTGGCTGAGCTCAGCCTCTGCCCGTCCCTAATCGGCTGTTTGTCAAGGCCCTGTGGTGCCGTGAAGCAATGGCCGCT  
 CGGCCTGCCAGGGCGCCAGACCCTGCGCTGTCCGCCGTGGCCGGCGCGTCCACACGGTGGCGCGCCGACAGCCTGTCCGCTCTGGCCC  
 GCCCGCTCGCTGGTGGCGCTGTGCGGGCGGGGCCGGAAGTGTGGGACAGCGCGGGGCCGAGAACCAGGAAAGTGGCGGGCGGGCGCG  
 GGGGACAGAGCAAAAGCTTGGAGACAGGTGCGGGCGGGTTCGGGTGCGGGAGCGGCTCCGGGCGGCAGCTATGGAACAAAAGTTGA  
 TTTCTGAAGAAGATTGGAAACAAAAGCTAATCTCCGAGGAAGACTTGAACAAAAAATTAATCTCAGAAGAAGACTTGGgGCCTCTCCGAGGA  
 CGTCATCAAGGAGTTTCATGCGCTTCAAGGTGCGCATGGAGGGCTCCGTGAACGGCCACGAGTTTCGAGATCGAGGGCCAGGGCCGAGGGCC  
 GCCCTACGAGGGCACCCAGACCGCCAAGCTGAAGGTGACCAAGGGCGGCCCTGCCCTTCGCTGGGACATCCTGTCCCTCAGTTCC  
 AGTACGGCTCCAAGGCTACGTGAAGCACCCCGCGACATCCCGACTACTTGAAGCTGTCTTCCCGAGGGCTTCAAGTGGGAGCGCGT  
 GATGAACCTCGAGGACGGCGCGTGGTACCGTGACCCAGGACTCCTCCCTGACAGGACGGCGAGTTTCATCTACAAGTGAAGCTGCGCGG  
 CACCAACTTCCCTCCGACGGCCCGTAAATGCAAGAAGACCATGGGCTGGGAGGCCTCCACCGAGCGGATGTACCCGAGGACGGCGC  
 CCTGAAGGGCGAGATCAAGATGAGGCTGAAGCTGAAGGACGGCGCCACTACGACGCGGAGGTCAAGACCACCTACATGGCCAAGAAGCC  
 CGTGACGCTGCCCGCGCCTACAAGACCGACATCAAGCTGGACATCACCTCCACAACGAGGACTACACCATCGTGGAAACAGTACGAGCGC  
 GCCGAGGGCCGCCACTCCACCGGGCGCGggtggcAGACGA GACGTGCGCATCCTGTTACTGGGCGAGGGTAGGGCGCGGCCCGGGGTCTC  
 GGAGCTGCGGGCGCGGTGAGGCGGGGTGAGGGTCTCGGGGGTGGGGGGCGCGGTGACCTTGGCCCTCGCGCTGACCGCCTCGCCCCG  
 CGACGCCAGGTGGGGAAGACGTCCCTGATCCTGTCCCTGGTGGCGAGGAGTTCCCGAGGAGGTAAAGGGCACGCCCGCCCGCGGGG  
 GTGGAGCGGGCCAGCCGGGGTCCCTGGTGGCGCGGGTCCCTTGACAGTCCCTCCCGCGCGGAGGAGATCACCATCCCCGCG  
 GACGTACCCCGGAGAAGGTGCCACCCACATCGTGGACTACTCAGGTAGCGGGCGTAGCCTCCCGGGGGCCCGGCCCGCAGCGGTCCG  
 GCGGGCTGCTGGGTCCGCAAGTGGAGTCTTTTGTCCCTTAGAAGCCGAGCAGACGAGCAGGAGAGCTGCGGGAGGAGATCCACAAGGTA  
 CCCGTGGTGCAGGGACGAGGGAGGGGCTGGCGCGGGCTCGGCCTAATCCGCTTCGACGCTGGGGGATTGGACCGAGGTGCTCCGG  
 GTGCTTGGCCCTGATAATTCTGTGACCTCCGCACTGAGGGTGTGCGGGGCCCTACAGCGCACCCCGCIGgAGCCGGCACCCGCTCAGT  
 CCAGTGGTCTCCAGGGATAACAGGACCCCTCCCGCGGGCTCTCCCTCCCTCTGCCGGGTGGCAGCAGCGTTTGTCTTCTCTGTGGG  
 CTCTGTGCGCCACGTCCCGTGTGTGTG

RHOT1HDR and RHOT2HDR were synthesized and cloned by Invitrogen, a subsidiary of Thermo Fisher Scientific, into the pMA-RQ and pMS vectors containing Ampicillin and spectinomycin/streptomycin resistance markers respectively (Figure 4-2).

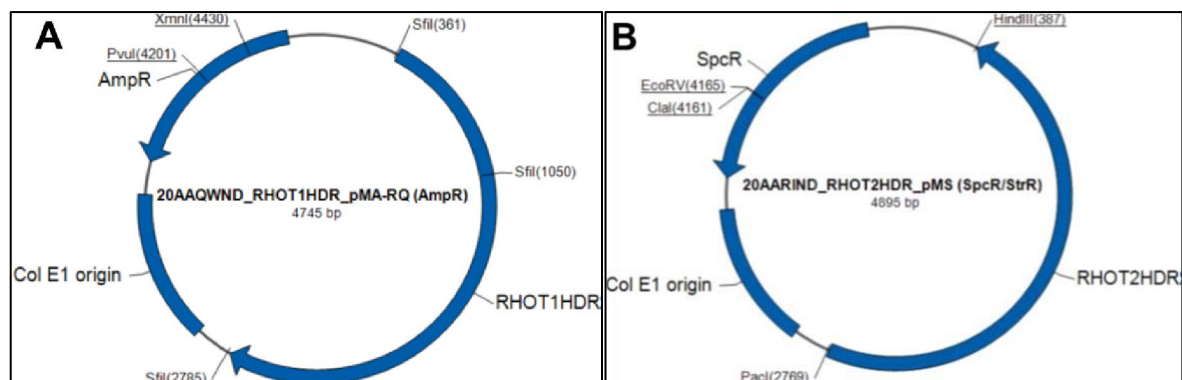


Figure 4-2 Vector map of RHOT1HDR (A) and RHOT2HDR (B) provided by Invitrogen (Picture is reproduced from Invitrogen.com).

#### **4.4 Co-transfection, puromycin selection and single colony expansion**

For co-transfection, cells were seeded in 3 cm<sup>2</sup> culture dishes (SH-SY5Y: 900.000/HeLa: 200.000 cells seeded on day one for transfection). Cells with 60% to 80% confluency were co-transfected, using the JetPrime transfection agent (#101000027, Polyplus, Illkirch – France) according to the company instruction. To co-transfection the cells 1 µg plasmid (0.5 µg of each gRNA/Cas9 and HDR plasmid) was diluted into 200 µl jetPRIME® buffer and mixed by vortexing for 15 seconds. For each gene, both of the designed gRNAs were individually used in separate experimental conditions along with the HDR plasmid to assess the combination of the HDR plasmid with which specific gRNA gives a higher the recombination efficiency. Afterwards, 2µl of jetPRIME® reagent added to plasmid and transfection buffer cocktail and mixed by vortexing for 15 seconds (DNA to jetPRIME® ratio was 1:2). Next, the co-transfection cocktail was spined down and incubated for 10 min at RT. In meantime old culture media were replaced with fresh medium. After the incubation time over, the co-transfection cocktail added dropwise onto the cells in serum containing medium, and distribute evenly by rocking the plates back and forth and from side to side. Cells were kept in culture incubator in controlled condition at 37°C and in 5% CO<sub>2</sub>. Five hours after transfection, transfection medium was replaced with fresh full culture medium in order to remove the transfection cocktail. 48 hours after co-transfection, Puromycin (1 µg/mL) selection was started by another media change. Puromycin selection was stopped after 48 hours by changing to full culture medium. After giving the cells two days more to recover from puromycin selection and to promote cell growth, we adapted two different approaches. The first approach included trypsinizing and counting the cells, followed by plating them into 96-well plates at a low density of 100 cells per plate. For each experimental condition, a total of ten 96-well plates were plated. Three to six weeks after single seeding of the HeLa and SH-SY5Y cells respectively, the single colonies displaying positive eGFP/mRFP fluorescence were selected and transferred to bigger culture dishes to expand the colonies in order to gain enough amount of material for PCR genotyping, which was necessary for the knock-in validation. The second approach which we named it enrichment phase, to increase the chances of identifying real positive knock-in cells. Two days after stopping puromycin selection, we trypsinized and counted the cells. This time, instead of single cell seeding, we seeded 2000 cells per plate. Once the cells were confluent enough,

two replicas out of them were made, one replica served as a reservoir and the other used for DNA isolation and PCR genotyping. Cells from the wells exhibited a positive band in the PCR results, were trypsinized and seeded at a density of 100 cells per well. Once more, after creating replicas of the plate and obtaining sufficient material for DNA isolation, another PCR analysis was done. Following this, we prepared ten 96-well plates, each containing 100 cells per plate derived from the well that displayed a positive PCR result. This approach aimed to increase the chances of obtaining positive colonies for further analysis and experimentation.

#### **4.5 Knock-in validation- PCR genotyping**

##### **4.5.1 DNA isolation**

For final Knock-in validation at the genomic and DNA sequencing, DNA from expanded single colonies was isolated with the DNeasy Blood & Tissue Kit (#69504, Qiagen Düsseldorf, Germany) according to the manufacturer's protocol: 80% confluent cells were harvested, centrifuged (400 g, 5 min, RT) and the supernatant was aspirated. The cell pellet was resuspended in Resuspend in 200 µl PBS plus 20 µl proteinase K. Thereafter, 200 µl Buffer AL (lysis buffer) was added and sample were incubated at 56°C for 10 min. After adding 200 µl Absolut ethanol, samples were added to a silica column, bound to the column, washed twice and eluted in a small volume ddh<sub>2</sub>o water. Finally, DNA concentration was measured photometrically (ND1000, Thermo Fisher Scientific, Waltham, MA, USA) and the DNA samples kept at -20 °C for long-term storage. For genomic validation in the enrichment phase, DNA was isolated with the QuickExtract™ DNA Extraction Solution (#M0492S, NEB, Frankfurt am Main, Germany) according to the manufacturer's protocol. After removing the culture media, 20 µL of extraction solution added to each well of 96 well plate. Next, the cells were scraped using pipet tips and transferred into PCR tubes. Thereafter, the samples were faced to different heat incubation started with incubation at 65°C for 15 minutes, followed by 68°C for 15 minutes and 98°C for 10 minutes. At the end, the DNA was stored at -80°C for long-term storage. No DNA concentration measurement was done due to the low volume of samples.

##### **4.5.2 Primer design and standard PCR**

For each gene, different sets of primers were designed using the NCBI website (<https://www.ncbi.nlm.nih.gov/tools/primer-blast/index.cgi>) and ordered from Sigma-Aldrich (Steinheim, Germany) (Table 2). The forward and reverse primers of left primer

sets bound outside the left homology arm inside the insert respectively. Whereas, the right set's forward primer binding inside the insert and a reverse primer binding outside the right homology arm. The reverse primer of the left set and the forward primer of the right set had overlapping regions to have a complete sequence coverage. The forward and reverse primers second primer set bound somewhere inside the insert and outside right homology arms. Using each of these primers set, PCR products will be observed as bands only if the insert has successfully integrated into the genome, since one pair of primers targets the insert region. Additionally, as we encountered challenges in amplifying the RHOT2 left and right regions, we had to designed two more additional pair of primers. The forward and reverse primers of RHOT2- third primer set were designed to bind within the left homology arm and outside the right homology arm, respectively. With the utilization of this primer set, we obtained a band that differed in size by the insert size (771 bp), indicating the presence or absence of the inserts. Initially, the RHOT2-forth primer set was designed as a nested primer set capable of amplifying a smaller PCR fragment from the PCR product generated by the RHOT2-left primer set. However, later on, due to challenges in amplifying the left region of the RHOT2 sequence, its forward primer was used in combination with the reverse primer of the left primer for PCR genotyping, named hereafter combination primer. It has to be noticed that, placing the either forward primer or the reverse primer each set outside the homology arms was necessary to avoid primer binding to the HDR plasmid, thereby getting false positive results.

Primer pair	Sequence	KI Size (bp)	WT size (bp)
RHOT1-left primer	Forward: ATCGAGTGCCACCTCCGTGTC Reverse: GCTCGATGCGGTTCAACAGGG	1324 bp	-
RHOT1-right primer	Forward: CAGCCGCTACCCCGACCAT Reverse: GAAGTCCCCGCTGTTGCGTCCT	1486 bp	-
RHOT2-left primer	Forward: CCGACCAGCATCATGCCAGTG Reverse: TAGGCCTTGGAGCCGTAAGG	1178 bp	-
RHOT2-right primer	Forward: TCCGAGGACGTCATCAAGGAGTTCA Reverse: CGCAGTGAGGGGTGCCAACA	1686 bp	-
RHOT1- second primer	Forward: ATATCATGGCCGACAAGCAGA Reverse: AATGTATGAAATTTCTGGGTGGGG	1175 bp	-
RHOT2- second primer	Forward: GAGGACGGCGCCCTGAAG Reverse: GACAGAGTGACAGGACCGCA	1174 bp	-
RHOT2- third primer	Forward: GGGCAGAGCGAAAGGCTTGAG Reverse: GAGGGCTCACCTTCTCAATGGTGG	2257 bp	1489 bp
RHOT2- forth primer	Forward: GGAGCCCTCTGAGTGCTG Reverse: GTTCACGGAGCCCTCCATG	988 bp	-
RHOT2- combination primer	Forward: GGAGCCCTCTGAGTGCTG Reverse: TAGGCCTTGGAGCCGTAAGG	1134 bp	-

**Table 4-2 List of PCR primers used for knock-in validation.**

For PCR genotyping of potential Miro1 knock-in cells, the RHOT1 right primer set was used in combination with Q5® High-Fidelity 2X Master Mix (#M0492S, Neb, Ipswich, MA, USA), while the left primer set was used with My Taq HS polymerase (#BIO-21111-BL, Biocat, Heidelberg, Germany). Likewise, for PCR genotyping of potential Miro2 knock-in cells, the RHOT2 right and left primer set was used along with My Taq HS polymerase (#BIO-21111-BL, Biocat, Heidelberg, Germany). Thereafter, all PCR products were electrophoresed in a 1% agarose gel supplemented with SERVA HiSense Stain G (#39805.01, Serva, Heidelberg, Germany) and visualized under UV light. The expected sizes of PCR products can be found in Table 4-2.

### 4.5.3 Sequencing

A pair of primers was designed for sequencing, specifically targeting the left and right homology arms regions. By using this primer set, it was possible to amplify the (WT) sequence with a size difference with KI size which was equal to the size of the inserts (Table 4-3). Once the PCR product was confirmed to have the correct size, the samples were submitted to LGC genomics for sequencing. In order to obtain sufficient DNA for sequencing, five PCR reactions were conducted for each knock-in (KI) clone. After extracting the bands from the agarose gel, the gel pieces were combined in a 1.5 mL reaction tube. The DNA was then isolated using the Nucleospin Gel and PCR Clean-Up kit (#740609.25, Macherey-Nagel, Düren, Germany).

Primer pair	Sequence	KI size(bp)	WT size(bp)
RHOT1- sequencing	Forward: GGGAGCGCTGTTCCGGCGCAG Reverse: GGGATGAGGTCCGGCGGTTAGGG	1456 bp	667 bp
RHOT2- sequencing	Forward: GCCAGGGCGCCAGACCCTGCG Reverse: GCGACGTCTTCCCCACCTGGGCTG	1188bp	417 bp

**Table 4-3 List of PCR primer used for sequencing.**

### 4.5.4 Knock-in validation- Western Blot analysis

In order to confirm knock-in at the protein level, western blot analyses were conducted on the sample that exhibited a positive PCR genotyping result. About one third of the cells from a confluent 10 cm dish were used for protein extraction. The cells were lysed using RIPA lysis buffer, supplemented with protease and phosphatase inhibitors (1:100 dilution) (Pierce, Rockford, IL, USA). The protein concentrations were determined using the BCA protein assay (Pierce, Rockford, IL, USA). Based on the measured concentrations, an equal amount of protein was loaded from each sample onto a discontinuous polyacrylamide gel (NuPAGE 4–12% Bis-Tris gel, Invitrogen).

The proteins were then separated by size and transferred to a PVDF membrane. The membrane was subsequently incubated overnight at 4°C with the primary antibodies after blocking the membrane with 2.5% BSA 2.5% milk in TBS-T at RT for one hour. To confirm the expression of tagged Miro1 protein, mouse anti-Miro1 antibody from Sigma-Aldrich (#WH0055288M1) and Rabbit anti-GFP antibody from Cell Signalling Technology (#2956) were used. The molecular weight of the endogenous Miro1 protein and the tagged version is approximately 70 kilodaltons and 120 kilodaltons, respectively. For confirmation of tagged Miro2 protein expression, mouse anti-Miro2 antibody from Neuromab (#N384/63) and mouse anti-Myc antibody from Cell Signaling Technology (#2276) were employed. The molecular weight of the endogenous Miro2 protein is 80 kilodaltons and the tagged version is approximately 120 kilodaltons. Rabbit anti-GAPDH antibody from Cell Signalling (#2118) was used as a loading control. All primary antibodies were diluted at a ratio of 1:1000. The following day, horseradish-peroxidase-linked secondary antibodies (anti-mouse at 1:3000 dilution, #115-035-003, or anti-rabbit at 1:10000 dilution, #111-035-003, both from Jackson Immuno Research, PA, USA) were added. Finally, the chemiluminescence signal was analysed using DocITLS image acquisition 6.6a (UVP BioImaging Systems, Upland, CA, USA).

#### **4.6 Immunocytochemistry (ICC)**

Due to the faint fluorescent signal of tagged Miro1 and Miro2 in live cells, the immunocytochemistry (ICC) method was employed to enhance the signals. The ICC protocol used was generously provided by Prof. Thomas L. Schwarz's lab at Boston Children's Hospital, Harvard Medical School. Briefly, Cells were seeded in glass bottom dishes (#D35-20-1.5-N, Cellvis, Mountain View, CA, USA) day before starting ICC protocol, placed on a hot plate set at 37°C, and fixed with 4% PFA for 5 minutes at RT. This was followed by three washes, each lasting 5 minutes. Subsequently, the cells were permeabilized using 0.5% Triton X-100 in PBS for 15 minutes. After blocking the cells with 5% BSA in PBS for one-hour, primary antibody incubation was performed overnight at 4°C using the same antibody as used for the western blot analysis. Following three washes with PBS for 5 minutes, secondary antibody incubation was carried out using anti-Rabbit FITC and anti-Mouse Cy3 secondary antibodies (1:700 dilution) for anti-GFP and anti-Myc, respectively. The cells were mounted using 20 µL of a hardening mounting medium, and the samples were stored

in a refrigerator until they were ready for image analysis. All the steps were done at room temperature, unless specifically mentioned otherwise. Pictures of the ICC-stained cells were captured using the Zeiss confocal laser scanning microscope 880 (CLSM880) with Argon laser 488 for GFP/FITC and laser 568 for MYC/Cy3, were used.

#### **4.7 Co-Immunoprecipitation (CoIP)**

Coimmunoprecipitation (CoIP) is the famous technique widely used to study protein–protein interactions. CoIP protocol starts with protein isolation, antibodies attachment to beads, protein complexes isolation, and protein complexes evaluation using Immunoblot analysis (western blot) or mass spectrometry analysis (Figure 4-3) (Lee, 2007). To preserve interaction between Miro proteins and their binding partner before sending samples for Mass spectrometry analysis we have applied two different protocol, ChromoTek and Ismael's protocol apart using different beads to pull down the fusion proteins. The main difference of these two protocols were the type of detergent and concentration of detergent (Table 4-4). Chromotek GFP (#gtma, Proteintech, USA) or MYC (#yta, Proteintech, USA) Trap Magnetic Agarose beads were utilized for affinity purification of Flag-GFP-Miro1 and Myc-mRFP-Miro2, along with their respective interactors, following the manufacturer's protocol. For each CoIP, three 10 cm dishes were used. When the cell confluence reached to at least 80%, cells were chilled on ice, washed twice with ice-cold PBS, and then scraped and collected in 1.5 mL of ice-cold PBS supplemented with protease and phosphatase inhibitors (1:100 dilution) from Pierce, Rockford, IL, USA. After five minutes centrifugation at 1000 rpm, the cell pellets were resuspended in 150 µL of ChromoTek or Ismael's protocol lysis buffer (Table 4-4) containing protease and phosphatase inhibitors (1:100 dilution) from Pierce, Rockford, IL, USA, followed by incubation on ice for 30 minutes. During the incubation, the samples were pipetted up and down three times to improve the efficiency of isolation. Subsequently, the samples were centrifuged at high speed for 10 minutes, and the supernatant was collected as the protein sample for the next step. Protein concentration was measured using the BCA protein assay (Pierce, Rockford, IL, USA) and equal amounts of protein samples, minimum 400 µg, from Knock-in and WT cells were taken and incubated with either GFP or MYC magnetic agarose beads, rotating end over end overnight at 4 °C. The following day, the samples were washed three time with a low salt (150 mM NaCl) and

one time with a high salt (500 mM NaCl) wash buffer to remove nonspecific interactions. Afterward, the beads were eluted in 2X SDS buffer and subjected to a heat incubation at 95 °C for 10 minutes. The supernatant containing the eluted proteins was separated from the beads using a magnetic stand. Subsequently, the samples were run on a discontinuous polyacrylamide gel (NuPAGE 4–12% Bis-Tris gel, Invitrogen), transferred to PVDF membrane and blotted with specific primary antibodies to confirm the success of the CoIP and assess whether the CoIP effectively pulled down the Miro interacting partners with the main protein. To blot Miro1 and Miro2, primary and secondary antibodies used were the same as those employed for Knock-in validation. In addition, antibodies such as mouse anti-TRAK2 from NeuroMab (# N390/43), rabbit anti-TRAK1 from Sigma (#HPA005853), and rabbit anti-Myo19 from Abcam (#ab174286) were used at a dilution of 1:1000. These antibodies were employed to determine the effectiveness of pulling down the known interacting partners of Miro1 and Miro2.

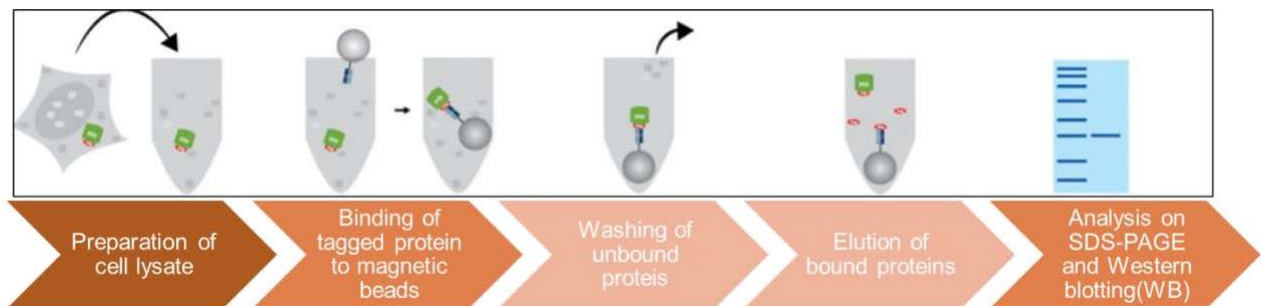


**Figure 4-3 Schematic illustration of Co-immunoprecipitation protocol (Picture is reproduced from <https://www.ptglab.com/>)**

	Chemical	Lysis Buffer		Wash Buffer	
		Ismaeel	Chromotek	Ismaeel	Chromotek
1	Tris-HCl	10mM pH7.4	10mM pH 7.5	10mM pH 7.5	10mM pH 7.5
2	NaCl	150 mM	150 mM	500 mM	150 mM
3	EDTA	5mM	5mM	1 mM	0.5 mM
4	MgCl <sub>2</sub>	1.5mM	-	1 mM	-
5	Triton	1%	-	1%	-
6	glycerol	10%	-	-	-
7	NaF	1mM	-	-	-
8	Protease Inhibitor	0.5%	-	-	-
9	Nonidet™ P40	-	0.5%	0.5%	0.05%
10	sodium azide	-	0.09%	-	0.018%
11	EGTA	-	-	0.5 mM	-

**Table 4-4 Comparative component of Lysis and washing buffers in ChromoTek and Ismael's protocol.**

#### **4.8 Formaldehyde cross linking**

Whole-cell cross-linking, coupled with mass spectrometry, stands as one of the few techniques capable of investigating weak or transient protein-protein interactions within intact cells. Formaldehyde, a small molecule with the ability to rapidly permeate all cellular compartments generates protein-protein cross-links, serves as a commonly employed reversible crosslinking agent in intact cells. It is used to maintain protein-protein interactions before immunoprecipitation and subsequent mass spectrometry analysis (Nowak et al., 2005; Tayri-Wilk et al., 2020; Vasilescu et al., 2004). We employed a cross-linking protocol provided by Postdoctoral Fellow Dr. Sindhuja Gowrisankaran from the Thomas Schwarz lab before Immunoprecipitation. Our objective was to preserve the interaction between Flag-GFP-Miro1 or MYC-mRFP-Miro2 with the motor-adaptor complex protein since these interactions are transient and weak, potentially susceptible to loss during the immunoprecipitation process. The protocol was carried out as follows:

- 1- Cell culture dishes were placed on ice and washed with wash with 1mL cold 1XPBS
- 2- 1X PBS was removed and 1 mL crosslink-quench solution (0.1% (v/v) formaldehyde in PBS) was added and dishes were kept for one minute on ice.
- 3- Crosslink-quench solution was replaced with 1 mL fresh crosslink-quench solution and cell dishes agitated gently for 9 minutes at room temperature
- 4- Crosslinking reaction was stopped by addition of 125mM glycine (1.2 M stock, in PBS) for 5 min at room temperature with a gentle agitation.
- 5- Cells were washed twice with 1 mL PBS
- 6- Cells were harvested in 1.5 mL ice cold PBS supplemented with protease and phosphatase inhibitor (1:100)
- 7- Experiment was continued using Immunoprecipitation protocol

#### **4.9 Duolink® Proximity Ligation assay (PLA)**

The proximity ligation assay (PLA) is a convenient method for detecting proteins and protein-protein interaction in situ in cells or tissues as long as suitable antibodies are available. In situ PLA offers an advanced method to detect protein interactions. The method depends on the recognition of target molecules in close proximity (<40 nm) by pairs of affinity probes, giving rise to an amplifiable detection signal with high sensitivity

and specificity. Being a sensitive method for detection and quantification, PLA can be considered as a complementary method for immunofluorescence analysis through reducing the unspecific staining and background that may be might be problematic while application of traditional immunofluorescence protocols (Hegazy et al., 2020). In PLA method, cells are stained against the two proteins of interest using two primary antibodies which are raised in two different species such as mouse/rabbit, rabbit/goat, or mouse/goat and are compatible with immunohistochemistry- or immunofluorescence method. Afterwards, cells are stained with PLA probes secondary antibodies (2°-Ab) (one PLUS and one MINUS). The PLA probes have a specific DNA strand and if the proteins of interest interact with each other they hybridize and form a circular DNA. The DNA will be amplified and illustrated through fluorescently-labeled complementary oligonucleotide probes (Figure 4-4) (Alam, 2018; Hegazy et al., 2020; Weibrecht et al., 2010; Zieba et al., 2010). Considering our aim to investigate the concurrent interactions of Miro1 and Miro2, as well as their associations with other proteins, such as motor-adaptor complex proteins, in order to determine whether they participate in distinct protein complexes or have shared interactions, purchasing PLA alongside mass spectrometry analysis would be a compelling approach for visualizing these interactions.

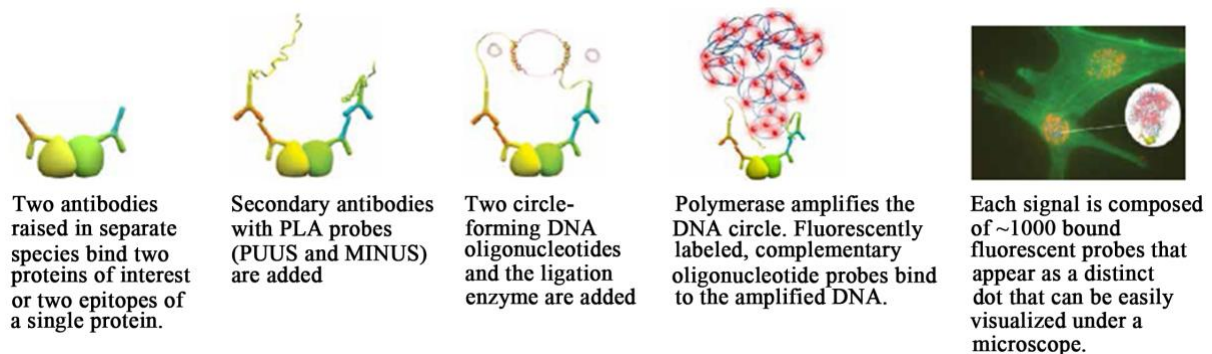


**Figure 4-4 Schematic detailing the procedure of Duolink® Proximity Ligation Assay (Picture is reproduced from [www.sigmaaldrich.com](http://www.sigmaaldrich.com)) .**

In this thesis, the *in-situ* PLA was performed by Duolink (DUO92101-1KT, Sigma-Aldrich) based on manufacturer protocol. 15000-30000 Cells were seeded in glass bottom 96 well plates. When cells were grown enough, ICC protocol applied to fix and permeabilize the cells as follows,

1. Fixation: 4% PFA for 5 minutes at 37 ° C.
2. permeabilization: 0.5% Triton X-100 for 15 minutes at RT.
3. Afterward this step, PLA protocol applied as described here:

4. Blocking: 40  $\mu$ l of Duolink Blocking Solution to each 1cm<sup>2</sup> sample. Incubate the samples in a heated humidity chamber for 60 minutes at 37 °C.

**Note:** Due to lack of humidity chamber availability, I filled the empty wells with water to humidify the samples in all the steps needed in all the steps.

5. Primary Antibody Incubation: Samples were incubated with either Rabbit anti-GFP CS antibody (1:400) and Mouse anti-MYC (1:700) or Rabbit anti-GFP CS antibody (1:400) and mouse anti-Flag (1:100), as a positive control, overnight at 4 °C.

6. Duolink PLA Probe Incubation: Samples were washed with 1x Wash Buffer A two times for 5 minutes and incubated with 40  $\mu$ l diluted (1:5) Rabbit-PLUS and mouse-MKNUS PLA probes were in an incubator for 1 hour at 37 °C.

7. ligation: Samples were washed with 1x Wash Buffer A two times for 5 minutes and incubated with ligation solution containing 39  $\mu$ l 1x Duolink ligation buffer supplemented with 1  $\mu$ l ligase and incubated in incubator for 30 minutes at 37 °C.

8. Amplification: Samples were washed with 1x Wash Buffer A two times for 5 minutes and incubated with amplification solution containing 39.5  $\mu$ l 1x Duolink amplification buffer supplemented with 0.5  $\mu$ l Polymerase in the incubator for 100 minutes at 37 °C.

9. final wash: Samples were washed with 1x Wash Buffer B for 10 minutes in at room temperature following by one time wash with 0.01x Wash Buffer B for 1 minute.

10. Preparation for imaging: Samples were mounted with a coverslip using a minimal volume of Duolink in-Situ Mounting Medium with DAPI. Samples were kept at -20 °C till image analysis.

#### **4.10 SH-SY5Y differentiation**

As mentioned before, we selected SH-SY5Y cell line for our knock-in experiments due to its ability to be differentiated into neuron-like cells with axons and growth cones. This provides a model system that closely resembles primary neurons but is more convenient to handle (Shiple et al., 2016). Once the SH-SY5Y cells expressing GFP-tagged Miro1 protein were ready, we followed the SH-SY5Y differentiation protocol originally established by Shiple et al. in 2016. This protocol is based on a gradual serum-starvation approach, coupled with the introduction of extracellular matrix proteins and neurotrophic factors (Figure 4-5). The differentiation protocol takes a period of 21 days, starting from the initial cell seeding until the fully differentiated cells are ready for final imaging or biochemical analyses. The protocol was followed as seen

below.

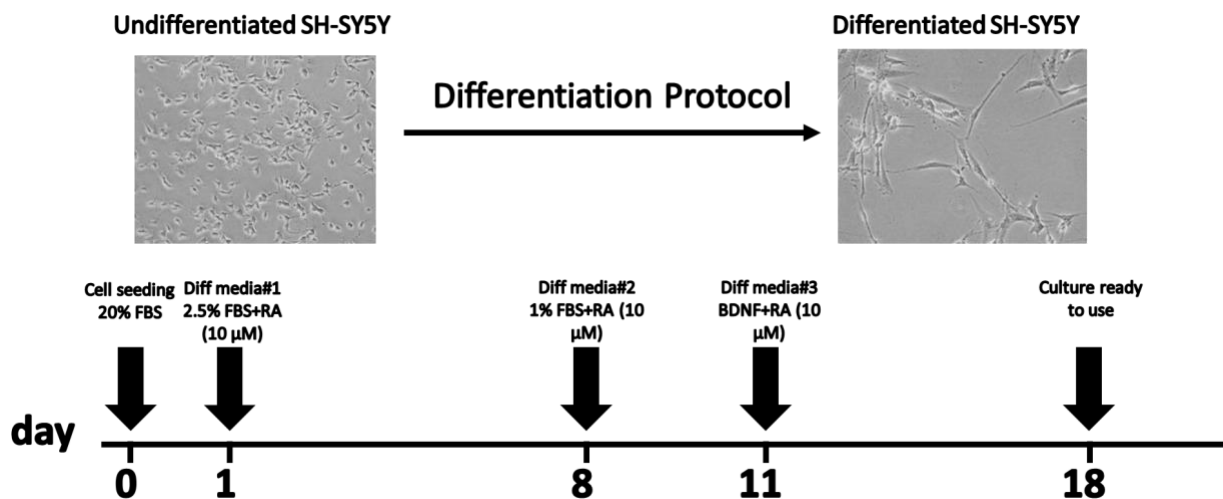


Figure 4-5 illustration of the differentiation process timetable.

which consists of 11 steps spanning a period of 21 days. Initially, between 25,000 and 100,000 cells are seeded onto uncoated 35 mm dishes on first day (day 0) of the differentiation protocol. On days 1, 3, and 5, the old media is replaced with fresh Differentiation Media #1. On day 7, the cells are divided equally onto uncoated 35 mm dishes, and Differentiation Media #1 is utilized. On day 8, the media is switched to Differentiation Media #2, and on day 10, the cells are again divided equally, but this time onto ECM-coated 35 mm dishes in Differentiation Media #2. On days 11, 14, and 17, the old media is replaced with Differentiation Media #3. By day 18, the differentiated neurons are prepared for downstream applications (Picture is reproduced from with slight modification from Lopes et al., 2017; Shipley et al., 2016)

Three days (day 0) prior to treating the cells with the Differentiation media #1, approximately 60,000 GFP-tagged Miro1 knock-in and WT SH-SY5Y cells were seeded into each 3.5 cm well. The cells were fed with RPMI culture media supplemented with 20% heat-inactivated FBS (hiFBS) for Miro1 knock-in cells and 10% hiFBS for WT cells, as well as 1% Pen/Strep. On day one, the media was replaced with Differentiation Media #1, which contained retinoic acid (RA) at a final concentration of 10μM and 2.5% hiFBS. The RA was dissolved in 95% ethanol (5mM stock solution). On day 3 and day 5, fresh Differentiation Media #1 containing RA and 2.5% hiFBS was replaced with the old media. On day 7, the cells were trypsinized for 1 minute and carefully transferred to a new 3.5 cm dish. This step aimed to remove the stronger adherent epithelial-like cells and retain the lightly adherent cells that had already transformed into neuron-like cells. One day after the first splitting (day 8), Differentiation Media #2, supplemented with 10μM RA and 1% hiFBS, was replaced with Differentiation Media #1. The second splitting (1:2) happened on day 10, and the cells were transferred to coated glass bottom 24-well plates. The plates were coated

by incubating them with 200  $\mu$ L of poly-D-lysine (20  $\mu$ g/mL) and 40  $\mu$ L of laminin (3.33  $\mu$ g/mL) in ddH<sub>2</sub>O overnight, covered with aluminum foil, and kept under culture hood. On the following day (day 11), Differentiation Media #3, supplemented with 10 $\mu$ M RA, was used. The media change with Differentiation Media #3 was repeated on day 14 and day 17. Finally, on day 18, the neuronal cultures were ready for use. The basic growth media used for Differentiation Media #1 and #2 was the same as the RPMI media used to seed the cells at the beginning of the protocol.

#### **4.11 Immunocytochemistry (ICC) of differentiated SH-SY5Y**

To validate the successful differentiation of GFP tagged Miro1 SH-SY5Y knock-in cells and WT control SH-SY5Y cells to neurons at the molecular level, the ICC protocol, provided by Thomas Schwarz lab, described earlier was employed, along with specific neuron-specific markers. Here's a summary of the procedure:

1. The differentiated cells were fixed using 4% PFA.
2. The fixed cells were permeabilized using 0.5% Triton X-100 for 15 minutes at RT.
3. A blocking step was performed using 5% BSA for 1 hour at RT.
4. The cells were then incubated overnight at a cold room with the following primary antibodies:
  - Mouse anti-Tubulin J1 (1:1000) from Bio Legend (#801213, CA, USA) - a neuron-specific tubulin marker.
  - Chicken anti-MPAP2 (#NB300-213, Novus Biologicals, CO, USA) - a neuron-specific microtubule binding protein found in perikarya and neuronal dendrites.
  - Rabbit anti-HSP60 (#NBP1-77397SS, Novus Biologicals, CO, USA) - a mitochondrial marker.
  - Chicken anti-GFP (#1010, Aves Labs, CA, USA) and Rabbit anti-GFP (#A-11122, Invitrogen, Waltham, MA, USA) - GFP antibodies against Miro1 protein.

5. On the following day, after washing the cells three times with PBS, the secondary antibodies were applied:
  - Goat anti-Rabbit or anti-Chicken Alexa Fluor™ Plus 488 (#A32790/#A32931) at a dilution of 1:500 for GFP-Miro1.
  - Goat anti-Chicken or anti-Mouse Alexa Fluor™ Plus 568 (#A-11041/#A-11011) at a dilution of 1:500 for MAP2 or TUJ1 neuronal markers.
  - Donkey anti-Rabbit or anti-Rabbit Alexa Fluor™ Plus 647 (#A-31573) at a dilution of 1:500 for HSP60 secondary antibodies.
6. All the secondary antibodies were purchased from Thermo Fisher Scientific.
7. Finally, 10 µL of VECTASHIELD® Antifade Mounting Medium (#H-1000-10, Vector Laboratories, CA, USA) was added, and the cells were covered with a cover glass and stored overnight at 4°C without further washing steps.
8. Pictures of the ICC-stained cells were captured using the Zeiss CLSM700 microscope, employing settings suitable for the three different secondary antibodies.

#### **4.12 Expansion microscopy**

Although conventional light and fluorescent microscopes have been instrumental in uncovering numerous biological insights by optically magnifying of structures in fixed cells and tissues, their resolution is constrained by the laws of diffraction, limiting the clarity of cellular details to a few hundred nanometers. Various strategies have been employed to overcome the limitations of traditional microscopy, such as image processing techniques that generate super-resolved images, optical imaging schemes that surpass the diffraction limit, and sample manipulations that expand the size of the biological sample (Jacquemet et al., 2020). Additionally, the advent of super-resolution microscopy techniques like Stimulated Emission Depletion Microscopy (STED) has enabled the capture of high-resolution images. However, the cost associated with such microscopes makes them inaccessible to many laboratories. To address this limitation, Chen et al. (2015) introduced a cost-effective super-resolution microscopy technique called Expansion Microscopy (ExM). ExM involves physically enlarging a specimen by

embedding it in a swellable polymer, thereby allowing features smaller than the diffraction limit of light (~250 nm) to become distinguishable in the expanded specimen. Remarkably, Chen et al. (2015) demonstrated a lateral resolution of approximately 70 nanometers in expanded cultured cells and brain tissue using a conventional confocal microscope. There are two general protocols for ExM: the first method, known as the "DNA method," involves sample staining with polymer-binding probes, growing an expandable polymer inside the sample that links to the probes, digestion of the sample using protease, and then polymer expansion through dialysis. The polymer-binding probes contains antibodies that are tagged with doubly modified DNA oligonucleotides containing a fluorophore and a methacryloyl group which are designed to be covalently amalgamated into the polymer (F. Chen et al., 2015). The second method, called the "MA/GA method," was established by Chozinski et al. (2016) as a modified version of the first method. In this protocol, standard fluorophore-labeled secondary antibodies, commonly used in immunocytochemistry, are employed instead of expensive custom-designed DNA-labeled antibodies to stain the sample. Methacrylic acid N-hydroxy succinimidyl ester (MA-NHS) or glutaraldehyde (GA) is then used to label the entire sample, which is crucial for linking the specimen to the hydrogel (Chozinski et al., 2016). The subsequent steps involve gelation, protease digestion, and expansion through dialysis into deionized water, similar to the "DNA method" (Figure 4-6).

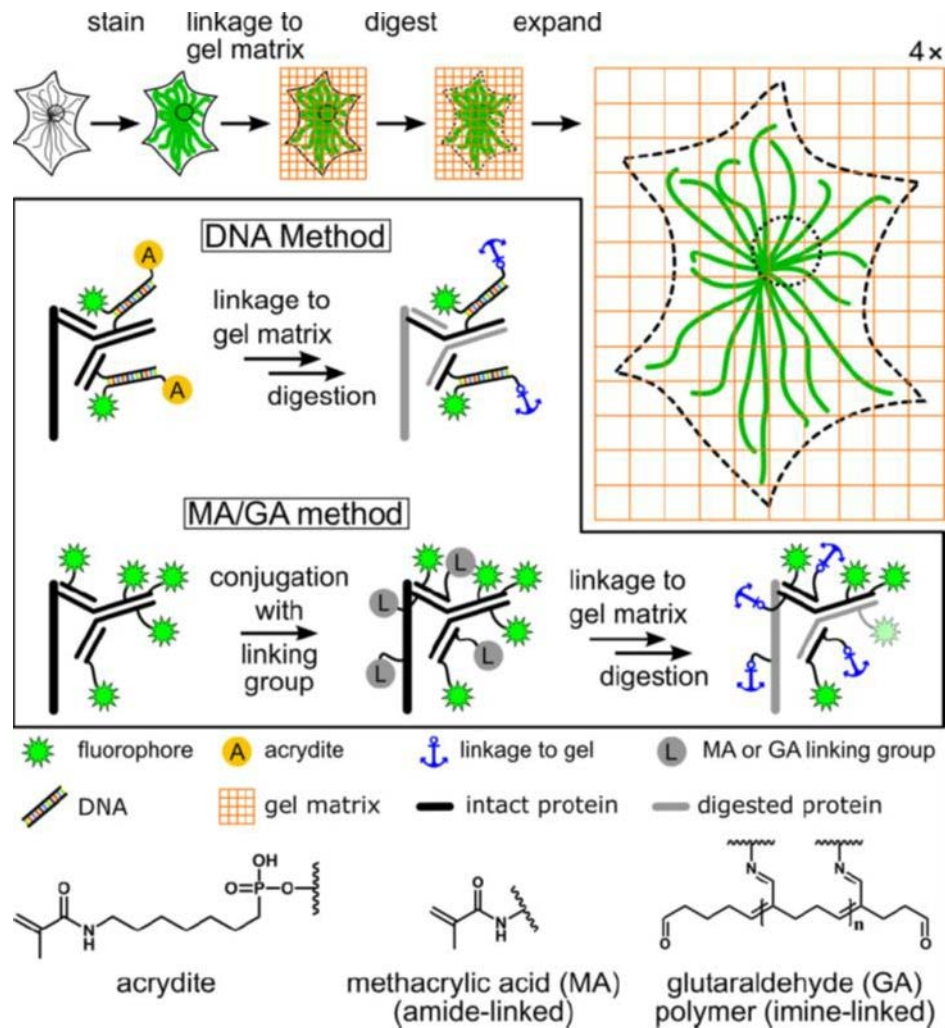


**Figure 4-6 Representative picture of expansion microscopy protocol and comparison between the DNA method and 'MA-NHS/GA' method in this study.**

In the DNA method, the specimen is immunostained using a tailor-made antibody that has doubly modified DNA, and linked to both an acrydite moiety and a fluorophore (A). In opposite, in the MA-NHS/GA methods, methacrylic acid N-hydroxy succinimidyl ester (MA-NHS) or glutaraldehyde (GA) is used in order to mark the whole sample with polymer-linking groups after application of general immunostaining with fluorophore-labeled antibodies (only secondary antibodies are shown). Although fluorescent proteins are also preserved by the MA-NHS/GA methods via the same mechanisms, they are not depicted in this picture for clarity (Picture is reproduced from Chozinski et al., 2016).

Since our objective was to investigate the localization and distribution of Miro1 and Miro2 within individual mitochondria, which was not feasible with an Epi-fluorescent microscope due to the diffraction limit of light, we opted to utilize the ExM method. This enabled us to take advantage of super-resolution imaging to capture detailed images of our knock-in cells. To initiate the expansion microscopy process, after fixing the samples with 4% PFA and performing the ICC protocol described earlier, we followed the expansion microscopy protocol established by Chozinski et al. (2016), as explained in detail below:

1. The cells were treated with 0.25% Glutaraldehyde (GA) (# 50-262-23, Fisher Scientific, MA, USA) diluted in PBS for 10 minutes at RT.
2. After three washes with PBS for five minutes, the samples were immersed in a monomer solution (1× PBS, 2 M NaCl, 2.5% (wt/wt) acrylamide, 0.15% (wt/wt) N,N'-methylenebisacrylamide, and 8.625% (wt/wt) sodium acrylate) for approximately one minute at RT.
3. Following this, 4  $\mu$ L of 10% tetramethylethylenediamine (TEMED) (#1610800, Bio Rad, and 4  $\mu$ L of ammonium persulfate (APS) were added to the monomer solution to create the gelation solution. This step should be done quickly to avoid solidifying the gelation solution before adding it to the samples.
4. Approximately 80  $\mu$ L of the gelation solution was placed on top of each sample, and a cover glass was applied to ensure an even gel surface. The gelation process was done at RT for 30 minutes.
5. The cover glass and gel were carefully removed using tweezers and transferred to a digestion buffer (1× TAE buffer, 0.5% Triton X-100, and 0.8 M guanidine HCl). Freshly added Proteinase K at a concentration of 8 units mL<sup>-1</sup> facilitated digestion, which took place at 37 °C for 45 minutes.
6. Following digestion, the digestion buffer was discarded, and the samples were gently washed three times with ddH<sub>2</sub>O.
7. To induce gel expansion, the samples were transferred to 10 cm dishes and submerged in ddH<sub>2</sub>O. The water was exchanged every 30 minutes until expansion was completed, typically requiring 3-4 exchanges.
8. The expanded samples were then cut to fit into glass bottom dishes using a blade.
9. Finally, 1% low melting agarose was added to each sample to fix samples after thoroughly removing any residual water.

## 5 Result

### 5.1 Utilizing the CRISPR-Cas knock-in technology, we aimed to add epitope and fluorescent tags in N-terminus of endogenous Miro1 and Miro2 proteins

As previously stated, the absence of specific antibodies targeting endogenous Miro1 and Miro2 in the market, coupled with the substantial risk of mis-localization of protein of interest to the locations that is absent in normal physiological condition by overexpression, prompted us using the CRISPR-Cas9 technique to tag the endogenous Miro1 and Miro2 proteins. This approach enables us to investigate Miro1 and 2 localization and functions under conditions that closely resemble their actual physiological environment. Using Crispr Cas9 technology necessitated the utilization of a guide RNA(gRNA) with a homology with the region of interest, Cas9 endonuclease protein to generate a double-stranded break where tags have to be inserted and a homology directed repair (HDR) template vector containing the desired tags and two arms with a homology to the upstream and downstream regions of the insertion site, called right and left homology arms respectively, facilitating specific integration of the tag to the region of interest. For Miro1, our strategy involved the incorporation of 3 repeats of the FLAG affinity alongside eGFP fluorescent tags. In the case of Miro2, 3 repeats of the MYC affinity and mRFP fluorescent tags were selected. Considering the fact that Miro proteins anchors to mitochondria through their C-terminal transmembrane domain, our decision was to situate the tags within the N terminus GTPase domain of Miro1 and Miro2 genes right away after the start codon to have less interference with the anchorage to mitochondria which is necessary for mitochondrial trafficking (Figure 5-1). To maintain the proteins' original folding characteristics, a linker consisting of one or two glycine residues was introduced between the two tags, as well as after the fluorescent tags. A pivotal consideration was the incorporation of the tags in a manner that they are translated under the endogenous Miros' promoter. Consequently, no additional promoters or start codons were introduced upstream of the tags within the HDR template vector. This strategic design aimed to ensure seamless integration and the preservation of the native regulatory context for the tagged proteins.

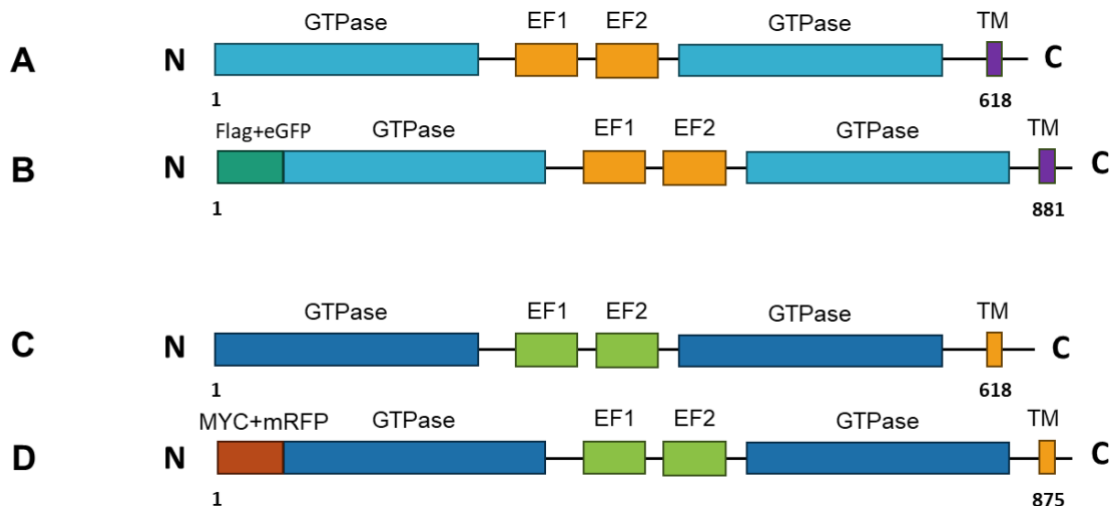


**Figure 5-1 Schematics illustration of the Miro1 and Miro2 proteins domains in wild-type (WT) and knock-in versions.**

Miro1 and Miro2 depict a unique arrangement of domains in their structure. They are characterized by the presence of two GTPase domains, strategically positioned at both the N and C terminus of their respective gene sequences. These GTPase domains are connected by two EF hand domains, positioned in the middle. The anchoring of Miro proteins to the outer mitochondrial membrane is facilitated by a transmembrane domain located at the C-terminus.

Panels **A** and **B** depict the wild-type (WT) and the knock-in versions of Miro1 protein respectively, while WT and Ki version of Miro2 protein represented in **C** and **D** picture respectively. In the knock-in versions, protein tags have been introduced at the onset of the N-terminal GTPase domain. To be specific, Miro1 (**B**) has been furnished with 3X FLAG and eGFP tags, while Miro2 (**D**) incorporates 3X MYC and mRFP tags. Notably, the insertion of these protein tags leads to a greater amino acid content in the knock-in versions of Miro proteins. Although both WT Miro1 and Miro2 protein have 618 amino acids in their sequence, mutant Miro1 and Miro2 consists of 263 and 257 amino acids more respectively due to the incorporation of the tagging elements.

## 5.2 Sanger sequencing confirmed gRNA cloning into CRISPR/ Cas9 vector

To establish a stable cell line with knock-ins for Miro1 and Miro2, we employed the Benchling website to design two distinct gRNA targeting their respective genes RHOT1 and RHOT2 respectively. These gRNAs were subsequently integrated into the PX459 vector plasmids, which featured a site for gRNA insertion and a gene cassette for expressing the Cas9 protein. The final vectors were named RHOT1-gRNA1/2 and RHOT2-gRNA1/2 corresponding the gene's name and gRNA number. Validation of the precise integration of gRNAs into the vectors was conducted through Sanger Sequencing (Figure 5-2).

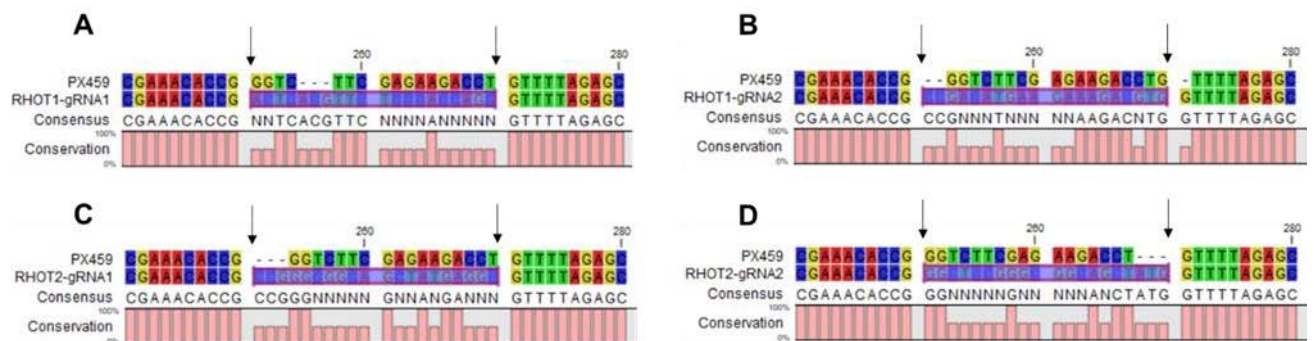


**Figure 5-2** The alignment of the PX459 sequence before and after gRNA cloning reveals a mismatch between BbsI cut sites (↓) where the gRNA has been inserted, confirming the successful cloning of the gRNA.

**A-B:** Alignment of the ligated RHOT1-gRNA1 and RHOT1-gRNA2 PX459 vectors with the PX459 backbone vector. **C-D:** Alignment of the ligated RHOT2-gRNA1 and RHOT2-gRNA2 PX459 vectors with the PX459 backbone vector.

### 3.3. HDR templates were successfully cloned into the vectors.

The RHOT1HDR and RHOT2HDR templates that we designed were successfully synthesized and cloned into pMA-RQ and pMS vectors by Invitrogen. The success of the cloning was confirmed through sequencing, and the vectors were shipped to us as vacuum-dried DNA. We further verified the success of the HDR template cloning by aligning our template sequences with the vector sequences, as shown in Figure 5-3.

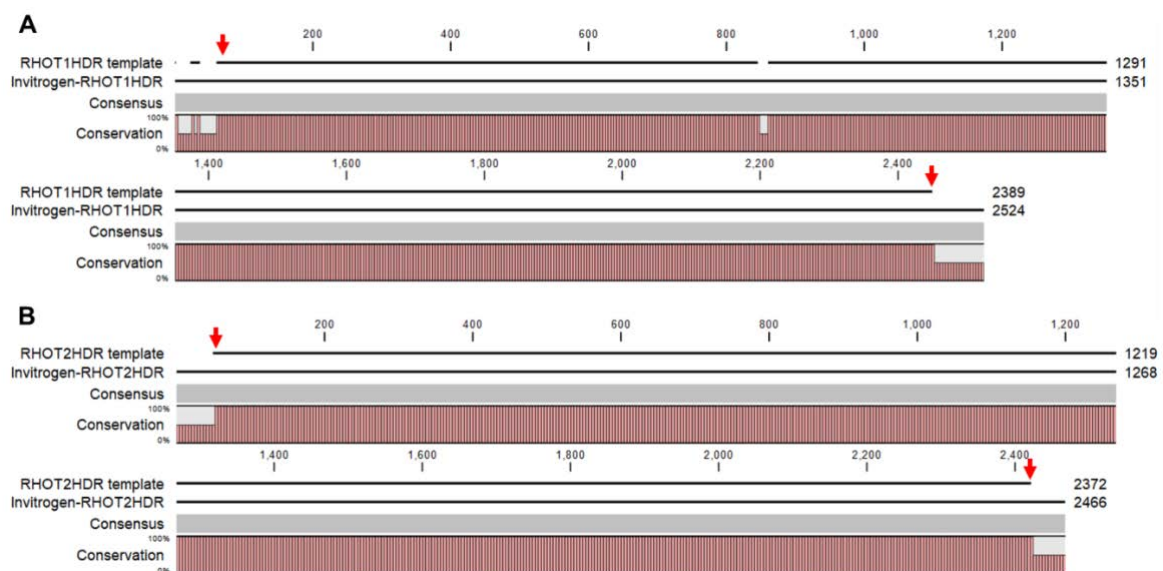


**Figure 5-3** The alignment of HDR templates and Invitrogen HDR vectors confirmed successful ligation of the HDR sequence into the vectors.

The alignment of RHOT1HDR template with Invitrogen RHOT1HDR vector sequences(**A**) and RHOT2HDR template with the Invitrogen RHOT2HDR vector(**B**) confirmed successful integration of the HDR template into the Invitrogen vectors. The start and end points of the HDR template sequences are indicated by red arrows.

**5.3 Screening for recombinant clones. Strategy 1. Screening for fluorescent cells did not succeed in identifying either FLAG-eGFP-Miro1 or MYC-mRFP-Miro2 Knock-in SH-SY5Y cells.**

Because we were introducing a fluorescent tag into each Miro gene, we anticipated that successful knock-in would yield cells with fluorescent mitochondria that we could select for establishing clonal lines from each construct. Even if the transfection and recombination efficiency were low (less than 1%), it would be relatively to identify the desired cells in each plate. When gRNA and HDR template vectors were ready, SH-SY5Y cells were co-transfected with equal amounts of each and presence or absence of fluorescent signal was counted. First the transfection efficiency was calculated by dividing the number of cells showing eGFP/mRFP signals, indicating as successful integration of the tags to the Miro1 and Miro2 gene, with the subsequence to total numbers of cells before and two days after puromycin selection (Figure 5-4).

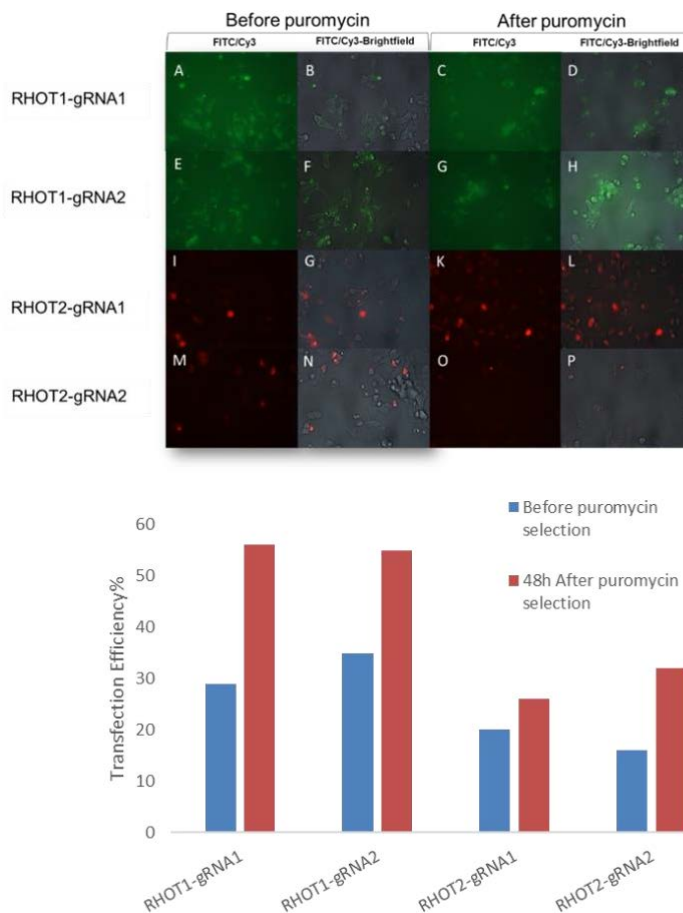


**Figure 5-4** Fluorescent imaging was performed using 60X oil objective lens of Nikon ECLIPSE Ti epi-fluorescent microscope on a mixed population of SH-SY5Y cells with the potential Miro1 and Miro2 Knock-in, both before and after puromycin selections.

**A-H:** Visualization of FLAG-eGFP-Miro1 using FITC channels, along with their merged images with bright field, in SH-SY5Y cells co-transfected with RHOT1gRNA1 or RHOT1gRNA2 and RHOT1HDR before and 48 hours after puromycin selection. **I-P:** illustration of MYC-mRFP-Miro2 using Cy3 channels, along with their merged images with bright field, in SH-SY5Y cells co-transfected with either RHOT2gRNA1 or RHOT2gRNA2 and RHOT2HDR before and 48 hours after puromycin selection, respectively.

Because such a high percentage of cells were fluorescent, we decided to take the cells to the next stage and try to isolate single cell clones. Cells were plated in low density of 100 cells per 96 well plate and 10 plates were made for each condition, total 40 plates. Later on, cells were checked on the microscope and the wells were containing single clones and showing fluorescent signals were selected and expanded as positive potential Knock-in clones. Since SH-SY5Y cells grow very slow and are sensitive to low density culture, most of them were died or did not grow enough to make colony. Therefore, For Miro1 we only found 17 clones and Miro2 10 clones showing fluorescent signal. When clones had expanded adequately, DNA isolation done in order to do PCR genotyping to confirm the knock-in at the genomic level. The genotyping strategy involved primer sets in which one primer was inside the tags to be inserted and the second was outside the HDR in the adjacent region of RHOT1 or RHOT2, so that only successful recombinations that placed the tags in the correct locus would be amplified. This required that one pair of each left and right primer binds to the intronic region which contained high GC content and repetitive sequences. Consequently, obtaining a specific PCR band was difficult and finding suitable primer pairs was challenging. Therefore, we had to design and test numerous primer combinations and different Taq polymerases and PCR conditions. This process spanned approximately six months until a specific desired band was finally achieved and the primer pairs listed in Table 4-2 represent the final set of primers that were successfully employed for all the PCR genotyping unless otherwise mentioned. Unfortunately, this first approach did not succeed, as the selected Miro1 (Figure 5-5) and Miro2 (Figure 5-6) clones exhibiting fluorescent signals tested negative in PCR genotyping and protein expression analysis by Western blot. This outcome could be attributed to two potential reasons. Firstly, since knock-in general transfection efficiency and also recombination efficiency is very low in SH-SY5Y, taking only 1000 cells from the mixed population was not enough to find positive colonies. Furthermore, the fluorescent signal from the tagged proteins was so faint, and what we initially counted as a signal from successful knock-in cells turned out to be primarily

background or autofluorescence indicating that the recombination/transfection efficiency that we calculated and displayed in figure 5-2-B based on these fluorescent signals did not accurately represent the actual efficiency. It should be noted that the primary antibodies used for Immunoblotting analysis against FLAG-eGFP-Miro1 fusion protein were anti-GFP (#2956, Cell signaling Technology), called hereafter anti-GFP CS, and mouse monoclonal anti-Miro1(#WH0055288M1, Sigma Aldrich), called hereafter anti-Miro1 Sigma. Whereas mouse monoclonal anti-Miro2(#N384/63 Neuromab), anti-Miro2 Neuromab and mouse Anti-MYC antibody (#2276, Cell Signaling Technology), called hereafter anti-MYC CS, were used against MYC-mRFP-Miro2 fusion protein. All the primary antibodies used in Western blot analysis at the dilution of 1:1000. The secondary antibodies, peroxidase AffiniPure Goat Anti-Rabbit (#111-035-003) and Peroxidase AffiniPure Goat Anti-Mouse IgG (#115-035-003) from Jackson ImmunoResearch company, were diluted at ratios of 1:10000 and 1:3000, respectively. Additionally, NuPAGE™ 4 to 12% gradient SDS-PAGE gel (#NP0322BOX, Invitrogen) was employed for western blot analysis. These conditions were consistently applied in all the protein studies experiments, unless stated otherwise. It has to be mentioned that the entire procedure, starting from transfection, followed by single cell seeding into multiple 96-well plates, and the subsequent search for single clones showing a positive signal under the microscope, as well as colony expansion and PCR genotyping of the chosen clones, has been done three times and the results presented here belongs to the last attempt using this strategy.

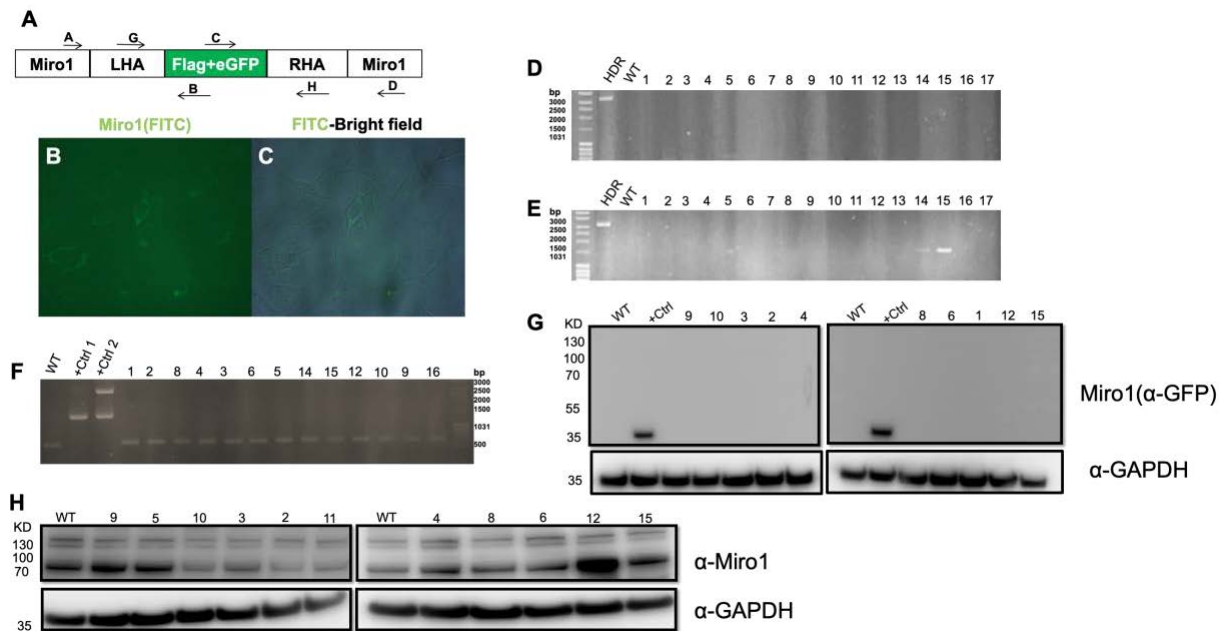


**Figure 5-5** Although some of the selected FLAG-eGFP-Miro1 SH-SY5Y clones exhibited positive fluorescent signals, neither PCR genotyping nor protein expression analysis could confirm the success of the knock-in experiment.

**A:** The diagram provides a visual representation of the binding sites for the forward and reverse primers utilized in this experiment. The forward primers from the left and right primer sets are denoted as **A** and **C**, bind outside the left homology arm (LHA) and inside the insert respectively. Similarly, the reverse primers from these sets are labeled as **B** and **D** binding inside the insert and outside right homology arm (RHA) respectively. The PCR products generated using the left and right primer sets result in sizes of 1324 bp and 1486 bp, respectively. Given that either the forward or reverse primer of each set binds to the insertion region, the PCR product will undergo amplification only if the insert has been successfully integrated, preventing the amplification of any WT bands. Additionally, the forward and reverse primers from the sequencing primer set, indicated by **G** and **H**, bind within the LHA and RHA homology arms, leading to the amplification of a 1456 bp fragment in Knock-in cells or a 667 bp fragment in WT cells.

**B -C:** Live imaging of one of the selected clones. The FITC and bright field channel were used in order to visualize GFP signals and the cells itself respectively. Images captured using 60X oil objective lens on a Nikon ECLIPSE Ti epi-fluorescent microscope.

**D-E:** PCR genotyping of the selected clones, which exhibited positive GFP fluorescent signals. The genotyping done using RHOT1 left and right primer sets (Table 4-2). If successful insertion occurred, the PCR genotyping using the left and right primer pair would result in amplification of PCR products with size of 1324 bp and 1486 bp, respectively. However, as evident from picture **D**, only clone numbers #14 and #15 exhibited bands and these bands were smaller than the expected size, while the PCR product of the same clones amplified by the right primer set did not display any bands(**E**). This outcome made us to think that incomplete insertion could be a possible explanation for these results.

**F:** PCR genotyping of some clones using RHOT1-sequencing primers listed in Table 4-3. In the image, all the clones exhibited the wild-type (WT) band size at 667 bp, while only the positive controls (+ctrl), which was the RHOT1HDR construct obtained from the company (+ctrl 1), and the same vector after retransformation (+ctrl 2) displayed a band at the correct knock-in size, indicating no insertion had taken place. The PCR products were loaded onto a 1% Agarose gel.

**G-H:** depict the SDS-PAGE analysis of selected clones using **G:** rabbit anti-GFP, Cell signaling Technology, #2956, called hereafter anti-GFP CS and **H:** mouse Monoclonal Anti-Miro1, Sigma, #WH0055288M1, respectively. Moreover, anti- GAPDH, Cell Signaling Technology, #2118, used as a loading control. To confirm the functionality of the anti-GFP CS antibody, cytosolic GFP with a molecular weight of approximately 35 KD was overexpressed in WT SH-SY5Y using pcDNA3-EGFP Addgene plasmid, #13031, and equal amount of total protein was loaded as a positive control (+Ctrl) alongside the potential KI clones. The endogenous Miro1 has a molecular weight of 70 KD, whereas the FLAG-eGFP-Miro1 fusion protein has a molecular weight of around 110-120 KD.

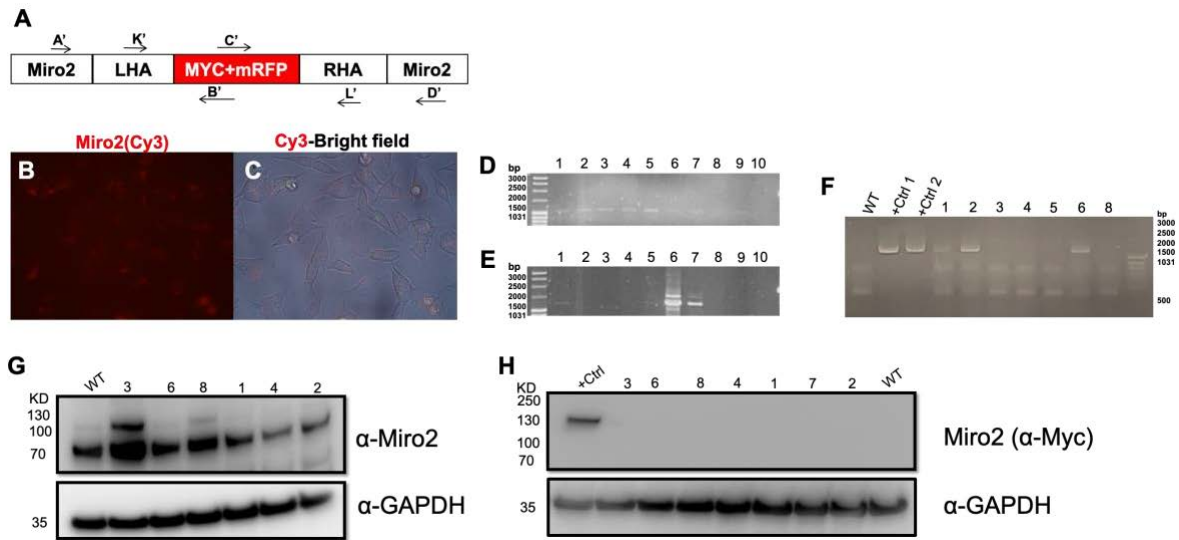


**Figure 5-6** Despite the promising results obtained from live imaging and PCR genotyping of the selected potential Miro2 Knock-in SH-SY5Y clones derived from the first approach, no active expression of the fusion protein was detected through western blotting analysis.

**A:** The picture presents the binding sites of the forward and reverse primers employed in this experiment. The forward primers from the left and right primer sets are indicated as **A'** and **C'**, respectively, with A' binding outside the Left Homology Arm (LHA) and C' binding inside the insert. Correspondingly, the reverse primers from these sets are marked as **B'** and **D'**, with B' binding inside the insert and D' binding outside the Right Homology Arm (RHA). Using left and right primer sets PCR genotyping yielded amplification of PCR products in sizes of 1117 bp and 1686 bp, respectively only if the successful integration of the insert has taken place. Furthermore, the forward and reverse primers from the sequencing primer set, designated as **K'** and **L'**, respectively, bind within the LHA and RHA homology arms. This results in the amplification of a 1188 bp fragment in Knock-in cells or a 417 bp fragment in WT cells.

**B-C:** Live imaging of the selected clones using Cy3 and brightfield channels employing a 60X oil objective lens on a Nikon ECLIPSE Ti epi-fluorescent microscope.

**D- E:** PCR genotyping of the selected clones, which exhibited positive Cy3 fluorescent signals. The genotyping was performed using RHOT2 left (**D**) and right primer (**E**) sets which amplify PCR products with sizes of 1178 bp and 1686 bp, respectively. As in the panel C, most of the selected clones showed a positive band of the correct size, while a few of them displayed a band of smaller than expected size in picture D (~1.2Kb).

**F:** PCR genotyping of selected clones using the RHOT2-sequencing primer set, listed in Table 4-3, and as it is obvious some of the clones exhibited a wild-type (WT) band size (417 bp), while others displayed a band of knock-in size equal to the two positive controls: +ctrl 1 (RHO21HDR vector obtained from Invitrogen) and +ctrl 2 (the same vector after retransformation). The PCR products were loaded onto a 1% Agarose gel.

**G- H:** SDS-PAGE analysis of selected clones using Mouse Monoclonal Anti-Miro2, Neuromab, #N384/63, anti-Miro2 Neuromab (**G**), and Mouse Anti-MYC CS (**H**) antibody from Cell Signaling Technology (#2276), called hereafter anti-MYC CS, respectively. Additionally, Rabbit anti-GAPDH antibody, Cell Signaling, #2118, was used as a loading control. To verify the specificity of the band obtained from the clones using the anti-MYC CS antibody, WT SH-SY5Y cells a MYC-tagged protein (130 KD) was overexpressed using a vector kindly provided by Dr. Kathrin Maedler's lab. An equal amount of total protein was loaded as a positive control (+Ctrl) alongside the potential knock-in clones. The endogenous Miro2 has a molecular weight of 80 KD, while the MYC-Miro2 fusion protein has a molecular weight of around 110-120 KD. Although some of the clones exhibited a band with a larger size compared to endogenous Miro2, the band was smaller than the expected KI molecular weight and

was also faintly present in the WT lane, which should not be the case. Moreover, probing the blot with the anti-MYC CS antibody did not reveal any bands in any lane except in the +Ctrl Lane. Therefore, despite some clones showing positive results in imaging and PCR genotyping, the protein expression analysis failed to confirm the successful expression of MYC-Miro2 knock-in protein, potentially due to incomplete insertion of tags leading to a lack of translation.

#### **5.4 Screening for recombinant clones. Strategy 2. The FLAG-eGFP-Miro1 but not MYC-mRFP-Miro2 Knock-in SH-SY5Y cell was successfully identified by direct PCR screening of clones.**

Given the failure of the first approach, we pursued a second approach, with PCR screening of pools of cells to increase the chance of finding positive knock-in cells in the mixed population. In summary, we performed PCR genotyping on a population of 2000 cells coming from a mixed population after puromycin selection using RHOT1 and RHOT2 second primer sets. For each condition, we had 12 wells, each containing 2000 cells. Among these, three wells exhibited a positive band. Afterwards, the cells from the wells showing positive genotyping results were taken and seeded in 100 cells per well. PCR genotyping of 100 cells per well pool was done using left and right primers set for RHOT1 (Figure 5-7) and RHOT2 (Figure 5-8) candidates respectively. It has to be noted that for each condition, we performed PCR genotyping on approximately 600 wells (equivalent to six 96-well plates) with 100 cells in each well, in order to identify positive cells. The presented agarose gel image represents the

PCR genotyping results exclusively from the plate exhibiting positive bands.

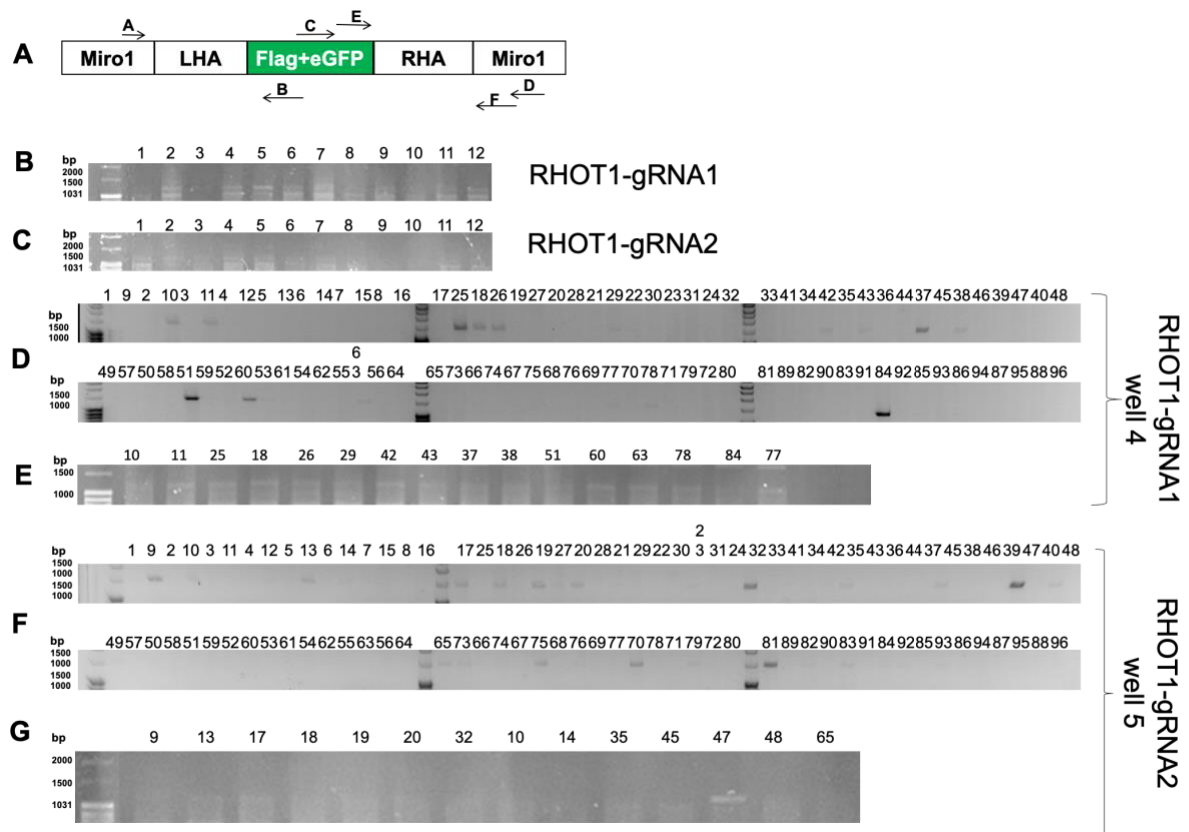


**Figure 5-7 Application of the PCR screen/enrichment approach as a valuable strategy, significantly increased the probability of identifying positive FLAG-eGFP-Miro1 knock-in cells within the mixed population of SH-SY5Y cells.**

**A:** Schematic representation of the binding sites for the forward and reverse primers of the left primer set (**A and B**), right primer set (**C and D**), and second primer set (**E and F**) used for PCR genotyping in this experiment. The left primer set amplifies a PCR product of 1324 bp, while the PCR product amplified by the right primer sets results in a size of 1486 bp. Additionally, the application of the second primer pair leads to the amplification of a 1175 bp PCR product. Amplification of PCR products using all three primer sets is only possible when the tags have been successfully inserted, as the reverse primer of the left primer set and the forward primers of the right and second primer sets bind to the insert region.

**B–C:** depict the PCR genotyping results of 12 wells, each containing 2000 cells derived from cells co-transfected with either RHOT1-gRNA1 or RHOT1-gRNA2 and RHOT1-HDR after puromycin selection. The RHOT1-second primer set was employed, resulting in the amplification of a 1175 bp PCR product of the correct size. Positive results were observed in wells 4, 6, and 10 for the RHOT1-gRNA1 condition (**B**), and wells 2, 3, and 6 for the RHOT1-gRNA2 (**C**) condition. These wells were selected as positive samples for next step of our experiment.

**D–G:** PCR genotyping results of 100 cells/well population derived from the previously selected positive cell population (2000 cells per well). Firstly, using the RHOT1-right primer set (1486 bp), the sequence from the insert to the outside of the right homology arm in all 96 wells was checked, as illustrated in pictures **D** and **F**. Subsequently, the wells displaying positive bands of the correct size were subjected to PCR amplification to test for the presence of the left region using the RHOT1-left primer set (1324 bp), as shown in pictures **E** and **G**. Notably, the analysis of 100 cells per well revealed the presence of positive cells within this smaller population, thereby increasing the likelihood of identifying pure positive cells in the subsequent steps.

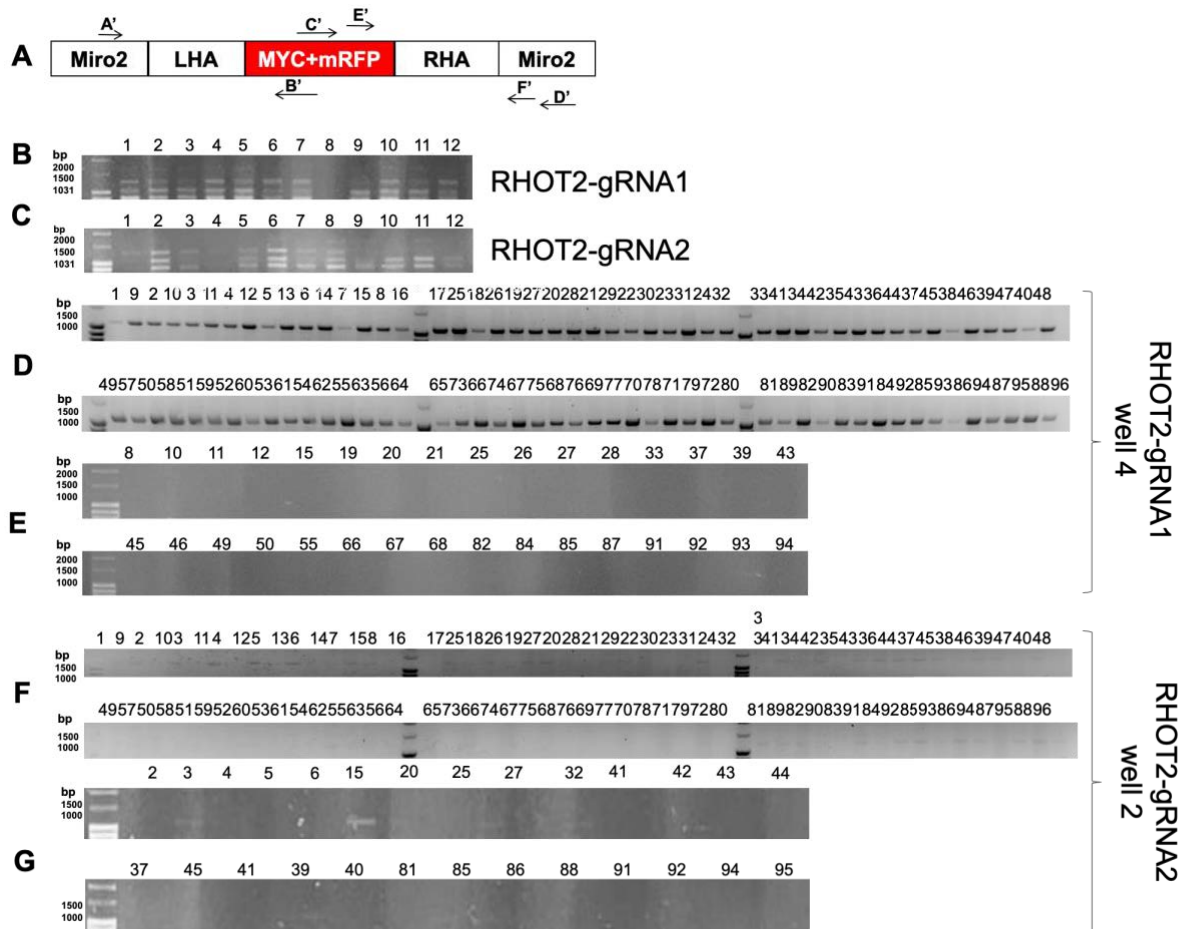


**Figure 5-8** The utilization of the enrichment approach raised the chance of identifying positive MYC-mRFP-Miro2 KI cells within the SH-SY5Y mixed population.

**A:** binding sites illustration of the forward and reverse primers of the left primer set (**A'-B'**), right primer set (**C'-D'**), and second primer set (**E'-F'**) employed for the present PCR genotyping. The left and right primer sets amplify PCR products with sizes of 1117 bp and 1686 bp, respectively. Additionally, the second primer set produces a 1174 bp PCR product. Notably, due to the reverse primer of the left primer set and the forward primers of the right and second primer sets binding to the insert region, successful PCR product amplification using all three primer sets is only achievable when the tags have been correctly inserted, resulting in the absence of a band from the WT DNA sample.

**B –C:** depict the PCR genotyping results of 12 wells, each containing 2000 cells derived from cells co-transfected with either RHOT2-gRNA1 or RHOT2-gRNA2 and RHOT2-HDR after puromycin selection. The RHOT2-second primer set was employed, resulting in the amplification of a 1174 bp PCR product of the correct size (**B**). Positive results were observed in wells 4, 6, and 10 for the RHOT2-gRNA1 condition, and wells 2, 3, and 6 for the RHOT2-gRNA2 condition (**C**). These wells were selected as positive samples for next step of our experiment.

**D-G:** PCR genotyping results of 100 cells population derived from the previously selected positive cell population (2000 cells per well). Firstly, using the RHOT2-right primer set (1686 bp), the sequence from the insert to the outside of the right homology arm in all 96 wells was checked, as illustrated in pictures **D** and **F**. Subsequently, the wells displaying positive bands of the correct size were subjected to PCR amplification to test for the presence of the left region using the RHOT1-left primer set (1178 bp), as shown in pictures **E** and **G**.

Lastly, cells from the wells, 100 cells per well stock, that exhibited a positive PCR result were subjected to trypsinization and subsequently plated in a low-density

manner, with 100 cells per 96-well plate. A total of 10 96-well plates were created for each Miro1 and Miro2 condition. This approach was undertaken to isolate single clones and identify positive pure Knock-in cells. After six weeks of growth, each well was carefully checked under a microscope to identify those containing single clones. Upon adequate growth, the selected single clones were PCR genotyped to identify Knock-in positive clones. In the case of Miro1, we found 140 single clones, and we genotyped them first using RHOT1-sequencing primer set. This set of primers binds to specific regions in the Left and Right homology arms. These primers targeted the genomic region, rather than the inserted sequence, resulting in PCR amplification regardless of integration of the insert. However, a size difference of 789 base pairs existed between the Knock-in clones, which yielded a larger band, and the Wild-Type (WT) clones, which produced a smaller band. Using this primer set, we could identify 19 clones that displayed a positive KI band along with a WT band, suggesting that these clones were either homozygous or a mixture of KI and WT cells. Subsequently, we analyzed the complete insert sequence using primer sets that covered both the left and right ends, allowing for a comprehensive read of the whole insert. The positive clones were later transferred to 10 cm dishes to expand them and collect sufficient material for subsequent analyses, such as western blotting analysis to confirm the active expression of the tagged Miro1 protein. While PCR genotyping using sequencing primers on certain positive clones revealed them to be heterozygous, showing both KI and WT size bands, we couldn't verify this through western blot analysis due to the lack of a suitable anti-Miro1 antibody. However, we managed to confirm the active expression of the FLAG-eGFP-Miro1 protein through western blotting and ICC method in the SH-SY5Y KI positive clones using an anti-GFP CS antibody (Figure 5-9).

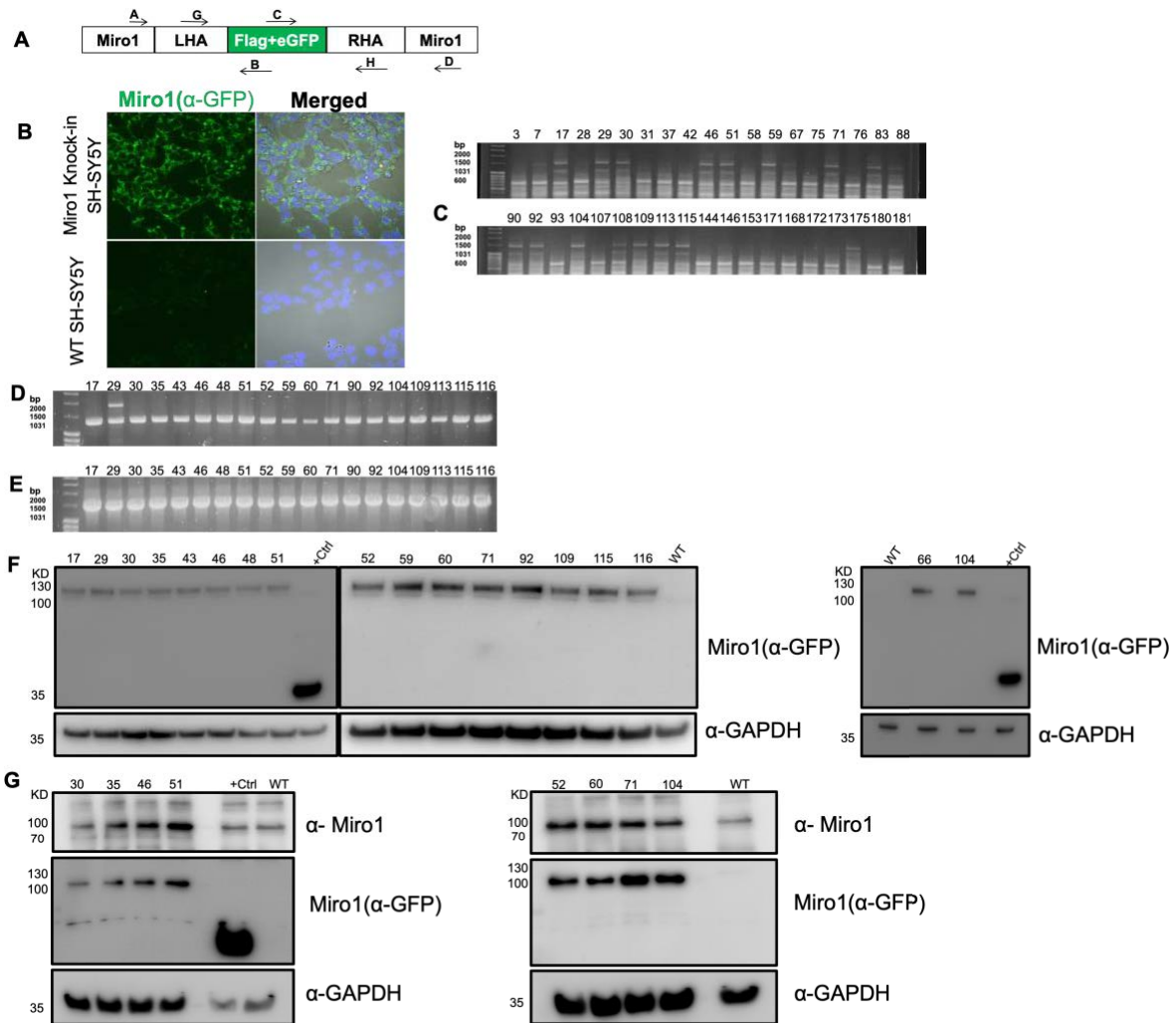


**Figure 5-9** Through comprehensive genomic and proteomic analysis, along with a protein localization study, it was confirmed that the GFP-FLAG tags were successfully inserted at the N-terminus of the endogenous Miro1 protein and actively expressed in the selected pure clones.

**A:** Graphical representation of the binding sites of the forward and reverse primers used for PCR genotyping of the chosen FLAG-eGFP-Miro1 single clones: the binding sites are labeled as follows: Left primer set: Forward primer (A) and Reverse primer (B), Right primer set: Forward primer (C) and Reverse primer (D), Sequencing primer set: Forward primer (G) and Reverse primer (H)

**B:** Immunocytochemistry results of one of the pure clones. The clone was fixed with 4% PFA and stained using anti-GFP CS (1:100) and FITC secondary (1:700) antibodies to visualize FLAG-eGFP-Miro1. Mounting media containing DAPI was used for mounting the samples and also nucleus staining, indicated in blue. Images were captured using FITC, DAPI, and brightfield channels with a 60X oil objective lens on a Nikon ECLIPSE Ti epi-fluorescent microscope. The merged image incorporates the FITC channel and merged pictures of FITC, DAPI channels along with the brightfield channel. The picture clearly demonstrates strong GFP signals exclusively present in the KI sample, confirming its specificity.

**C -E:** PCR genotyping was conducted on the isolated pure selected clones. Initially, we employed the sequencing primer set, where the forward primer (G) binds to the LHA and the reverse primer (H) binds to the RHA. Given the varied growth rates among the 140 chosen single clones, multiple PCR reactions and agarose gel analyses were run and only a snapshot of one PCR reaction featuring some of the clones is presented in image C. This image indicates that some of the clones were heterozygous, as both the WT band (667 bp) and the KI band (1456 bp) were present in the pattern and some like clone number #104 were homozygote based on showing only KI size band. Consequently, 19 clones demonstrating this positive band pattern were identified and subjected to genotyping using the RHOT1

left primer (**D**) and right primer (**E**) sets, which generate PCR products of sizes 1324 bp and 1486 bp, respectively. As depicted in the provided images, all the chosen clones exhibit positive bands of the correct size, affirming the precise integration of the insert within the region of interest.

**F-G:** Two separate SDS-PAGE analysis were conducted on the selected clones using the same anti-GFP CS antibody employed for immunocytochemistry to confirm the insertion of the tag and anti-Miro1 antibody (#WH0055288M, Sigma Aldrich) to assess the homo or heterozygosity of the FLAG-eGFP-Miro1 Knock-in SH-SY5Y clones. The Rabbit anti-GAPDH antibody (Cell Signaling, #2118) was used as a loading control. To verify the specificity of the GFP antibody, a protein sample from Wild-Type (WT) SH-SY5Y cells overexpressed with cytosolic GFP protein was included as a positive control (+Ctrl). It's important to note that the endogenous Miro1 protein carries a molecular weight of 70 KD, while the FLAG-eGFP-Miro1 fusion protein possesses a molecular weight of around 110-120 KD. In Western blot picture **F**, it is evident that all the selected clones actively express the FLAG-eGFP-Miro1 protein. The specificity is affirmed by the absence of a band in the WT lane, and presence of the expected cytosolic GFP band size at around 40 KD in the +Ctrl Lane. Picture **G** illustrates the Western blot result using the anti-Miro1 Sigma and anti-GFP CS antibodies. As previously stated, there's a lack of a suitable antibody against Miro1, and this antibody recognizes various unspecific proteins which makes identifying the endogenous WT Miro1 challenging. While faint band at 70 KD present in some of the KI lanes could be represent WT Miro1, it's difficult to conclude its identity since it's absent in the WT and +Ctrl lanes. Furthermore, the strong bands at 100 KD could correspond to the tagged version of Miro1. Notably, this antibody recognizes an unspecific protein with a molecular weight of 100 KD, which is why it's present in both the +Ctrl and WT lanes, though less strong compared to the KI lane. In conclusion, due to the confusions arising from the Miro1 antibody's recognition of unspecific proteins, we couldn't definitively conclude the homo or heterozygosity of the clones using this anti-Miro1 antibody.

In the context of MYC-mRFP-Miro2 knock-in SH-SY5Y cells, we followed a procedure similar to that used for FLAG-eGFP-Miro1 cells. After six weeks of low-density single-cell seeding (100 cells per 96-well plate), we observed the presence of 96 wells with single clones out of a total of 9600 wells (equivalent to 10 96-well plates) using microscopy. During PCR genotyping, we encountered an issue with the RHOT2-left and right primer sets. We found that the forward primer of the left primer set and the reverse primer of the right primer set could generate a PCR product of the same size as the KI band. Consequently, the positive results we obtained from the enrichment phase using these primer sets turned out to be false positives. Despite this setback, we remained determined to genotype the selected clone, hoping to identify any clones that carried the MYC-mRFP-Miro2 insertion. To proceed, we performed PCR genotyping on the clones using RHOT2-sequencing primers after expanding the colonies and obtaining sufficient cellular material for DNA isolation. This primer set allowed for the amplification of both the WT and KI bands, as the forward and reverse primers targeted the genomic region. Across all the clones, we observed multiple bands in addition to the KI band at approximately 1188bp and the WT band at around 500bp. This suggested that the clones were either heterozygous or comprised a mixture of KI and WT populations. Due to the potential for false positive results caused

by the targeting of the genomic region (LHA and RHA) shared with the HDR template, we decided to verify the accuracy of the positive outcomes by using another primer set, RHOT2-third primer. Notably, the reverse primer of this set binds to a location outside the right homology region. Surprisingly, all the tested clones displayed a negative result for the KI band, with only the WT band (approximately 1500bp) being detected. Furthermore, the western blot analysis conducted on a subset of the chosen clones revealed no positive signals indicating active expression of the MYC-mRFP-Miro2 protein, as detected by the anti-MYC CS antibody. This result served as a confirmation that despite our efforts and several repetition of the entire process—from co-transfection to single clone genotyping—we were unable to achieve the successful generation of MYC-mRFP-Miro2 KI SH-SY5Y cells (Figure 5-10).

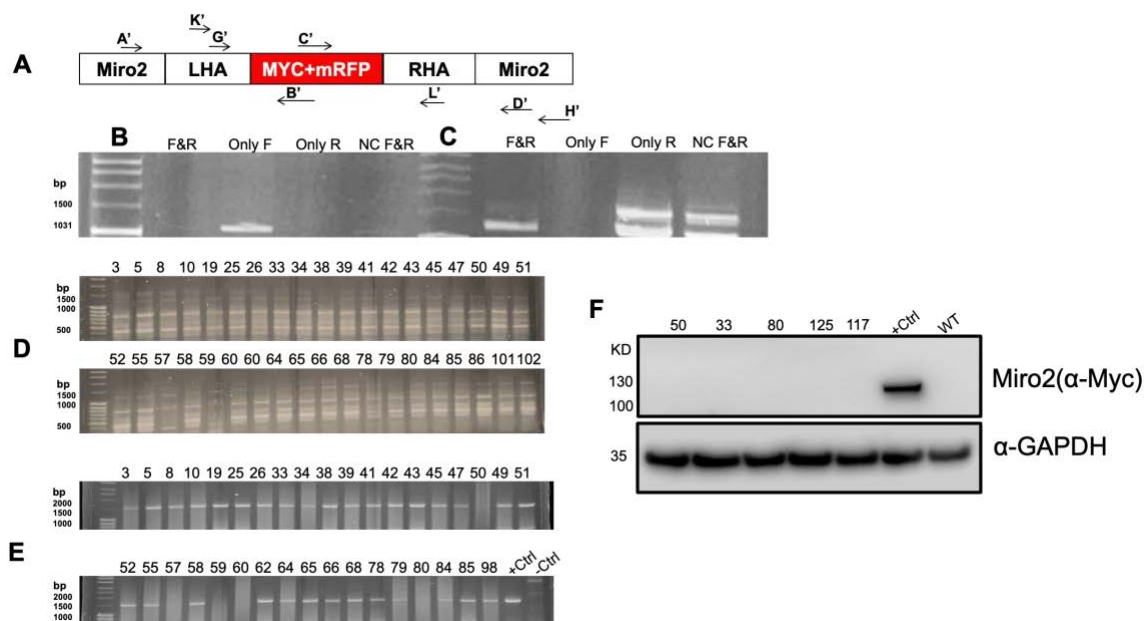


**Figure 5-10** Despite obtaining a positive result during the enrichment phase, neither PCR genotyping nor western blotting of potential pure single clones could confirm the insertion of tags and expression of the MYC-mRFP-Miro2 fusion protein in HeLa cells.

**A:** Graphical representation of primer binding sites used for PCR genotyping of MYC-mRFP-Miro2 potential KI SH-SY5Y clone. Left primer set: Forward primer (A') and Reverse primer (B'), Right primer set: Forward primer (C') and Reverse primer (D'), Third primer set: Forward primer (G') and Reverse primer (H') and Sequencing primer set: Forward primer (K') and Reverse primer (L').

**B-C:** PCR genotyping of a selected clone revealed false positive results, indicating that the forward primer of the left primer set (**B, 1178 bp**) and the reverse primer of the right primer set (**C, 1686 bp**) alone could amplify a band of the same size as the expected knock-in band. This implies that the positive result obtained during the enrichment phase was not accurate and was a false positive result.

**D-E:** PCR genotyping of selected potential MYC-mRFP-Miro2 clones using the sequencing and third primer sets. Although some clones showed a correct knock-in size band amplified by the sequencing primer set (**D**), we could reproduce the result using sequencing primer sets (**E**) since we only got WT size band, around 1.5 Kb. The -Ctrl indicates PCR amplification performed out of the RHOT2HDR vector, while the +Ctrl represents the result of WT SH-SY5 DNA amplification.

**F:** SDS-PAGE analysis of some clones that showed a PCR band using the sequencing primer set. To

verify the authenticity of the positive PCR bands, total protein was isolated, and western blotting was performed using a mouse anti-MYC CS antibody (1:1000) to detect the MYC-mRFP-Miro2 fusion protein with a molecular weight of around 110-120 KD. Rabbit anti-GAPDH antibody (1:1000) from Cell Signaling (#2118) was used as a loading control. Additionally, to confirm the specificity of the band obtained from the clones using the anti-MYC CS antibody, total protein from overexpressed Myc-tagged WT SH-SY5Y cells (130 KD) was included as a control (+Ctrl). To sum up, the blot picture clearly shows no expression of the protein, indicating that the PCR results were false positive.

### **5.5 The combination of using HeLa cells and the second strategy resulted in the successful establishment of stable MYC-mRFP-Miro2 Knock-in cells.**

Due to the difficulties encountered when attempting to create FLAG-eGFP-Miro1 KI SH-SY5Y cells and the lack of success in generating MYC-mRFP-Miro2 KI SH-SY5Y cells, we decided to use HeLa cells as an alternative model to try establishing our KI desired cells. HeLa cells were chosen due to their higher transfection efficiency and faster growth rate, as previously mentioned. Since our efforts to generate MYC-mRFP-Miro1 KI SH-SY5Y cells were unsuccessful, our initial focus shifted to creating MYC-mRFP-Miro2 KI HeLa cells. Building on the successful PCR screening and enrichment strategy used to create FLAG-eGFP-Miro1 KI SH-SY5Y cells, we applied the same approach to generate the desired KI HeLa cells. To create MYC-mRFP-Miro2, we co-transfected wild-type (WT) HeLa cells with either RHOT2-gRNA1 or gRNA2 alongside RHOT2HDR vectors. The enrichment process commenced 48 hours after co-transfection. We set up one 96-well plate with 2000 cells in each well for each condition, including cells co-transfected with gRNA1 or gRNA2, and the HDR template. Once a sufficient number of cells was obtained, we isolated DNA and initiated PCR genotyping. It's worth noting that the use of AmpliTaq Gold™ 360 Master Mix from Thermo Fisher (#4398881), specifically designed for amplifying complex and high GC content genomic regions, enabled us to employ RHOT2-left and right primer sets. These primer sets had previously yielded false positive results since the only forward or reverse primer could make primer dimer and amplify a non-specific PCR product equal size of KI expected product size. With this PCR master mix we only got PCR product amplified when we had KI sample and had both forward and reverse primers in our PCR master mix. For PCR genotyping of the pools containing 2000 cells per well, we utilized the RHOT2-second primer sets. Cells from wells number #86 and #64, which showed positive results, were trypsinized and seeded at 1000 cells per well, totaling 96 wells, for the next round of the enrichment phase. For this phase, we employed a combination primer, where the forward primer was derived from a

nested PCR set and bound outside the left homology arm (LHA), while the reverse primer remained the same as the reverse primer of the left primer set and bound to the insert region. Positive results were obtained from wells number #2, #4, and #5, and we subsequently tested them using RHOT1-right primer sets. Positive wells were further analyzed using right primer sets to obtain a full sequence read. Continuing with the enrichment steps, we seeded 500 cells per well from well 5 that had shown positive results in the previous steps, resulting in a total of 32 wells. When the cells were grown enough, we proceeded with PCR genotyping using the combination primer. Subsequently, the positive cells were subjected to another round of testing using the right primer set. Following this, we plated 100 cells per well from wells 1 and 16, both of which had exhibited positive results in the 500cells per well enrichment steps. This marked the final stage of the enrichment process, and PCR genotyping was conducted using the initial combination primer, followed by testing with the right primer sets. Fortunately, we were able to identify several wells that displayed positive bands with both primer sets. This success significantly increased our chances of identifying single MYC-mRFP-Miro2 Knock-in clones for the next phase (Figure 5-11).

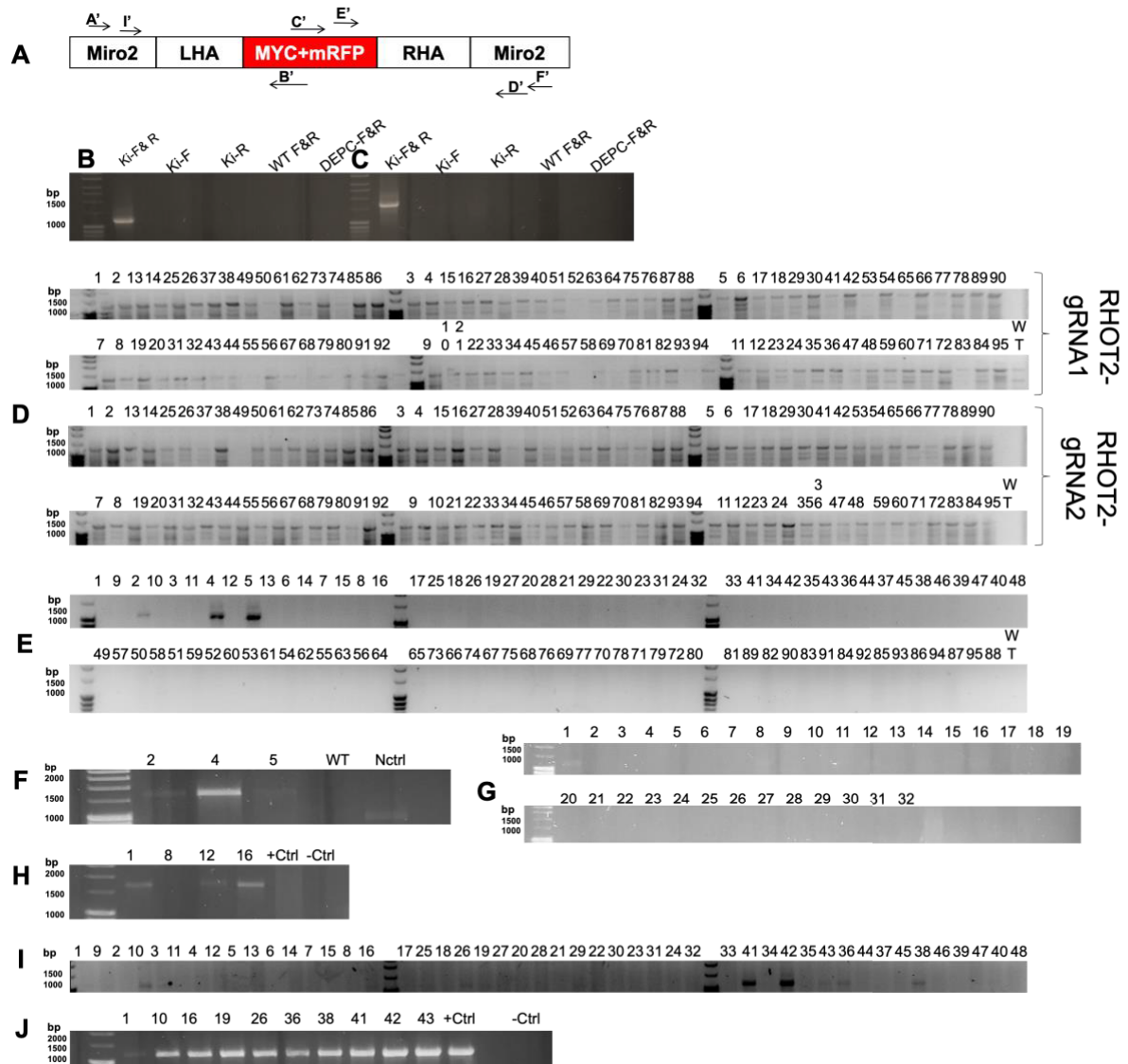


**Figure 5-11 The application of an enrichment approach, coupled with low-density cell seeding, led to the successful finding MYC-mRFP-Miro2 Knock-in HeLa pure clones.**

**A:** Schematic illustration of binding sites of primer sets used for identification of MYC-mRFP-Miro2 potential KI HeLa pools in mixed population. Left primer set: Forward primer (**A'**) and Reverse primer (**B'**), Right primer set: Forward primer (**C'**) and Reverse primer (**D'**), second primer set: Forward primer (**E'**) and Reverse primer (**F'**) and Combination primer set: Forward primer (**I'**) and Reverse primer (**B'**). **B-C:** By utilizing the AmpliTaq Gold™ 360 Master Mix from Thermo Fisher, we were able to achieve specificity in PCR genotyping of the mixed MYC-mRFP-Miro2 population using the Left (**B**) and Right (**C**) primer sets. As evident in the provided images, the distinct bands were exclusively present in the lane where we had the Knock-in DNA sample, along with both the reverse and forward primer pairs. To ensure the reliability of our results, we included negative controls in the experiment. These controls consisted of samples with various configurations, including KI DNA template paired with only the Forward or Reverse primer, Wild Type (WT) DNA template or DEPC water in place of DNA template paired with both the forward and reverse primer pairs.

**D:** PCR genotyping of 2000 cells/well using transfected with RHOT2-GRNA1 or RHOT20gRNA2 using RHOT2-second primer pair. Although in some of the wells showed positive bands, 1174bp, WT well showed the same size band but less strong compare to some of the KI band.

**E-F:** PCR genotyping of left part of the RHOT2 region of 1000 cells/well derived from number #64 positive well in 2000cells/well stage using RHOT2- combination primer set (**E**). Positive wells (2,4 and 5) showing positive band were PCR amplified using RHOT2-right primer set to make sure that whole

insert is present(F).

**G-H:** PCR genotyping of 500 cells/well derived from number #5 positive well in 1000cells/well stage using RHOT2- combination primer set (G). PCR genotyping of the positive wells done using RHOT2-right primer set to check the other side of sequence (H).

**I-J:** PCR genotyping of 100 cells/well derived from number #1 and #16 positives well in 500cells/well stage using RHOT2- combination primer set(I). The wells showing positive band were PCR amplified using RHOT2-right primer set to make sure that whole insert is present(J).

The expected PCR product size using Combination and right primer sets is 1134bp and 1686bp respectively.

To encourage the formation of single colonies Cells from well numbers #42 and #43, taken from a stock of 100 cells per well, underwent trypsinization and were subsequently seeded at a low density of 100 cells per 96-well plate. In total, ten plates were prepared, and after three weeks, the wells were examined under a microscope. This examination revealed the presence of 24 wells containing the desired single clones. Following this, the pure single clones were subjected to PCR genotyping, initially using a combination of primers and subsequently with the right primer sets. The results showed that ten clones exhibited a positive band when both primer sets were used. Notably, when PCR genotyping was performed using sequencing primer sets, all the clones displayed band sizes corresponding to the Knock-in template (around 1188bp) as well as the Wild Type (WT) (approximately 500bp). However, upon conducting SDS-PAGE analysis with an anti-Miro2 Neuromab antibody, it was observed that all clones, except for clone number #7, exhibited a single band at a size consistent with MYC-mRFP-Miro2 KI (around 120KD) size. In the case of clone number #7, both KI and WT sizes were evident, with a band size of 80KD. These results strongly suggest that the majority of the clones were homozygous, signifying the successful insertion of the Knock-in template into both copies of the chromosome. Furthermore, probing the blot using anti-MYC CS antibodies confirmed the active expression of MYC-mRFP-Miro2 protein in the selected positive clones as well. We suspect that the 100 KD band in the anti-MYC CS blot might result from either intracellular cleavage of MYC-mRFP-Miro2 or protein degradation during the protein isolation process. This inference is drawn from its larger size compared to the expected WT band size, which is approximately 70 KD. (Figure 5-12).

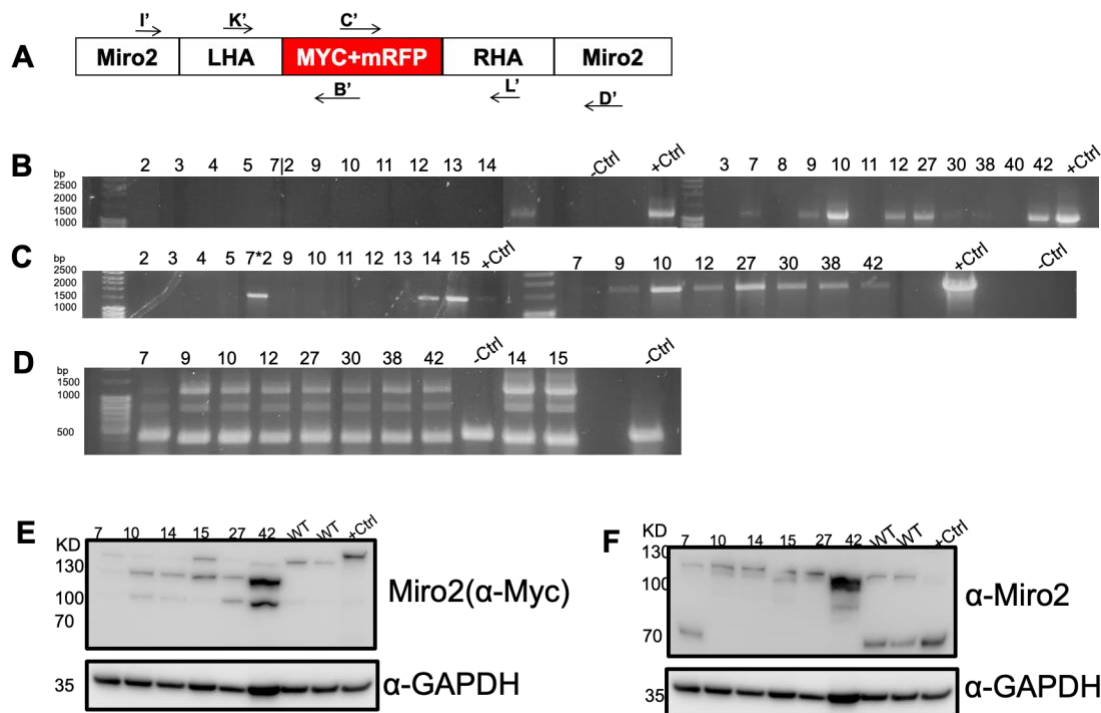


**Figure 5-12** The PCR genotyping and protein expression analysis of the selected pure potential MYC-mRFP-Miro2 HeLa clones provided conclusive evidence of the homozygous insertion of MYC-mRFP tags at the N-terminus of the endogenous Miro2 protein.

**A:** Representative picture of primer binding sites employed for PCR genotyping of MYC-mRFP-Miro2 potential KI HeLa selected single clones. Combination primer set: Forward primer (**I'**) and Reverse primer (**B'**), Right primer set: Forward primer (**C'**) and Reverse primer (**D'**), sequencing primer set: Forward primer (**K'**) and Reverse primer (**L'**) and.

**B-D:** PCR genotyping of the selected clones was carried out using the RHOT2-Combination primer set (**B**), the RHOT2-Right primer set (**C**), and the RHOT2- sequencing primer set (**D**). The Combination and Right primer sets were designed to amplify PCR products of expected sizes, 1324bp and 1686bp, respectively, only if the samples were positive for the Knock-in. In contrast, the Sequencing primer set could amplify PCR products from both KI-positive (1188bp) and Wild Type (WT) samples (417bp). As illustrated in the provided images, ten clones exhibited positive PCR bands with both primer sets, indicating successful integration of the tags into the targeted genomic region. The use of the sequencing primer confirmed the heterozygous nature of these positive clones, as they all displayed both KI and WT band sizes. The positive control (+Ctrl) employed in this analysis was derived from well number #64, which originated from a screening of 2000 cells per well.

**E-F:** Western blot analysis of the positive clones was conducted using two distinct antibodies: the anti-Mouse Anti-MYC CS antibody (**E**) and Miro2 Neuromab (#N384/63) (**F**). The application of the anti-MYC CS antibody confirmed the expression of the fusion protein at 120 kDa. Furthermore, the presence of a sample with an overexpressed MYC-tagged protein (at 130 kDa) as a positive control (+Ctrl) validated the specificity of the observed bands in the Knock-in lanes. Utilizing the anti-Miro2 antibody not only confirmed the active expression of the MYC-mRFP-Miro2 protein but also indicated that most of the clones were homozygous, implying that the tags had been successfully inserted into both copies of the chromosome.

In our efforts to establish FLAG-eGFP-Miro1 Knock-in (KI) HeLa cells, we employed a strategy similar to the one that successfully created FLAG-eGFP-Miro1 KI SH-SY5Y cells. We co-transfected wild-type (WT) HeLa cells with RHOT1-gRNA2, the same gRNA used to create the SH-SY5Y KI cells, and the RHOT1HDR vector. The

enrichment phase began 48 hours post-transfection by trypsinizing the cells and seeding 2000 cells per well, resulting in one 96-well plate with 2000 cells per well, totaling 192,000 cells. Once these cells reached confluence, we initially conducted PCR genotyping using the RHOT1-right primer sets. From the 17 wells that showed positive results, we selected well #28, which tested positive with both the RHOT1-right and RHOT1-left primer sets. Cells from this well were trypsinized and plated at a density of 100 cells per well in 40 wells of a 96-well plate. Subsequent PCR genotyping of the cells derived from this 100-cell-per-well stock using both the right and left primer sets identified well numbers #9 and #26 as positive wells. To isolate pure FLAG-eGFP-Miro1 KI HeLa cells, we trypsinized cells from these two wells and continued with low-density cell seeding, placing 100 cells per plate in seven 96-well plates. After three weeks, since HeLa cells grow faster than SH-SY5Y cells, we searched for single clones by checking each well under a microscope. In total, we identified 94 single clones. Once the selected single clones had grown sufficiently for DNA isolation, we isolated DNA and genotyped them using both the RHOT1-left, right and sequencing primer sets. However, despite significant efforts involving the screening of a large number of cells (192,000 cells) and narrowing down the screening to cells from positive wells, we did not achieve success in producing a stable FLAG-eGFP-Miro1 KI HeLa cell line (Figure 5-13). It's important to note that the reasons for this failure remain unknown. This failure cannot be attributed to the gRNA or HDR vector used, as we employed the same gRNA and HDR vector to create FLAG-eGFP-Miro1 KI SH-SY5Y cells and it worked well. Additionally, the genomic sequence of Miro1 in HeLa and SH-SY5Y cells is identical, and a similar enrichment approach was applied. One possibility is that the issue lies with the primer sets used for PCR genotyping, similar to the problem encountered with the Miro2-left and right primer sets that resulted in false positive results. However, it's worth noting that these primer sets were effective in identifying FLAG-eGFP-Miro1 KI SH-SY5Y cells. Given the aim of establishing double Miro1 and Miro2 KI stable cells, the decision was made to discontinue efforts to establish FLAG-eGFP-Miro1 single KI HeLa cells and to proceed with the creation of double KI HeLa cells instead.

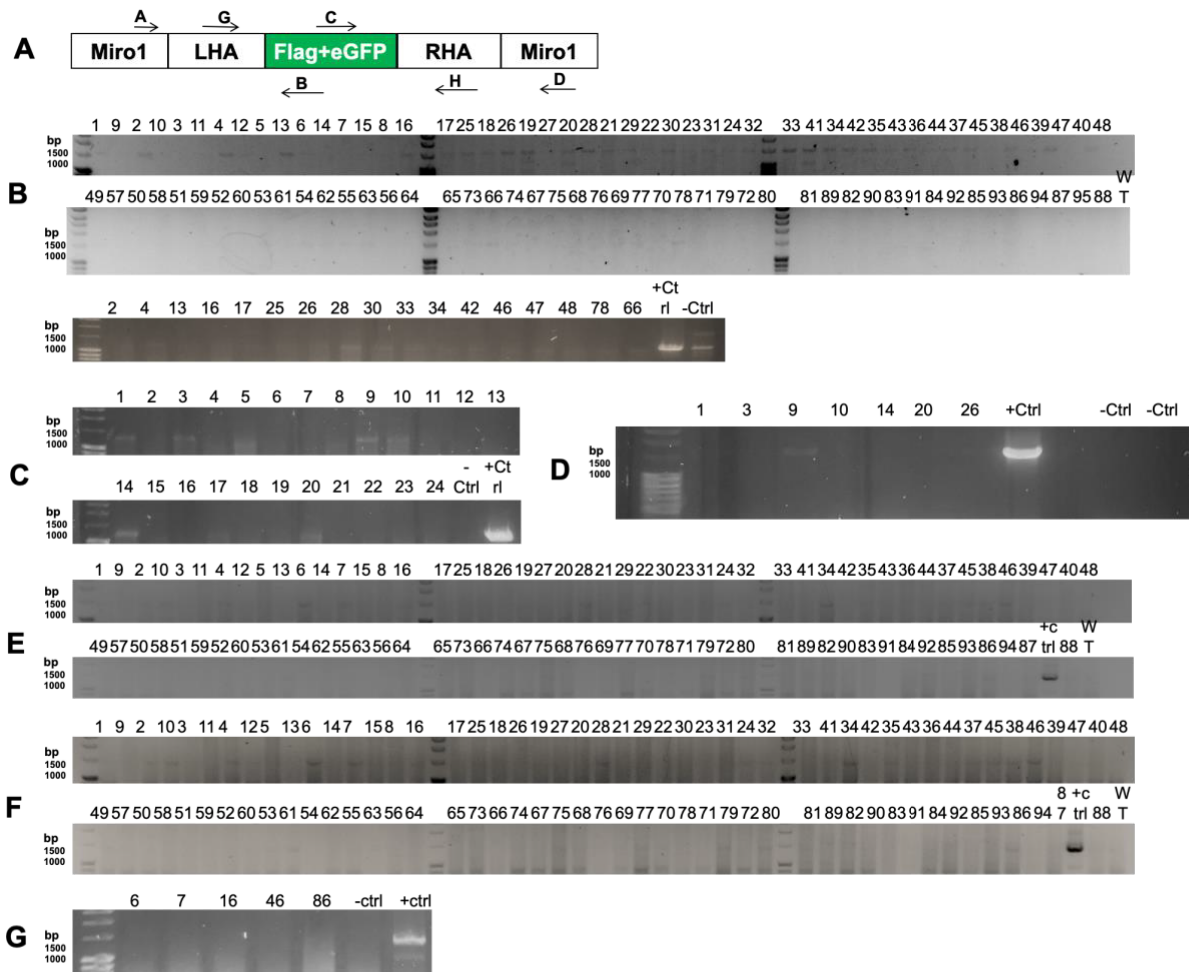


**Figure 5-13** Despite obtaining positive PCR genotyping results for some wells during the enrichment phase, PCR genotyping of selected pure clones derived from those wells failed to confirm the integration of the fusion tags in the N-terminus of the Miro1 gene in HeLa.

**A:** Binding sites illustration of RHOT1-left primer set (**A-B**), 1324 bp, RHOT1-right primer set (**C-D**), 1486, and sequencing primer set (**G-H**), 1456bp, used for PCR genotyping of FLAG-eGFP-Miro1 KI HeLa cells in enrichment and single colony screening.

**B:** PCR genotyping of 2000 cells/well, taken from a mixed population 48 hours after co-transfection. The cells were initially PCR genotyped using RHOT1-right primer sets, pictured in **upper panel**. Subsequently, cells with positive results were tested for the left side of the sequence using RHOT1-left primer sets, **pictured in lower panel**. Cells from well number #28 were selected for further analysis.

**C-D:** From the positive well number #28 of the 2000 cells/well step, 100 cells/well stock prepared and when cells were confluent, PCR genotyping was done using the first RHOT1-left primer sets(**C**). Positive wells were further tested using RHOT1-right primer sets (**D**).

**E-G:** The Potential FLAG-eGFP-Miro1 HeLa pure clones, originating from well number #9, which showed positive results in the 100 cells/well step, underwent PCR genotyping using first RHOT1-left (**E**) and right primer (**F**) sets, as well as RHOT1-sequencing primer(**G**). Although some of the clones showed positive band using left and right primer sets, we could not reproduce the result using sequencing primer set.

It should be noted that a DNA template of one of the FLAG-eGFP-Miro1 SH-SY5Y clones was used as the positive control(+Ctrl) in this analysis. Additionally, the PCR products were loaded onto a 1% agarose gel for PCR analysis.

## 5.6 Double Miro1/Miro2 Knock-in cells were successfully generated in the background of MYC-mRFP-Miro2 Knock-in HeLa cells.

As previously mentioned, in our research we aimed to explore the functional distinctions between Miro1 and Miro2 in terms of their localization, distribution, and identification of their binding partners. While having single Miro1 and Miro2 Knock-in (KI) cells was valuable, it posed certain limitations. One significant limitation was that we could only investigate one of the proteins at a time due to the absence of specific antibodies for detecting the other endogenous Miro protein. Additionally, overexpressing tagged forms of these proteins was not an ideal solution because it could potentially lead to mis-localization and distribution of the proteins, which might not accurately represent their behavior under normal physiological conditions. Hence, the most suitable approach for conducting a reliable comparative study was to generate a cell line expressing both tagged endogenous Miro1 and Miro2 proteins, referred to as Double Miro Knock-in (DMKI) cells. With this cell line, we could circumvent potential artifacts arising from overexpression and study both proteins simultaneously, allowing us to observe their localization and distribution closely resembling their natural state. To make DMKI cells as a starting material we could use either MYC-mRFP-Miro2 KI HeLa cells to make FLAG-eGFP-Miro1 KI or FLAG-eGFP-Miro1 KI SH-SY5Y cells to make MYC-mRFP-Miro2 KI SH-SY5Y cells. Due to the challenges, we had faced for making FLAG-eGFP-Miro1 SH-SY5Y KI cells and the previous unsuccessful attempts to establish MYC-mRFP-Miro2 KI in this cell line, we decided to make FLAG-eGFP-Miro1 KI using the MYC-mRFP-Miro2 Knock-in HeLa cells to have DMKI HeLa cells at the end. The process began by co-transfecting the MYC-mRFP-Miro2 Knock-in HeLa cells with RHOT1-gRNA2 and RHOT1-HDR. After 48 hours, we initiated the enrichment phase. In the first step, we made 12 wells, each containing 1700 cells, for a total of 20,400 cells. Cells from well numbers #4 and #5 showed positive results with both RHOT1-left and right primer sets and were trypsinized. These cells were further plated at a density of 100 cells per well, resulting in a total of 286 wells, each containing 100 cells. Upon reaching confluence, these cells underwent PCR genotyping using RHOT1-second primer sets. Cells from well #58 exhibited the most prominent results and were trypsinized and seeded at low density (100 cells per plate) to enable the isolation of single clones. In total, 10 plates were prepared. Three weeks later, single clones were identified by visual inspection under a microscope, resulting in the discovery of 286 single clones. PCR genotyping using RHOT1-left primer sets confirmed the integration of GFP-FLAG tags into the Miro1 gene in the background of MYC-mRFP-Miro2 Knock-in HeLa cells at the

genomic level some in some of the clones. Afterwards, RHOT1 and RHOT2 sequencing primer sets were used to further verification of this integration. Ultimately, we identified two clones out of the 286 clones that were positive for FLAG-eGFP-Miro1 Knock-in, in the MYC-mRFP-Miro2 background. While PCR genotyping using RHOT1-sequencing primers indicated that these two clones were heterozygous, displaying both KI (1456 bp) and WT (667 bp) band sizes, we were unable to confirm their heterozygosity or homozygosity of the clones at the protein level due to the lack of suitable Miro1 antibodies. However, protein expression analysis of these positive clones using anti-GFP CS and anti-MYC CS antibodies provided confirmation of the correct integration and active expression of the tags into the Miro1 gene in MYC-mRFP-Miro2 HeLa cells. This signifies the success of our endeavor to generate DMKI HeLa cells using this approach. (Figure 5-14).

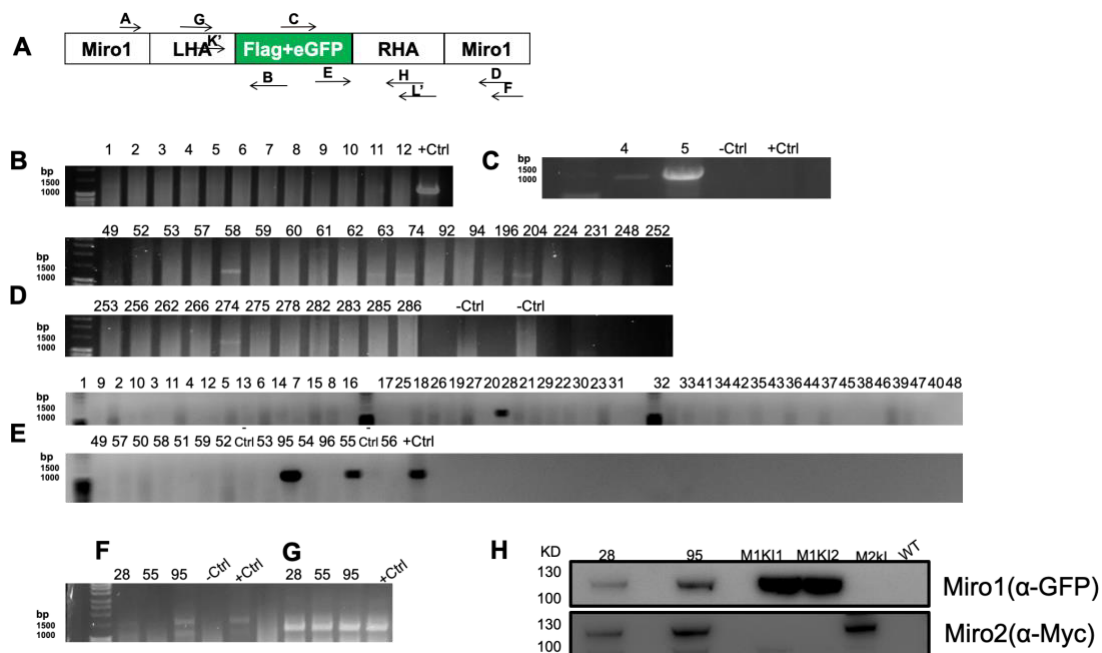


**Figure 5-14 Confirmation of GFP-FLAG tags integration into the endogenous Miro1 in MYC-mRFP-Miro2 Knock-in HeLa cells was achieved through PCR genotyping and protein expression analysis. The cells with successful integration were referred to as Double Miro Knock-in.**

**A:** Binding sites illustration of RHOT1-left primer set (**A-B**), 1324 bp, RHOT1-right primer set (**C-D**), 1486, RHOT1-second primer set (**E-F**), 1174bp, RHOT1-sequencing primer set (**G-H**), 1456bp and RHOT2-sequencing primer set (**K'-L'**), 1188bp used for PCR genotyping of FLAG-eGFP-Miro1 KI HeLa cells in the enrichment and single colony screening.

**B:** PCR genotyping of 1700 cells/well stock obtained from a mixed population 48 hours after co-transfection, using RHOT1-left and right primer sets respectively.

**C:** PCR genotyping 100 cells/well population from two positive wells (numbers #4 and #5) of the initial enrichment phase (1700 cells per well), using the RHOT1-second primer set.

**D-F:** PCR genotyping was performed on selected potential pure FLAG-eGFP-Miro1 and MYC-mRFP-Miro2 clones using the RHOT1-second primer pair (**D**), RHOT1-left primer set (**E**), and RHOT2

sequencing primer sets (F), respectively.

**G:** FLAG-eGFP-Miro1 and MYC-mRFP-Miro2 fusion proteins expression in DMKI HeLa cells was verified through SDS-PAGE analysis, using anti-GFP CS and anti-MYC CS antibodies. Protein samples from FLAG-eGFP-Miro1 (M1KI1, M1KI2) KI SH-SY5Y cells and MYC-mRFP-Miro2 (M2KI) KI HeLa cells were loaded beside the DMKI samples as controls to confirm the specificity of the results. The samples were loaded on a 4-12% gradient SDS-PAGE gel for this analysis.

### **5.7 The Immunoprecipitation (IP) of either FLAG-eGFP-Miro1 or MYC-mRFP-Miro2 was successful in terms of pulling down the bait proteins, but it did not result in the convincing capture of the prey proteins.**

After establishing Miro KI stable cell lines, our goal was to use these cells for immunoprecipitation (IP) of either FLAG-eGFP-Miro1 or MYC-mRFP-Miro2 and subject the samples to mass spectrometry analysis. This approach aimed to provide us with a deeper understanding of the roles of Miro1 and Miro2 by identifying their interacting proteins, shedding light on their diverse functions and interactions within mitochondrial trafficking and cellular machinery. Before proceeding with mass spectrometry analysis, it was crucial to optimize the IP conditions to make sure that we preserve the specific interactions while minimizing nonspecific bindings. Initially, our focus was on IP of the MYC-mRFP-Miro2 protein using ChromoTek MYC Trap magnetic beads (#ytma) and the corresponding ChromoTek protocol. To verify the specificity of the band obtained in the MYC IP lane from MYC-mRFP-Miro2 HeLa cells (M2KI-MYC IP), we did an IgG IP from MYC-mRFP-Miro2 HeLa cells and MYC IP from WT HeLa cells as negative controls. It has to be noted that IgG magnetic beads are particularly useful for detecting nonspecific interaction in IP since they are not conjugated to any specific antibodies. While the MYC Trap beads captured the MYC-mRFP-Miro2 protein with 100% efficiency since there is no band in MYC-mRFP-Miro2 Flow through (M2KI- FT) in Figure 5-15A blotted by anti-MYC CS, we were unable to successfully pull down Miro1 and Kinesin known as potential Miro2 binding partners with Miro2. Nevertheless, the absence of any bands in the WT MYC IP and M2KI IgG Lane in the anti-MYC CS probed blot confirmed the specificity of the M2KI-MYC IP band. As an alternative approach, we had the opportunity to use an IP protocol established by a Postdoctoral fellow in Thomas Schwarz's lab, Ismael. The primary difference between the ChromoTek protocol and the Ismael protocol was in the detergent and salt concentrations used in the lysis and washing buffers. Specifically, the ChromoTek lysis buffer contained 0.5% NP40, and the washing buffer had a salt concentration of 150mM, while the Ismael protocol's lysis buffer contained 1% Triton

X100, and the washing buffer had 500mM NaCl. Using the Ismael IP protocol, he has demonstrated that Miro1 homodimerizes with Miro1 and heterodimerizes with Miro2 when different tagged versions of Miro1 protein were overexpressed. Additionally, successful pull-down of overexpressed TRAK1 with overexpressed Miro1 was achieved by him. Given that our goal was to study the binding patterns of endogenous Miro1 and Miro2, we hoped that using Ismael's protocol would enable us to IP Miro2 with its binding partners as well. While it's known that overexpressed proteins may behave differently compared to endogenous ones, we remained optimistic about the possibility of immunoprecipitating endogenous protein using Ismael's protocol. Surprisingly, the use of Ismael's protocol did not facilitate the pull-down of Miro1 with Miro2. Furthermore, when comparing Ismael's protocol to the ChromoTek protocol, we found that the ChromoTek protocol was more efficient in pulling down the Miro2 protein itself (Figure 5-15 B). Given that Miro2 was tagged with MYC and mRFP tags, we speculated that using mRFP magnetic beads might aid in pulling down the binding partners of Miro2. Subsequently, we conducted two separate IP experiments using ChromoTek mRFP magnetic beads (#rtma, ChromoTek) and ChromoTek MYC magnetic beads with two different incubation times: 2.5 hours and overnight. Both experiments utilized the ChromoTek protocol. While the overnight incubation with mRFP beads resulted in a higher pull-down efficiency of the MYC-mRFP-Miro2 protein, longer incubation with MYC magnetic beads did not significantly increase the pull-down efficiency and in general, we observed that the MYC-mRFP-Miro2 pull-down efficiency using MYC magnetic beads was higher. Moreover, altering incubation times and using different magnetic beads did not successfully pull down TRAK1 and Miro1 along with Miro2 (Figure 5-15 C, D). As a result, we made the decision to proceed with shorter incubation times and continue using MYC magnetic beads for our further experiments and test other conditions. Further investigations revealed that the expression level of TRAK1 protein in HeLa cells was exceptionally low, which could be a contributing factor to our inability to IP it with Miro2. Consequently, we decided to overexpress GFP-TRAK1, vector kindly provided by Thomas Schwarz lab, MA, USA, in MYC-Miro2 Ki HeLa cells to test whether this approach would enable successful IP of these proteins together. However, even with elevated TRAK1 protein levels beside using MYC magnetic beads from ChromoTek or Cell signaling (# 5698) with ChromoTek buffers (Figure 5-15 E, F), or ChromoTek MYC magnetic beads along ChromoTek protocol and Ismael's protocol (Figure 5-15 G, H), neither resulted in

coming down of TRAK1 or MYO19 with Miro2. In summary, our attempts to replicate Ismael's success in pulling down Miro1, Miro2, and TRAKs together using the same protocol were unsuccessful. This disparity could be attributed to the fact that overexpressed proteins behave differently compared to their endogenous counterparts. Overexpression often leads to a high abundant of protein within cells, potentially causing it to localize differently and interact with other proteins that it might not do at endogenous levels. Furthermore, Ismael's experimental model was HEK cells, while we were using our KI HeLa cell line. It's well-known that protein expression levels and functions can vary between different cell types, which could contribute to the differences in our results using the same IP protocol. To test this hypothesis, our plan is to overexpress the same tagged protein in HeLa and HEK cell lines and do the IP and see if we can reproduce Ismael's result or not. Additionally, our attempts to detect interacting partners were hindered by the use of antibodies designed for detecting endogenous proteins, which we suspected might not be sufficiently specific to our target proteins which was confirmed by the presence of non-specific bands, making it challenging to identify the main specific band. For instance, in the case of Miro1, we observed a band of the correct size in both the M2KI IP Lane and the WT IP Lane, suggesting the possibility of non-specific binding, potentially due to cross-reactivity or other factors. In Ismael's experiment he didn't have problem regarding the antibody he used. He could rely on antibodies targeting specific tags like MYC or GFP when studying overexpressed GFP or MYC tagged Miro or TRAK proteins. This allowed for more dependable data, as there's a wide array of highly specific antibodies for MYC and GFP readily accessible in the market. Moreover, anti-MYC and anti-GFP antibodies usually have high sensitivity and can detect even low levels of tagged protein, making it easier to observe interactions with low protein levels. This option wasn't available to us when working with single KI cells. Moreover, the interactions between Miro2 and the tested proteins might be weak, making them undetectable by Western blotting. More sensitive methods, such as mass spectrometry analysis, could be beneficial in identifying potential interactors with greater precision. Furthermore, given that Miro1 and Miro2 are outer mitochondrial membrane proteins, the detergent concentration had to be sufficiently high to solubilize them. However, a high detergent concentration can negatively impact protein-protein interactions, potentially leading to interaction loss. Therefore, it's also possible that our current IP conditions may not be optimal for preserving protein-protein interactions, and the protein complexes might

disassemble during the IP protocol. Exploring milder detergents like Digitonin with lower concentrations may help in solubilizing the Miro proteins while preserving their interactions. Finally, it is also possible that there is no natural interaction between these proteins at the endogenous level, and the reported interactions might be artifacts resulting from the overexpression of the proteins, which could lead to abnormal localization within the cell, such as the mitochondria but we cannot be 100% sure since we think we need to further optimize our IP condition before make the final conclusion. In summary, our journey to elucidate the interactions of Miro1 and Miro2 has faced various challenges, including differences between overexpressed and endogenous proteins, the specificity of antibodies, the sensitivity of detection methods, and the optimization of IP conditions. Addressing these issues will be critical in advancing our understanding of these protein interactions and their roles within cellular processes at the endogenous level.

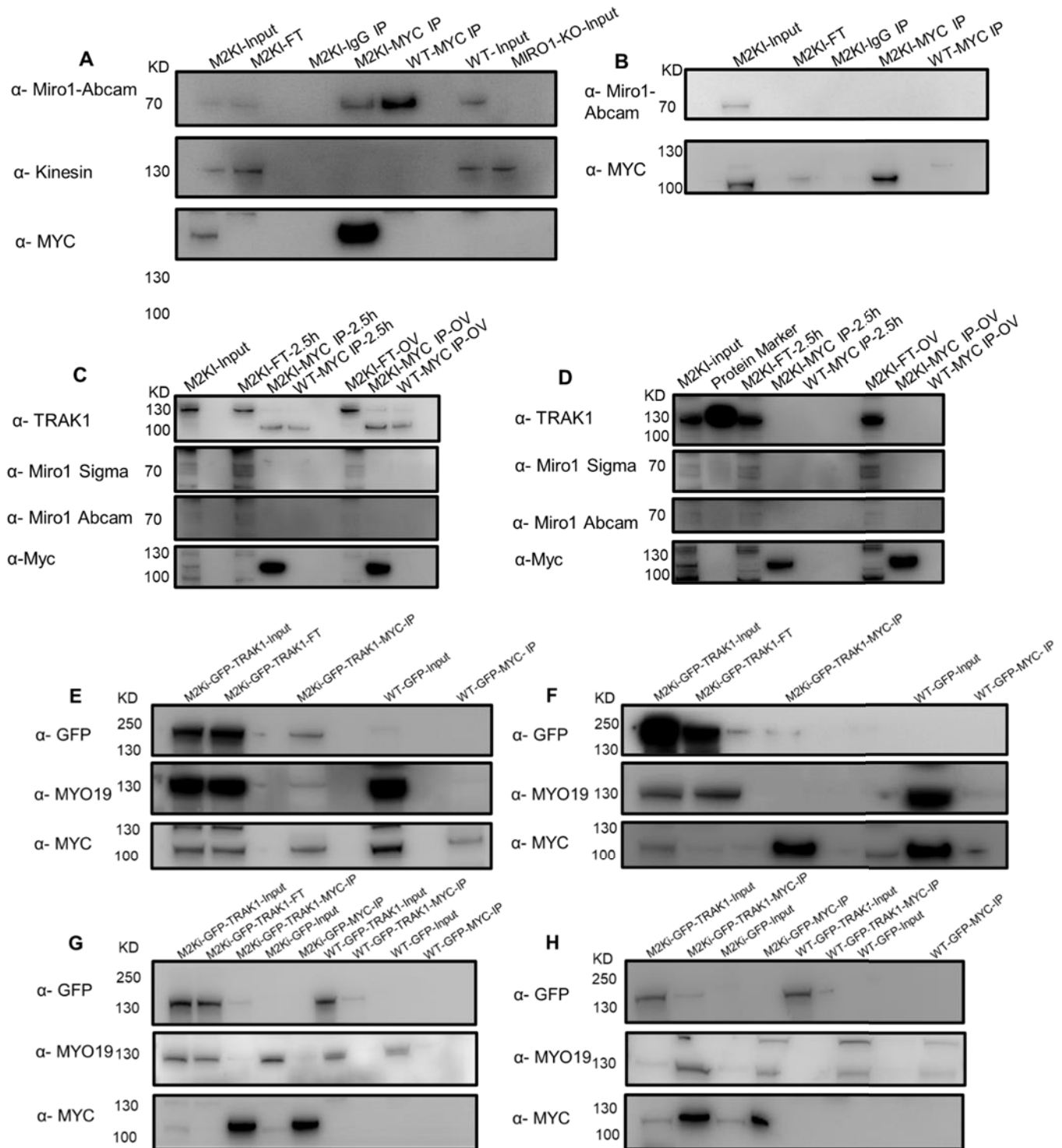


**Figure 5-15** Despite using different lysis buffers with varying detergent composition and concentration, utilizing different magnetic beads and different MYC Magnetic beads from different companies, overexpressing well-known interactors, we were not able to pull down the potential known binding partner of Miro2 in the Miro2 Immunoprecipitation (IP) experiments.

**A-B:** MYC-mRFP-Miro2 KI HeLa cells were immunoprecipitated using MYC magnetic (M2Ki-MYC IP) and IgG (M2Ki-IgG IP) magnetic beads. After lysing the cells with ChromoTek buffer containing 0.5% NP40 (**A**) or Ismael's buffer containing 1% Triton X100 (**B**) equal amount of total protein added to 25  $\mu$ l

beads and samples were incubated overnight Rotating end-over-end at 4 °C. On the following day flowthrough (M2KI-FT) was collected as output to estimate IP efficiency. For ChromoTek protocol we had 3 washes with 150mM NaCl containing washing buffer and one wash with 500 mM NaCl containing washing buffer, whereas in Ismael protocol 5 times washes with 500mMNaCl washing buffer was done. Afterwards, beads were eluted in 2X SDS buffer and samples were ran on 4-12% gradient SDS-PAGE for further analysis. 10% of total lysate and supernatant after bead incubation were loaded as input and flowthrough (FT) respectively. Mouse monoclonal anti- Kinesin, heavy chain (#MAB1614, Merk Millipore) and mouse monoclonal anti-Miro1 (#CL1083, Abcam), anti-Miro1 Abcam were used against endogenous Kinesin and Miro1. MYC-mRFP- Miro2 was probed using mouse anti-MYC CS antibody. Although using both protocol the pull down of MYC-mRFP-Miro2 protein was successful, we couldn't IP Miro1 or Kinesin with Miro2. M2KI is abbreviation of MYC-mRFP-Miro2 KI HeLa cells and WT stands for WT HeLa cells. IgG IP and MYC IP stands for eluted IP sample, either M2KI or WT, from MYC and IgG beads respectively. Equal amount of total protein from Miro1 Crispr Knock-out HeLa cells loaded beside other samples to test the specificity of anti-Miro1 Abcam antibody.

**C-D:** ChromoTek MYC magnetic beads (**C**) and ChromoTek mRFP magnetic beads (**D**) was used to do a MYC IP out of MYC-mRFP-Miro2 KI HeLa cells(M2KI) and WT HeLa cells (WT) (as a negative control). IgG IP out of both M2KI and WT cells was done as an additional control. After lysing the cells with ChromoTek lysis buffer containing freshly added protease and phosphatase inhibitor samples were splitted and incubated with either MYC, mRFP and IgG beads separately. To test the efficiency of IP with different incubation time we put two time point for bead incubation 2.5 hours (2.5h) and overnight (OV). After each incubation time the flowthrough (FT) of the beads incubated with MYC-MRF-Miro2 sample (M2KI-FT) were collected and beads were washed in the way explained before with ChromoTek washing buffer and eluted in 2X SDS buffer. The following antibodies used for immunoblotting of our proteins of interest showed in this. Anti- TRAK1 (#HPA005853, Sigma-Aldrich), anti-Miro1 (#H0005288-M01, Sigma Aldrich), Anti-Miro1 Sigma, anti-Miro1 Abcam, anti-MYC CS. As it is shown using MYC magnetic beads from different companies and testing different incubation time did not resulted in pulling down of either Miro1 or TRAK1 protein, although the pulling downing of Miro2 protein itself was successful in any conditions. Equal amount of total protein was used as starting material in all the conditions. 10% of total protein as lysate and and supernatant after bead incubation as FT were loaded.

**E-H:** MYCMiro2 KI HeLa cells were overexpressed with GFP-TRAK1(M2KI-GFP-TRAK1) vector, while the WT HeLa cells were overexpressed with the pcDNA3-EGFP plasmid (#13031, Addgene) as a control (WT-GFP). After 48 hours, the cells were lysed using ChromoTek lysis buffer with added protease and phosphatase inhibitors (at a 1:100 ratio). Subsequently, IP was carried out using MYC magnetic beads from ChromoTek (**E**) and Cell Signaling Technology (**F**). In another experiment, MYC-mRF-Miro2 KI HeLa were overexpressed with GFP-TRAK1(M2KI-GFP-TRAK1) and pcDNA3-EGFP(M2KI-GFP) separately. Additionally, WT HeLa cells were overexpressed with either the pcDNA3-EGFP (WT-GFP) plasmid or the GFP-TRAK1 (WT-GFP-TRAK1) plasmid serve as additional control groups. For each condition, two dishes were prepared, and after 48 hours, the cells were lysed using either ChromoTek lysis buffer (**G**) or Ismael's protocol lysis buffer (**H**), with freshly added protease and phosphatase inhibitors. Subsequently, the cells were incubated with either ChromoTek MYC magnetic beads. In the experiment using the ChromoTek protocol, the beads were washed three times with a low salt concentration (150mM) washing buffer and once with a high salt concentration (500mM) washing buffer. Whereas, in the experiment using Ismael's protocol, five washes were performed using a 500mM NaCl washing buffer. After the washing steps, the beads were eluted using 2X SDS buffer, and the IP samples were run on an SDS-PAGE gel for further analysis. For validation purposes, anti-GFP CS was used against GFP-TRAK1 and cytoplasmic GFP protein, Rabbit anti-MYO19 (#ab174286, Abcam) was used against endogenous MYO19 protein, and anti-MYC CS was used against MYC-mRFP-Miro2 to confirm the success of the experiment in pulling down the Miro2 tagged protein itself. The results, as evident from the blot images, indicate that regardless of variations in the beads used, lysis and washing buffer compositions, incubation times and overexpression of TRAK1, was not successful in pulling down of TRAK1 or MYO19 with MYC-mRFP-Miro2 protein under any condition. However, in all conditions,

the IP was successful in terms of pulling down the MYC-mRFP-Miro2 protein itself.

For all the experiment 10% of IP starting material and Supernatant after bead incubation loaded as input and Flowthrough (FT).

Subsequently, our aim was to investigate whether we could IP Miro1 and its known binding partners using our FLAG-eGFP-Miro1 KI SH-SY5Y cells. Additionally, we wanted to determine if Miro1 and Miro2 exist in the same complex and heterodimerize, or if they are present in separate protein complexes, labeling different mitochondrial populations. To initiate this investigation, we utilized ChromoTek GFP Trap magnetic beads (#gtma) and IgG magnetic beads (as a negative control) followed the recommended protocol from the same company. This combination of ChromoTek beads and protocol allowed us to successfully pull down the FLAG-eGFP-Miro1 tagged protein, however Miro2 couldn't be detected by Western blotting (Figure 5-16 A). Given this outcome, we decided to repeat the IP using Ismael's protocol to explore if using a different detergent could facilitate the pull-down of endogenous Miro2 with FLAG-eGFP-Miro1 protein. Unfortunately, using different buffers didn't yield any success in pulling down Miro2 with FLAG-eGFP-Miro1, but the FLAG-eGFP-Miro1 pull-down was successful (Figure 5-16B). Considering the possibility of a weak interaction between Miro1, Miro2, and TRAK1 (a reported main partner of Miro1 in mitochondrial movement) that might not be preserved during IP, we applied a crosslinking protocol to preserve protein-protein interactions. Despite conducting the IP with crosslinking and a comparison experiment without crosslinking (Figure 5-16 C and 5-16 D, respectively), we couldn't bring down TRAK1 with FLAG-eGFP-Miro1. Additionally, there was a band with the same molecular weight as endogenous Miro2 in the Miro1KI GFP IP lane, but the same size band was also present in the IP lane from WT SH-SY5Y cells, indicating it may be a non-specific binding. However, the IP with crosslinking was successful in pulling down FLAG-eGFP-Miro1, as well as the IP without crosslinking. Based on these results, it can be concluded that there is no direct interaction between Miro1 and Miro2 at least under the experimental conditions employed in this study. It is possible that they either reside in distinct mitochondrial populations or coexist within the same mitochondrion without engaging in direct interactions. To explore the potential interaction of Miro1 and Miro2 protein, it may be worthwhile to apply other IP conditions. For instance, using a different detergent such as Digitonin as a weak nonionic detergent could facilitate to IP Miro2 with Miro1. This adjustment in the experimental protocol may provide insights into the potential

interactions between Miro2 proteins that were not observed in the previous experiments.

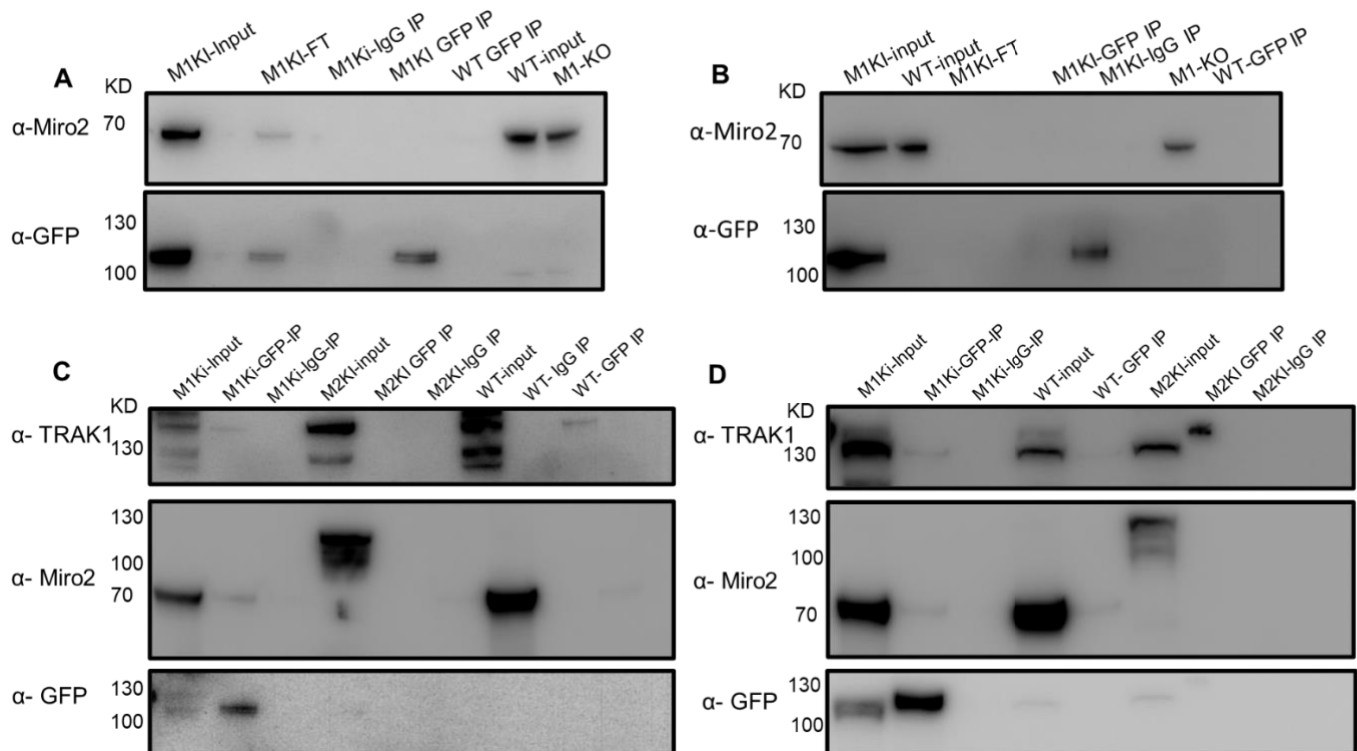


**Figure 5-16** Despite applying different IP protocols and crosslinking techniques, the immunoblotting of the GFP IP samples did not yield any detectable results for Miro2 and TRAK1, in contrast to the successful pull-down of FLAG-eGFP-Miro1.

**A-B:** FLAG-eGFP-Miro1 KI (M1KI) and WT SH-SY5Y(WT) were immunoprecipitated using ChromoTek GFP-Trap magnetic beads. For the IP we used either ChromoTek protocol and buffers (**A**) or Ismael's protocol and buffers (**B**). After lysing the cells, samples were incubated overnight either with GFP magnetic beads. To test the specificity of the band we get in MM1KI-GFP IP lane, IgG IP out FLAG-eGFP-Miro1 KI (M1KI-IgG IP) SH-SY5Y was done as well with the same strategy. The following day, beads were washed according the ChromoTek or Ismael's protocol instructions and eluted in 2X SDS buffer. To analyze the IP result, samples were loaded on to 4-12% gradient SDS-PAGE gel. Endogenous Miro2 (70KD) and TRAK1(around 130KD) were targeted using anti-Miro2 Neuromab, anti-TRAK1 Sigma, and anti-GFP CS antibody was employed against the tagged Miro1 (110-120 KD). Despite successful enrichment of FLAG-eGFP-Miro1 protein using both protocols, neither TRAK1 nor Miro2 co-immunoprecipitated with FLAG-eGFP-Miro1 protein.

**C-D:** To investigate whether crosslinking could be used to preserve interactions between FLAG-eGFP-Miro1 KI protein and its binding partners like TRAK1 and Miro2, we applied a crosslinking protocol to FLAG-eGFP-Miro1 KI (M1KI) and WT SH-SY5Y (WT) cells, as well as MYC-mRFP-Miro2 KI (M2KI) HeLa cells using 0.1% formaldehyde. Subsequently, we proceeded with IP using ChromoTeK GFP-Trap magnetic beads and followed the recommended protocol (**C**). The inclusion of MYC-mRF-Miro2 KI HeLa cells (M2KI) in this experiment served the purpose of examining any nonspecific binding of MYC-tagged proteins to the GFP beads, as we had observed significant nonspecific binding of GFP-tagged proteins to the MYC beads (as shown in the next panel). In addition to performing GFP IP, we also included IgG IP for all the samples as an additional negative control. To compare the IP results with and without crosslinking, we conducted an IP without crosslinking as well (**D**) After washing and eluting the beads, we ran an SDS-PAGE gel to observe the outcomes. The same antibodies used in blot pictures **A-B** were employed for immunoblotting the samples in this experiment. As obvious in the

blot images, there is a band corresponding to the molecular weight of TRAK1(130KD) and Miro2(80KD) in the M1KI-GFP IP lane. However, a similar-sized band is also present in the GFP IP lane from the WT sample (WT-GFP IP) in both the crosslinking and non-crosslinking experiments. These results led us to believe that these bands represent nonspecific protein binding to the beads and do not reflect real interactions. Nonetheless, FLAG-eGFP-Miro1 protein was successful in both experiments. It has to be mentioned that 10% of IP starting material and Supernatant after bead incubation loaded as input and Flowthrough (FT).

After successfully establishing DMKI HeLa cells, we transitioned our IP experiments to these cells, which enabled us to utilize tag-specific antibodies, overcoming previous challenges associated with the lack of specific and reliable antibodies for endogenous Miro1 and Miro2. To pull down FLAG-eGFP-Miro1 and MYC-mRFP-Miro2 fusion proteins, we started by using ChromoTek GFP Trap Agarose beads (#gta) and MYC Trap Agarose beads (#yta), respectively, following Ismael's protocol (Figure 5-17 A-B). While both IP were successful in pulling down the main proteins, specifically MYC-mRFP-Miro2 in MYC IP and FLAG-eGFP-Miro1 in GFP IP, we were unable to detect any co-precipitation of the other form of Miro in either pull-down, regardless of whether we used anti-Miro1/Miro2 antibodies or tag-specific antibodies. We also probed for the presence of TRAK1, but our results did not indicate any success in pulling down TRAK1 with FLAG-eGFP-Miro1 fusion protein in GFP IP. To address these challenges, we modified our approach by utilizing magnetic beads while following the ChromoTek protocol for the IP experiments. With the use of MYC magnetic beads and ChromoTek buffers, we successfully pulled down Miro1 (the bait protein) with Miro2 (the prey protein) (Figure 5-17 C). To validate the specificity of the FLAG-eGFP-Miro1 band obtained in the MYC IP experiment, we repeated the MYC IP using FLAG-eGFP-Miro1 KI SH-SY5Y cells, which do not express any MYC fusion protein, in addition to DMKI cells. Surprisingly, we observed a band of the same size as FLAG-eGFP-Miro1 in the MYC IP lane from FLAG-eGFP-Miro1 KI cells (M1KI-MYC IP), and it was even stronger than the band in the DMKI cells IP lane (DMKI-MYC IP). This indicated that GFP protein had nonspecific affinity binding to the MYC magnetic beads we used for IP, raising concerns about the reliability of the data regarding the pull-down of FLAG-eGFP-Miro1 with MYC-mRFP-Miro2. Additionally, we probed for MYO19 and TRAK2, which are known interactors of Miro2, and detected them in the IP lane from DMKI cells (DMKI-MYC IP). However, in the M1 KI cells IP lane (M1KI-MYC IP), there was a band with a slight size difference in the case of TRAK2 or a strong, same-size band in the case of MYO19 (Figure 5-17 D). Furthermore, we conducted another IP using

DMKI cells, where we used GFP Trap magnetic beads to pull down FLAG-eGFP-Miro1 protein. To assess nonspecific binding of MYC tagged protein to the GFP beads, we included GFP IP out of MYC-mRFP-Miro2 KI HeLa cells. As shown in Figure 5-17 E, our attempt to pull down MYC-mRFP-Miro2 protein with FLAG-eGFP-Miro1 protein was unsuccessful, as the band of equal size present in the DMKI GFP IP lane was also detected in the M2KI-GFP IP lane. Additionally, there was no success in pulling down TRAK1 with FLAG-eGFP-Miro1. Nevertheless, the IP procedure worked well for FLAG-eGFP-Miro1 pull-down.

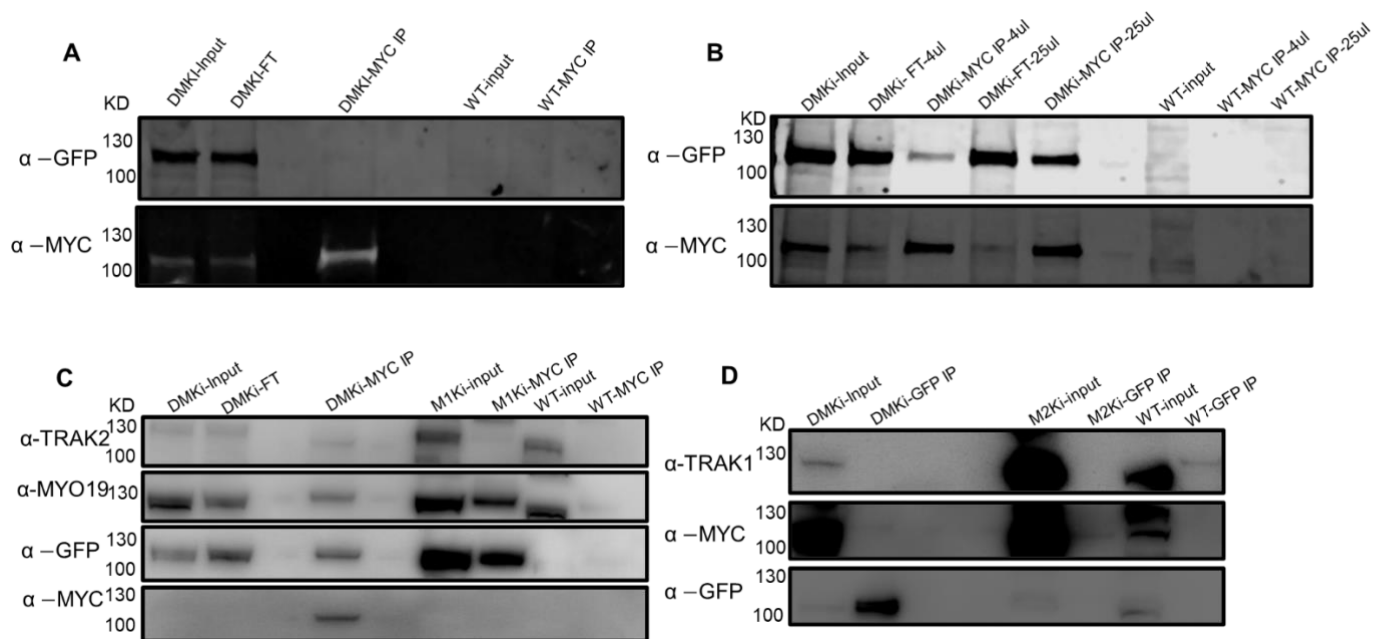


**Figure 5-17 non-specific binding of GFP-Miro1 to the MYC beads when MYC IP was performed from FLAG-eGFP-Miro1 KI samples. Although we got initial promising result from MYC IP experiment carried out in DMKI cells to pull down GFP-Miro1 with MYC-mRFP-Miro2 using ChromoTek MYC magnetic beads and ChromoTek protocol, it was later discovered that the interaction observed was due to non-specific binding of GFP-Miro1 to the MYC beads when MYC IP was performed from FLAG-eGFP-Miro1 KI samples.**

**A:** We performed MYC IP out of DMKI cells using ChromoTek MYC Trap agarose beads to pull down MYC-mRFP-Miro2 fusion protein and its binding partner. We followed Ismael's protocol for this experiment. The cells were lysed using a 1% Triton-based lysis buffer, and the samples were incubated with the beads overnight. After five washes with a wash buffer containing 500mM NaCl, we eluted the samples in 2X Lammeli buffer and loaded them onto an 8% straight Acrylamide gel for IP analysis. For immunoblotting, we used a rabbit anti-GFP CS antibody to check for the presence of FLAG-eGFP-Miro1 protein alongside a mouse anti-MYC CS antibody for MYC-mRFP-Miro2. Despite a successful result in pull down MYC-mRFP-Miro2 proteins, we were unable to detect FLAG-eGFP-Miro1 in association with Miro2 fusion protein.

**B:** We ran MYC and IgG IP experiments out of DMKI (DMKI MYC/IgG IP) and WT HeLa cells (WT MYC/IgG IP) with two different volumes of MYC magnetic agarose beads: 4  $\mu$ l and 25  $\mu$ l. This was done to assess whether reducing the bead volume affected the efficiency of protein pull down beside investigation of MYC-mRFP-Miro2 and FLAG-eGFP-Miro1 fusion protein association. We followed ChromoTek's protocol for this experiment. After cell lysis using a 0.5% NP40-based lysis buffer, equal

amounts of protein were added to the beads and incubated overnight at a cold room. The following day, after three washes with a low salt (150mM) washing buffer and one wash with a high salt (500mM) washing buffer, samples were eluted in 2X Lammeli buffer and loaded onto an 8% straight Acrylamide gel. We used anti-GFP CS and anti-MYC CS antibodies for immunoblotting. With this setup, we successfully isolated FLAG-eGFP-Miro1 along with MYC-mRFP-Miro2 using either bead volume. However, the efficiency was higher with a larger bead volume, especially regarding the pull-down of FLAG-eGFP-Miro1 with MYC-mRFP-Miro2, prompting us to use this bead volume for future experiments.

**C:** To validate the specificity of the FLAG-eGFP-Miro1 band obtained in the previous experiment (Figure 5-16 B), we included MYC and IgG IP from Miro1KI SH-SY5Y (M1KI) cells in addition to the DMKI and WT HeLa cells. We used ChromoTek buffers and NP40-based buffers for this IP experiment. After lysing the samples, we added 25  $\mu$ l of either MYC or IgG magnetic beads to the sample and incubated them overnight in a cold room. After washing, samples were eluted in 2X SDS buffer and run on SDS-PAGE gel. We used anti-GFP CS and anti-MYC CS antibodies against FLAG-eGFP-Miro1 and MYC-mRFP-Miro2 fusion proteins. For endogenous TRAK2 and MYO19, we used anti-TRAK2 (clone N390/43) from NeuroMab and anti-MYO19 Abcam antibodies. The blot revealed a non-specific strong band in the M1KI MYC IP lane when probed with anti-GFP CS antibody, which should not have been present since there is no MYC-tagged protein in FLAG-eGFP-Miro1 KI cells. This suggests that the band in DMKI MYC IP is also non-specific and does not represent a real interaction between MYC-mRFP-Miro2 and FLAG-eGFP-Miro1 fusion proteins. Similar results were obtained when probing for endogenous MYO19. The same-sized band was present in DMKI MYC IP and M1KI MYC IP, indicating it is not due to a specific interaction between MYO19 and MYC-mRFP-Miro2 protein too. However, the result for endogenous TRAK2 protein was promising, as only one specific band was present in DMKI MYC IP when probed using a mouse anti-TRAK2 antibody.

**D:** GFP IP out of DMKI cells was done by utilizing the ChromoTek GFP Trap magnetic beads and ChromoTek protocol and buffers. GFP IP and IgG IP were also carried out on MYC-mRFP-Miro2, and WT HeLa cells as negative control to test the specificity of the band we get in DMKI GFP IP lane. Cells were lysed using a 0.5% NP40 lysis buffer and incubated with beads overnight. The following day, after washing with low(150mM) and high(500mM) salt washing buffers, samples were eluted in 2X SDS buffer and run on an SDS-PAGE gel for IP analysis. We probed the blot for FLAG-eGFP-Miro1, MYC-mRFP-Miro2, and endogenous TRAK1 proteins using anti-GFP CS, anti-MYC CS, and anti-TRAK1 Sigma antibodies. Unfortunately, the IP experiment failed regarding specific pull down of either MYC-mRFP-Miro2 fusion protein or endogenous TRAK1 with FLAG-eGFP-Miro1 fusion protein, despite the pull-down of FLAG-eGFP-Miro1 fusion protein was quite successful.

For the experiment shown here that 10% of IP starting material and Supernatant after bead incubation loaded as input and Flowthrough (FT).

## **5.8 Proximity ligation assay (PLA) confirmed Miro1 and Miro2 are in close proximity on mitochondria, although it cannot be concluded that they form heterodimerize**

Since our attempts to investigate the potential interaction between Miro1 and Miro2, as well as to identify their respective binding partners, using the IP method have not yielded any successful results so far, we have decided to use an alternative approach, the Proximity Ligation Assay (PLA), as an in-situ method for visualizing protein-protein interactions, to study the Miro proteins interactions in DMKI cells. To carry out this study, we utilized the Duolink® In Situ Red Starter Kit Mouse/Rabbit (#DUO92101, Sigma Aldrich). Initially, our primary focus was on examining the interaction between

Miro1 and Miro2. To achieve this, we incubated samples (DMKI cells and WT cells as a control) with rabbit anti-GFP CS and mouse anti-MYC CS primary antibodies after fixing the cells. Given that Miro1 is tagged with FLAG-GFP tags, we also conducted a separate PLA experiment in which we co-labelled DMKI cells with rabbit anti-GFP CS and mouse anti-FLAG antibodies as a positive control, demonstrating the specificity of the PLA puncta obtained. After the primary antibody incubation, we followed the PLA protocol using rabbit plus and mouse minus PLA probs. Additionally, since our interest lay in studying the interaction between Miro1 and Miro2 within the context of mitochondria, we stained the samples against HSP60 protein, serving as a mitochondrial marker, using the anti-HSP60 antibody from Novus Biological following the completion of the PLA protocol. Subsequently, we proceeded with image acquisition. As Figure 5-18 A and C illustrates, we observed positive red PLA puncta in both conditions, FLAG-GFP and MYC-GFP, confirming the success of the experiment and indicating that Miro1 and Miro2 are in close proximity to each other, within a range of less than 40 nm. While there were some background signals in the WT samples, the signals in DMKI cells were more abundant. Quantification of the images further confirmed that the overlap of PLA signals with mitochondrial signals was significantly higher in DMKI cells compared to WT cells (Figure 5-18 B and D). Although our preliminary PLA results have indicated that Miro1 and Miro2 are in close proximity to each other, we are still uncertain about whether they interact and form heterodimers or not. This uncertainty arises from the fact that different IP conditions have failed to co-immunoprecipitated FLAG-eGFP-Miro1 and MYC-mRFP-Miro2 together. Therefore, we suspect that they may be in close proximity but not necessarily interacting with each other. Further experiments, particularly IP experiments under varying conditions, might provide additional insights and enable us to draw more robust conclusions in this regard.

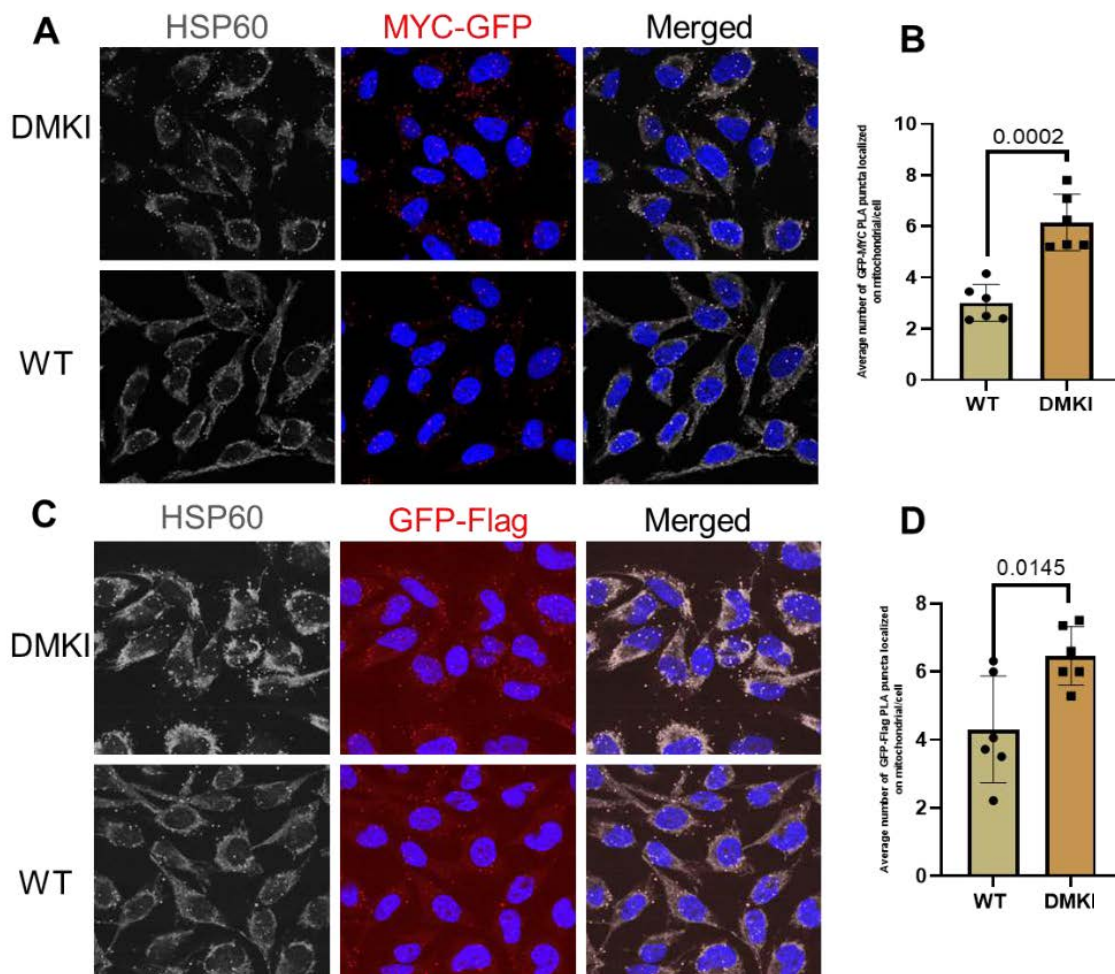


**Figure 5-18** The analysis of PLA data has confirmed the interaction between Miro1 and Miro2 localized within the mitochondria.

**A-B:** To investigate the distribution of FLAG-eGFP-Miro1 and MYC-mRFP-Miro2 on mitochondria in DMKI cells, we employed a Proximity Ligation Assay (PLA). The experimental process involved fixing both DMKI cells and WT cells, as a negative control, using a 4% PFA solution. Following this, after permeabilization and blocking, the samples were subjected to an overnight incubation with either mouse anti-MYC CS and rabbit anti-GFP CS primary antibodies. On the subsequent day, the samples were incubated with mouse Minus and rabbit Plus PLA probes, followed by ligation, signal amplification, and imaging. In order to visualize the endogenous HSP60 protein, as a mitochondrial marker, we utilized an anti-HSP60 antibody and Alexa 674 at a dilution of 1:500. To mount the samples and stain the cell nuclei, we used the provided mounting media containing DAPI from the kit. **A:** The visualization of signals was conducted using a 60X oil objective lens on the Zeiss confocal laser scanning 880 system. The HSP60 grey signal was detected in the far-red channel, facilitated by a Laser HeNe at 633 nm. The visualization of MYC-GFP red PLA signals occurred through the mCherry channel, employing an Argon laser at 543 nm. The visualization of DAPI-stained nuclei was achieved using a laser Diode at 405 nm. **B:** The Image quantification which confirmed that the MYC-GFP red PLA puncta is significantly higher in DMKI cells compare to WT indicating that the signal is specific and confirmed that Miro1 and Miro2 are localized to mitochondria in a close proximity of each other.

**C-D:** Since Miro1 fusion protein has FLAG and GFP tags, as a positive control, DMKI and WT cells were co-stained using rabbit anti-GFP CS and mouse anti-FLAG primary antibodies followed by PLA protocol. The expectation here was to obtain specific signals using antibodies targeting the FLAG and GFP tags verifying PLA experiment success. We applied the same protocol, antibody dilution and setting for this experiment as we did for MYC-GFP PLA experiment. **C:** As evident in both Panel C in

general the number of PLA red puncta is higher and more colocalized with the mitochondrial marker HSP60 in DMKI cells compared to WT HeLa cells. **D**: The statistical analysis also confirmed the PLA success and our observation and showed significant higher number of FLAG-GFP PLA red puncta localized on mitochondria in DMKI cells compare to WT cells.

Statical analysis was done using t. test at a significance level of  $P < 0.05$ . Number of puncta was normalized with respect to the number of cells.

### **5.9 Although MYC-mRFP-Miro2 signal is vary from cell to cell, there is co-localization of the MYC-mRFP-Miro2 signal and HSP60 signals in most of the cells in DMKI cells.**

One of the key objectives of our research was to investigate the localization and distribution patterns of Miro1 and Miro2 on mitochondria, with the intention of exploring whether any heterogeneity existed in this context or not. In other words, we aimed to determine whether Miro1 and Miro2 marked distinct mitochondrial subpopulations or if they are present across all mitochondria. For that we started with the study of Miro2 localization and we employed the general ICC protocol outlined in the material and methods section. In brief, DMKI cells were subjected to fixation using 4% PFA. Following permeabilization and blocking steps, cells were co-stained overnight with mouse monoclonal anti-MYC (#05-724, Sigma Aldrich) and anti-HSP60 Novus Biological antibodies. The subsequent day, anti-Mouse Alexa Fluor 488 and anti-rabbit Alexa Fluor 647 antibodies were applied. Finally, the samples were mounted using appropriate mounting media and imaging was done. Figure 5-18 A clearly illustrates that the MYC signal, stand for MYC-mRFP-Miro2 fusion protein depicted in red, exhibited specificity by its abundance and colocalized with the green HSP60 mitochondrial signal within DMKI cells, as compared to the WT samples. Due to our interest in investigating the localization of Miro proteins on individual mitochondria we needed to capture super resolution images, which unfortunately was not possible due to the lack of super resolution microscope. Therefore, we employed the expansion microscopy method recommended by a post-doctoral fellow in Thomas Schwarz lab, Guoli Zhao. This innovative approach involves increasing sample size to capture super-resolution imaging with conventional microscopes like confocal microscopes. Following this, we initiated the standard ICC protocol using the same antibodies as employed in the ICC experiment depicted in Figure 5-19 A. Following the washing step after the secondary antibody incubation, we initiated the expansion protocol. This involved the introduction of linker groups, followed by embedding the samples in a swellable gel, a digestion process, and ultimately, sample expansion and finally

imaging. As illustrated in figure 5-19 B, expansion microscopy allowed us to acquire close-up images of mitochondrial signals and MYC-mRFP-Miro2 localization on mitochondria. Notably, specific MYC signals, shown in red, were predominantly present in DMKI cells, mainly displaying colocalization with the green HSP60 mitochondrial marker. Moreover, we believe that some of the MYC-mRFP-Miro2 signals co-localized with mitochondria were lost during the expansion microscopy protocol since they are less abundant compare to MYC signal in DMKI cells in general ICC experiment. This could be due to enzymatic digestion and other treatments applied during expansion microscopy. Therefore, optimizing the protocol to preserve the original signals could enhance the reliability of our findings for all parties involved. Statistical analysis of the data is in progress and need to be optimized according to our experimental condition and purpose of our work. In summary, ICC and expansion microscopy results confirmed the localization of Miro2 on mitochondria. Nevertheless, there was variability in MYC signal intensity among cells (indicated by white and blue arrows in Figure 5-19 A), and in specific regions, the yellow-marked area in merged image in Figure 5-19 A, we were unable to detect any overlap between HSP60 and MYC. Several factors may account for these variations. Firstly, differential expression of the MYC-mRF-Miro2 fusion protein by cells may explain the observed differences in MYC signal from one cell to another. In addition, it is possible that a portion of Miro2 exclusively labels a subset of mitochondria, while the rest may be associated with other organelles. To investigate this hypothesis, co-staining MYC-mRFP-Miro2 protein with organelle-specific antibodies could provide valuable insights. Nevertheless, it's important to say that technical factors may also contribute to this variation. For example, uneven staining could be attributed to differences in cell permeability scores or the presence of the protein within complexes with other proteins which could restrict antibody access to all the proteins evenly, resulting in signal variations and lack of overlap. Furthermore, the absence of signal overlap might be due to weak MYC signals which hided by strong HSP60 signals and made us unable to capture. Repeating this experiment and using different antibodies dilution and detergent concentration might be a good strategy to examine the reliability of the result we got. It has to be mentioned due to the lack of biological replicate and since the experimental condition is not set, I was unable to make any statistical analysis.

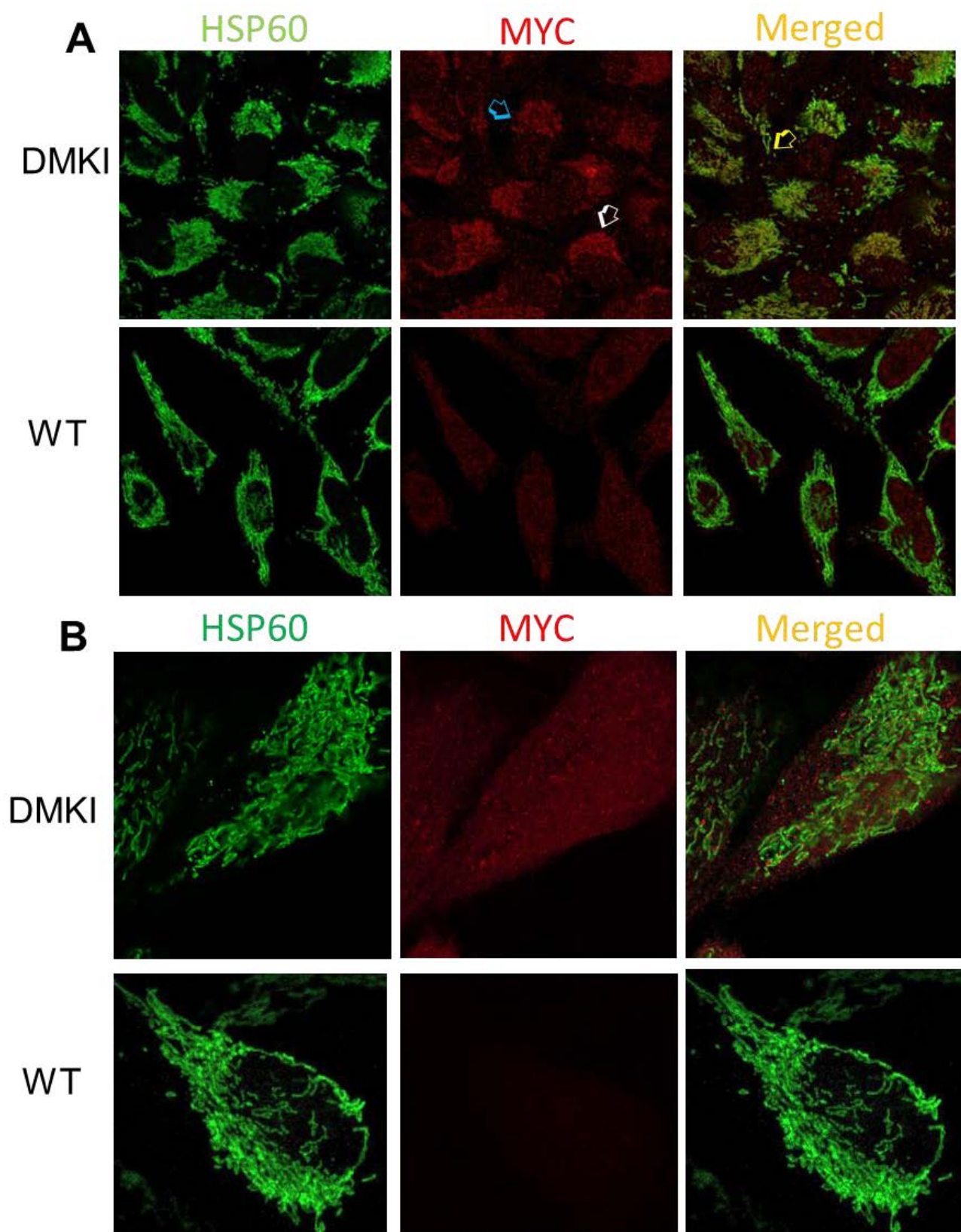


**Figure 5-19 Application of expansion microscopy in combination with conventional co-staining verified the mitochondrial localization of Miro2 in DMKI cells.**

**A:** Since the endogenous MYC-mRFP-Miro2 protein's signal was too faint in the live cells, to study the

diversity in proteins localization and distribution in DMKI cells, we applied the general ICC protocol for signal enhancement. For that, DMKI cells were first fixed with 4% PFA and co-stained anti-MYC from Santa Cruz Biotechnology (diluted at 1:500) and anti-HSP60 from Novus Biological (diluted at 1:500), as a mitochondrial marker, primary antibodies against MYC-mRFP-Miro2 and endogenous HSP60 respectively. anti-mouse Alexa Fluor 488 and anti-rabbit Alexa Fluor 647 secondary antibodies were applied to label the MYC-mRFP-Miro2 protein and endogenous HSP60 proteins, respectively (A). Subsequently, the samples were mounted in the mounting medium, and images were acquired using a Zeiss LSM700 microscope equipped with a 60% oil objective lens

**B:** In order to capture super resolution images using conventional microscope we applied the expansion microscopy experiments we followed the same ICC protocol and employed the same primary and secondary antibodies as used in panel **A**. Following the secondary antibody incubation and thorough washing, we initiated the expansion microscopy process, involving the introduction of linker groups, enzymatic digestion, and sample expansion. The expanded samples were then fixed in glass-bottom dishes using low melting agarose gel, and imaging was performed using SP8 LIGHTNING Confocal Microscopes. In both experiments, we included WT HeLa cells as a negative control.

As it is obvious in both images, there is a more pronounced MYC signaling in DMKI cells compared to WT. Furthermore, in panel A, it is apparent that there is a possible heterogeneity among cells in terms of MYC-mRFP-Miro2 protein expression levels, with some cells exhibiting higher expression than others. As an example, cell pointed by white arrow shows brighter MYC signals compare to the cell pointed by blue arrow which could be due to higher expression of MYC-mRFP-Miro2 protein in that cell.

### **5.10 The FLAG-eGFP-Miro1 fusion protein showed partial co-localization with mitochondria in differentiated KI SH-SY5Y cells.**

In the context of cellular health and survival, particularly in neurons characterized by their distinct morphology, the proper motility of mitochondria holds significant importance. Miro1 plays an essential role in mitochondrial trafficking by serving as an anchor for the motor-adaptor protein complex on the outer membrane of mitochondria. One of the distinct advantages of working with SH-SY5Y cells lies in their capability to be differentiated into neuron-like cells. To address our objective of studying the diversity in the mitochondrial distribution and localization of Miro1 and Miro2 in neuronal cells, we aimed to introduce tagged Miro1 and Miro2 proteins into SH-SY5Y cells. While we succeeded in generating FLAG-eGFP-Miro1 KI SH-SY5Y cells, our efforts to tag the Miro2 gene in this cell line did not yield success. To achieve our goal of studying Miro1 in neuronal settings, we initiated the differentiation of FLAG-eGFP-Miro1 KI SH-SY5Y cells. The detailed protocol is outlined in the materials and methods section. Due to the relatively weak fluorescence signals of endogenous FLAG-eGFP-Miro1 fusion protein in live cells, we opted to fix and stain the cells to enhance the signals. Consequently, upon completing the neuronal culture and subsequent fixation, cells were co-stained for the FLAG-eGFP-Miro1 fusion protein, ATP5A (served as a mitochondrial marker), to observe Miro1 fusion protein localization and distribution on mitochondria in axons. To confirm the success of differentiation, along with FLAG-

eGFP-Miro1 and ATP5A, cells were stained for microtubule-associated protein 2 (MAP2) highly expressed in neuronal soma and dendrites. As it is shown in the figure 5-20, the GFP signals are specific to Miro1, as they are present in KI cells and display overlap with a subset of HSP60 mitochondrial signals. The magenta staining representing MAP2 confirms that both Miro1 KI SH-SY5Y and WT SH-SY5Y cells have successfully transitioned into neuron-like cells. In conclusion, Miro1 exhibits an uneven distribution and localization across different mitochondrial subpopulations in axons. This can be understood as some mitochondria lacking Miro1 protein, potentially implying the presence of other proteins, like Miro2, anchoring the motor-adaptor protein complex in differentiated SH-SY5Y cells. The subsequent step involves co-staining the cells against Miro1 and Miro2 proteins alongside a mitochondrial marker to exploring their distribution patterns, thereby testing this hypothesis. Furthermore, technical factors, as explained in the previous section, could potentially influence this matter. At the end it has to be mentioned that these data are preliminary result and repetition of the experiment is necessary for final conclusion and statistical analysis.

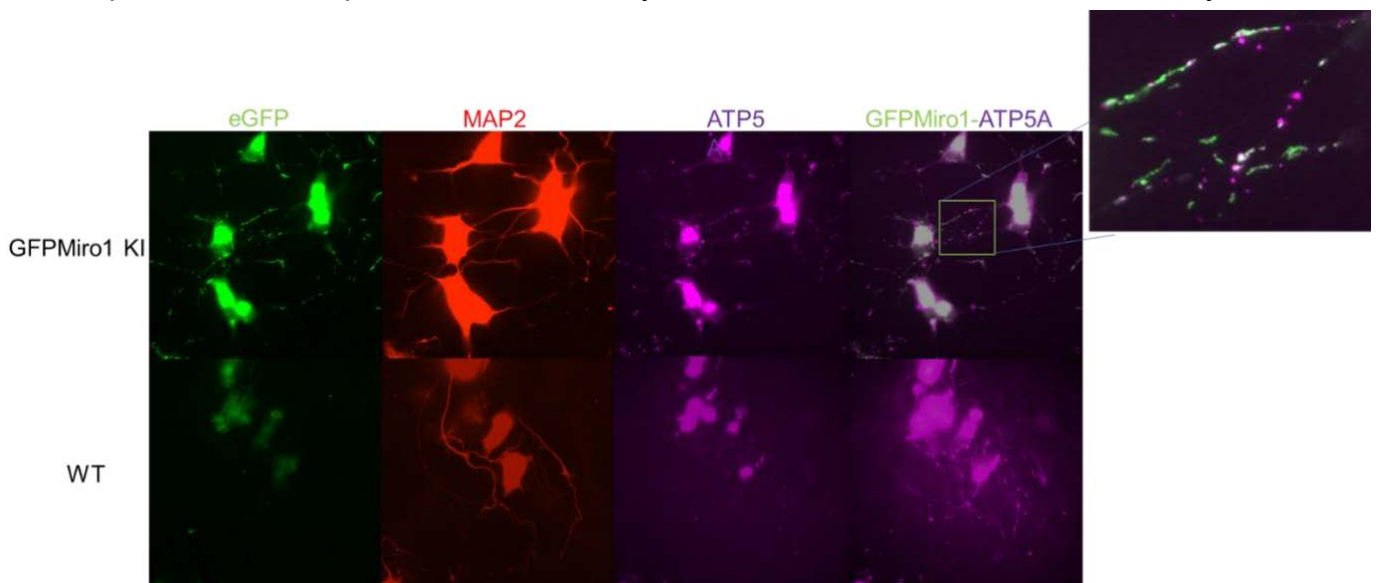


**Figure 5-20** In differentiated SH-SY5Y cells, the co-staining procedure revealed a partial co-localization pattern between FLAG-eGFP-Miro1 and HSP60 signals specifically within the FLAG-GFP- Miro1 KI cells, while no such co-localization was observed in the WT cells.

FLAG-eGFP-Miro1 KI SH-SY5Y cells and WT SH-SY5Y cells, used as a control, were subjected to a differentiation protocol to investigate the localization and distribution of FLAG-eGFP-Miro1 in neuron-like cells. After 21 days of following the protocol, the differentiated FLAG-eGFP-Miro1 KI SH-SY5Y and WT SH-SY5Y cells were fixed with 4% PFA. They were then co-stained against FLAG-eGFP-Miro1 using a rabbit anti-GFP (#A-11122, Invitrogen), 1:1000, ATP5A, as a mitochondrial marker, using a mouse anti-ATP5A antibody, 1:500, and MAP2, as a neuronal marker localized specifically in soma and dendritic regions, using a chicken anti-MAP2(# NB300-213, Novusbio) antibody, 1:1000. Subsequently, secondary antibodies were applied, with Alexa Fluor 488 and 568 (both at 1:700) used for FLAG-eGFP-

Miro1 and MAP2, respectively, and Alexa Fluor 647 (at 1:500) used for ATP5A. The samples were then mounted in mounting media, and images were acquired using a Nikon ECLIPSE Ti2 microscope equipped with a 60X oil objective lens. In the merged image, differences in the localization of the FLAG-eGFP-Miro1 signal on mitochondria (HSP60) can be observed. While there is overlap between the two signals in certain regions of axons, there are also areas where one of the signals are absent and there is no overlap between them.

## **6 Discussion:**

The goal of my Ph.D. research, as part of the MitoDive consortium with the focus on mitochondrial diversity, was to investigate the potential functional and biochemical diversity between endogenous Miro1 and Miro2 proteins as outer mitochondrial membrane protein involved in mitochondrial trafficking within neuronal and non-neuronal cells. My aim was to gain insight into how it influences the characteristics of mitochondrial movement, which is highly important for cellular health and survival. There is a connection between impaired mitochondrial trafficking and the onset and disease progression, especially neurodegenerative diseases, such as Parkinson and Alzheimer's. To achieve our goal, I employed Crispr Cas9 Knock-in technology to specifically label endogenous Miro1 and Miro2 proteins, enabling us to study them under conditions that closely mimic normal physiological condition. Due to the critical role of mitochondrial trafficking in maintaining the health and functionality of neurons, our ultimate goal was to investigate the distinction between Miro1 and Miro2, key components of the mitochondrial motility machinery, specifically within neuronal cells. However, I encountered several limitations when setting up our experimental model. We were confronted with the challenge of not being able to utilize the Crispr knock-in technique in neurons. This limitation stemmed from the fact that neurons are primary cells with a limited lifespan in vitro, making them not suitable for long experiments involving Crispr technology. Because neurons do not divide, every neuron would need to undergo its own Crispr even and might therefore be a heterogenous collection of recombination events some of which might include deletions or partial insertions. Creating Crispr Miro1 and Miro2 Knock-in mouse lines and subsequently extracting neurons from these mice for our experiment was a feasible option. However, there were practical challenges that I encountered. Firstly, our laboratory lacked the necessary facilities for generating mouse knock-in lines. Additionally, the process of developing these mouse lines was time-consuming. An alternative option was to generate our knock-in of interest in human induced pluripotent stem cells (iPSCs) and then differentiate them into neurons for our experimental model. However, there were limitations for using this approach, mainly due to the absence of iPSC culture facilities in our laboratory and lack of experience. While we considered the possibility of establishing iPSC lines in my supervisor's lab

in Boston, the global health crisis caused by the COVID-19 pandemic prevented us from pursuing this avenue.

Consequently, we decided to use a cell line that could be differentiated into neurons to facilitate the creation of knock-ins for our study. We selected the SH-SY5Y neuroblastoma cell line, which originates from humans and can be induced to differentiate into neuron-like cells. Working with these cells posed its own set of challenges, including very low transfection efficiency and slow growth rates. Additionally, the high sensitivity of SH-SY5Y cells to in vitro culture conditions required special maintenance. Moreover, generating the desired knock-ins in this cell line proved to be challenging, not only due to the low transfection efficiency, but also due to the infrequent occurrence of recombination events occurring during mitosis in the G2 and S phases as is needed to knock-in a gene. These limitations significantly reduced the probability of obtaining the desired knock-ins. Nevertheless, our research goal forced us to accept these challenges. I pursued the creation of SH-SY5Y cells expressing stably Miro1 and Miro2 knock-ins. Initially, I adopted the general approach widely employed for establishing stable knock-in cell lines. This process involved transfection, puromycin selection, seeding single cells at low density, identifying wells containing single clones displaying a positive fluorescent signal, expanding the colonies, conducting PCR genotyping, and analyzing protein expression in the selected clones. Regrettably, despite multiple attempts utilizing this method, I did not achieve our objective of generating Miro1 and Miro2 knock-in cell lines. Several potential factors contributed to this outcome. The exceptionally low transfection and recombination efficiency, low survival and growth rate of single clones combined with the screening of a small fraction of the cell population, made the identification of positive cells within a large population exceedingly challenging. Additionally, our reliance on fluorescent signals for the selection of single clones led to chasing false positives from background or autofluorescence. I could not discern a clear and legitimate signal over this background and therefore could never select single clones that lacked a convincing fluorescent signal but may have possessed the desired knock-in modification. Subsequently, we came up with a novel strategy, referred to as the "enrichment approach," to increase the chance of finding positive cells within a large population. This method involved PCR pools of cells, rather than relying on a fluorescent signal, to find a pool that contained the desired positive cells prior low-density cell seeding and further PCR genotyping. While sorting the cells based on

fluorescent signals using FACS machine was an option, we were concerned that weak signals over background fluorescence might also prevent the sorter from differentiating between genuine signals and auto-fluorescent false positives. PCR genotyping proved to be a reliable strategy, although finding an appropriate primer set that would yield specific results was challenging too. To ensure that the PCR band originated from the genomic region rather than the HDR template, I designed the primer pairs in such a way that either the forward or reverse primer bound outside the homology arm, while the other primer bound inside the insert. In theory, this approach should have provided a straightforward PCR result. However, in practice, I encountered an unexpected outcome: unspecific bands of the same size as the expected Knock-in band appeared in the Wild type sample I used as a negative control. To prevent the unintended integration of inserts at nonspecific sites, I made the strategic choice to have a long homology arm of 800 base pairs. Since the genomic region of both Miro1 and Miro2 genes for the left homology arm were relatively small, I incorporated sequences from an upstream neighbor gene, which was part of a long non-coding RNA containing high GC and repetitive sequences. In addition, the reverse primer of the right primer set primarily targeted the intronic region, which also exhibited a high GC content and contained repetitive sequences. Ultimately, having these features increased the probability of binding the primers to other sites in the genome even with partial homology and result in unspecific amplification. I always checked for unspecific binding of primers using PrimerBlast and I picked ones that were theoretically negative. This issue kept me busy over a span of more than six months and I dedicated considerable time to designing tens of primer pairs, utilizing different Taq polymerases and varying PCR conditions, and running hundreds of agarose gels to identify suitable primer pairs that would yield specific results. Finally, the combination of the enrichment approach and reliance on PCR genotyping proved successful in identifying several pure clones with the desired Flag-GFP-Miro1 Knock-in. Unfortunately, even this approach failed to identify MYC-mRFP-Miro2 Knock-in SH-SY5Y. I later realized that the primer sets I initially used for PCR genotyping in the enrichment step to find positive MYC-mRFP-Miro2 Knock-in population was misleading, as the forward and reverse primers of the left and right primer sets themselves could amplify a PCR product of the same size as the Knock-in size (Figure 5-10 A). Later, I overcame this challenge by using AmpliTaq Gold™ Fast PCR Master

Mix from Thermo Fisher, specifically designed for amplifying high GC content and complex sequences (Figure 5-10 B).

The difficulties of working with the SH-SY5Y cells prompted me to switch to HeLa cells, an easier cell with a higher transfection efficiency and faster growth rate. Because it is also a human cell line, it did not require redesign of the HDR, gRNA, or primer sets. Application of the enrichment approach beside PCR genotyping using AmpliTaq Gold™ Fast PCR Master Mix and RHOT2-combination and right primer sets enabled me successfully to identify MYC-mRF-Miro2 Knock-in pure homozygous HeLa clones (Figure 5-11). I am proud that I could make Miro1-Miro2 double Knock-in HeLa cells too, which is a precious tool to achieve our study objectives.

Reflecting on the challenges encountered while working to establish a stable Knock-in cell line, especially in SH-SY5Y has prompted me to consider what changes I would make if I was to embark on this journey again. To start anew, I would opt for a more manageable cell line, such as HeLa or Hek293, for initial protocol development rather than starting with SH-SY5Y cells. After successfully establishing the protocol with these cell lines, I would then transition to working with SH-SY5Y cells, leveraging the experience and protocol gained to create Knock-ins in this specific cell line. Using HeLa or Hek293 cells offers several advantages for establishing a Knock-in protocol. Firstly, these cell lines exhibit higher transfection efficiency, increasing the number of positive Knock-in cells and simplifying their identification within a mixed population. Additionally, their rapid growth rate proves beneficial, particularly when dealing with the establishment of stable cell lines, which typically spans several weeks. In the case of HeLa cells, the entire process took only two months until I obtained single clones, whereas the SH-SY5Y Knock-in protocol required almost double the time, spanning four months. Furthermore, I realized that HeLa cells are less sensitive to low-density culture and less prone to dissociation-induced apoptosis compared to SH-SY5Y cells. This observation was supported by our findings that I obtained more single clones when single-seeding HeLa cells, increasing the likelihood of discovering positive clones among them. Moreover, it's worth noting that the faint signals observed hindered our ability to perform live imaging, a crucial aspect of my project aimed at studying the impact of each Miro isoform's localization on mitochondrial dynamic parameters such as run and pause times, direction, and velocity of movement. Therefore, in a fresh attempt, I would select a highly bright and live imaging-compatible

fluorescent tag, such as tdTomato and mCherry, both of which are brighter and more photostable than eGFP and mRFP (Campbell et al., 2020; Shaner et al., 2005). Another viable option would involve utilizing the Halo tag to create a Knock-in protein instead of tagging the protein with both epitope and fluorescent tag. This tag can covalently bind to a Halo tag ligand, enabling protein purification, labeling, immobilization, and imaging (England et al., 2015). Regarding the components required for Crispr Knock-in of a gene, instead of using a plasmid, I would opt for Ribonucleoprotein (RNP). RNP is less toxic to cells, reducing the incidence of cell death. It does not integrate into the host genome and accelerates genome editing due to the elimination of the need for intracellular transcription and translation. This approach also reduces off-target effects, since RNP has a shorter lifespan compared to plasmids inside cells (F. Chen et al., 2020; Vakulskas et al., 2018; Z. Zhang et al., 2017). Considering the opportunity to work in my supervisor's lab in Boston, where there are well-equipped facilities for to work with induced pluripotent stem cells (iPSCs), another available alternative approach is the utilization of these cells to make Miro1 and Miro2 Knock-ins. iPSCs can be derived from either embryonic cells or adult somatic cells, exhibiting a remarkable capacity for reprogramming, rapid proliferation, and differentiation into a diverse array of highly specialized cell types, including neurons. This aligns with our primary objective of studying functional differences of Miro1 and Miro2 in neuronal cells. Moreover, iPSCs mimic the authentic human physiological conditions, making them an interesting experimental model for both fundamental research and studies related to diseases and the obtained data from them are more reliable compared to data derived from animal models. Notably, the CRISPR-Cas9 technology has been extensively employed for gene Knock-out, Knock-in, correction, activation, and repression in iPSCs for both basic research and disease-focused inquiries, offering a plenty of references for troubleshooting if the need arises (X. F. Li et al., 2019; Z. Zhang et al., 2017). Additionally, it's worth noting that HeLa cells, HeK cells, and iPSCs all originate from human cells. Consequently, if I decide to establish Knock-in protocol first in one of HeK or HeLa cell line and then move to iPSC I can be confident that the same protocol can be readily adapted for use with iPSCs because of their similar origin.

For the immunoprecipitation (IP) aspect, my initial approach involved utilizing Flag-GFP-Miro1 Knock-in SH-SY5Y and MYC-mRFP-Miro2 Knock-in HeLa cells to pull down either Miro1 fusion protein or Miro2 fusion protein. The goal was to investigate whether the other Miro isoform acted as a binding partner and if they formed heterodimers. Various IP conditions were tested, including different detergents (Triton and NP40), high and low salt washing buffers, diverse types of beads (MYC agarose beads, MYC, mRFP, and GFP agarose magnetic beads from ChromoTek, and MYC agarose magnetic beads from Cell Signaling Technology), and varying incubation times. Additionally, both tag-specific and endogenous antibodies were used to detect Miro1 or Miro2 as interacting partners. Immunoblotting analysis was performed using anti-Miro1 and anti-Miro2 endogenous antibodies in the IP experiments conducted on single knock-in cells (MYC-mRFP-Miro2 Knock-in HeLa cells and Flag-GFP-Miro1 Knock-in SH-SY5Y cells). However, the results obtained from these efforts either showed no association or revealed bands at the expected size in both the Knock-in IP lane and the WT IP Lane. One common method to preserve protein-protein interactions involves using Paraformaldehyde (PFA) as a cross-linker, which is widely used to maintain such interactions in cells, tissues, and sometimes entire organisms (Sutherland et al., 2008). I attempted to crosslink the Flag-GFP-Miro1 SH-SY5Y knock-in cells with 0.1% PFA before conducting IP experiments to preserve interactions between Miro proteins. But this approach did not yield different results (Figure 5-16 C). Besides the possibility that endogenous Miro1 and Miro2 do not interact with each other, another potential issue could be the lack of a good and specific antibody for detecting endogenous Miro1 and Miro2. This is especially relevant since I detected unspecific bands in the WT IP Lane using these antibodies. Given this context, the creation of double Flag-GFP-Miro1/MYC-mRFP-Miro2 Knock-in HeLa cells became a valuable tool since I could use tag specific antibodies which are more specific than endogenous antibodies and can detect even weak signals in cases of weak interactions between the proteins of interest. Having DMK1 cells, I applied all the aforementioned conditions to perform GFP or MYC IP experiments out of DMK1 cells. Immunoblotting analysis of GFP IP and MYC IP was carried out using anti-MYC CS and anti-GFP CS to determine whether MYC-mRFP-Miro2 or Flag-GFP-Miro1 was pulled down with the other Miro fusion protein. Through this strategy, I was

unable to detect specific interactions between Miro fusion proteins. In particular, in the case of the MYC IP experiment, including Flag-GFP-Miro1 Knock-in SH-SY5Y cells as an additional negative control revealed that the GFP fusion protein exhibited high nonspecific binding affinity to MYC magnetic beads, even when no MYC fusion protein was present. Consequently, I could not consider the GFP band in the Miro DK1 MYC IP Lane as a genuine interaction. These IP results, in conjunction with preliminary Proximity Ligation Assay (PLA) results using anti-GFP and anti-MYC CS antibodies (which were also used for IP samples' immunoblotting analysis), suggest that Miro1 and Miro2 are in close proximity to each other on the mitochondria. This led us to consider that they might interact with different protein complexes rather than directly interacting with each other. However, Ismael, a postdoc in the Schwarz Lab in Boston, found that tagged Miro1 forms homodimers and heterodimerizes with tagged Miro2 when overexpressed in HEK293T cells. Additionally, it has been reported that endogenous Miro1 co-immunoprecipitated with overexpressed peroxisomal Miro1 (PEX-Miro1) in HEK293 cells (K. J. Davis, 2020). Furthermore, in addition to investigating Miro1-Miro2 interaction, I explored interactions between Flag-GFP-Miro1 and MYC-mRFP-Miro2 proteins and the motor-adaptor protein complex TRAK1/TRAK2 and kinesin in every MYC or GFP IP experiment conducted on single or double Miro Knock-in cells. However, I did not detect any specific interactions between TRAK1/2 and kinesin with either Miro1 or Miro2 fusion proteins. Even overexpressing GFP-TRAK1 did not yield any differences in pulling down TRAK1 with Flag-GFP-Miro1 protein. Nevertheless, it has been demonstrated that KiF5C and TRAK1/TRAK2 colocalized on peroxisomes when co-expressed with PEX-Miro1, but no co-assembly of TRAK1/2 or Kinesin was reported when PEX-Miro2 was overexpressed in HEK293T cells (K. Davis et al., 2023). On the other hand, another study showed that in Double Miro Knock-out Mouse embryonic fibroblast cells, TRAK1 and TRAK2 could still localize on mitochondria, suggesting the possibility of the presence of other protein acceptors for TRAK1/2 on the mitochondria (Norkett et al., 2018). Moreover, in the immunoblotting analysis of MYC IP samples, I probed for endogenous MYO19, as it has been reported as a binding partner of Miro2. Under none of the different IP conditions did endogenous MYO19 interact with Miro2 fusion protein. This finding contradicts reports that describe Miro1 and Miro2 as the mitochondrial receptors of MYO19 and assert that MYO19's interaction with Miro1/2

is essential for MYO19 stability (Bocanegra et al., 2020; K. Davis et al., 2023; Norkett et al., 2018; Oeding et al., 2018).

As stated in the results section, in general there are some possible explanations for these opposing IP outcomes. Firstly, all the studies that reported these interactions relied on an overexpression system. Though overexpressing a protein has some advantages, it also comes with disadvantages too. In these systems, target proteins are often overexpressed as fusions with a reporter, easing purification and localization studies by usage of tag-specific antibodies rather than endogenous antibodies, which are typically less specific and may detect many non-specific proteins. Furthermore, increasing the protein expression levels are particularly advantageous for investigating low-abundance proteins that are challenging to detect at their endogenous levels. However, the overexpression of proteins typically results in significantly higher cellular protein levels compared to their endogenous counterparts, potentially leading to an imbalance in stoichiometry. This disruption of the natural protein stoichiometry within a cell could contribute to expression artifacts, such as non-specific protein-protein interactions (Moriya, 2015; Schwinn et al., 2020). Therefore, the reported Miro1-Miro1 or Miro1-Miro2 interactions may be due to the nature of the overexpression system which is not reflecting their real interactions at the endogenous level. Based on our IP result saying that there is no interaction between Miro1 and Miro2 and the PLA result which showing that Flag-GFP-Miro1 and MYC-mRFP-Miro2 are located in a close proximity of each other on mitochondrial surface, we conclude that Flag-GFP-Miro1 and MYC-mRFP-Miro2 mark the same mitochondrial population and there is no diversity in this regard but they are not present in the same protein complex meaning there might be a diversity in terms of their interaction partner. It has been reported that the number of micro-tubule-mediated mitochondrial trafficking events was significantly reduced in Miro1<sup>KO</sup> cells but was not changed in Miro2<sup>KO</sup> cells (Norkett et al., 2018). In another study, it was demonstrated that TRAK1/2 and kinesin did not co-assemble with PEX-Miro2 on peroxisomes, and no peroxisomal movement was observed. However, in the case of PEX-Miro1, TRAK1/2 and kinesin were found to colocalize with it on peroxisomes, leading the movement of peroxisomes from the prenuclear region to the cell periphery.(K. Davis et al., 2023). All these data support our hypothesis that there should be a diversity in regarding Miro1 and Miro2 binding partners resulting to their functional differences. To confirm this hypothesis mass

spectrometry analysis would be the best option. Sending sample for mass spectrometry would give us the possibility of finding each Miro isoform binding partners and see if they have overlapping or complementary functions regarding to mitochondrial movement characteristics like the directionality of movement, stop and run time, velocity and other mitochondrial functions. We believe, Due to the high abundance of overexpressed proteins, more interactions may occur, increasing the likelihood of detecting them through immunoprecipitation methods, even if some interactions are lost during the immunoprecipitation (IP) process. Conversely, the lower abundance of endogenous proteins and the transient nature of interactions between Miro proteins and motor-adaptor protein complexes may result in the loss of interactions during IP. Therefore, the cross-linking method is a good strategy to preserve protein-protein interaction before doing IP. For this purpose, setting up the cross-linking protocol is necessary. Application of a higher concentration of PFA, previously I used 0.1 %, extending the incubation time, or employing an alternative cross-linker such as Disuccinimidyl Glutarate (DSG), which has been successfully used to maintain protein-protein interactions in HeLa cells(Nowak et al., 2005), might help us preserve these interactions, if there are any, and detect them after IP experiments through immunoblotting. Furthermore, we believe that the IP conditions I have used may not be optimal for preserving transient interactions between Miro proteins and motor-adaptor protein complex. Therefore, further optimization of these conditions could be beneficial in co-precipitating these complexes effectively. Moreover, blocking the beads with BSA or pre clearing beads with plain magnetic beads might be helpful to reduce the non-specific binding of the protein to the beads thereby increasing the chance of specific interaction detection. In the context of our imaging efforts, while I have obtained promising results, there is still a need to improve our protocol to enhance the overall outcome. This is particularly critical for expansion microscopy, where a significant portion of the signals has been lost, necessitating further optimization to improve signal retention. One crucial aspect of achieving this improvement lies in enhancing the attachment of linker groups to the primary amines within the samples, as a crucial step in preserving a greater number of fluorophores. Notably, since some fluorophores are sensitive to acidic pH levels, a recommended adjustment involves diluting the anchoring solution in sodium bicarbonate pH of 8.3 instead of PBS pH 7.0–7.5. This modification has been reported as effective in

increasing anchoring efficiency, ultimately resulting in enhanced fluorophore retention. (Truckenbrodt et al., 2019).

## 7 Summarizing Remarks and future perspectives

In summary, given the limited three-year timeframe for this PhD project, I was able to successfully establish Flag-GFP-Miro1 knock-in stable SH-SY5Y cell line, MYC-mRFP-Miro2 knock-in stable HeLa cell line and Flag-GFP-Miro1/MYC-mRFP-Miro2 double knock-in stable HeLa cell line, Miro<sup>DKI</sup>. Using immunoprecipitation, I could show that endogenous Flag-GFP-Miro1 and MYC-mRFP-Miro2 proteins do not interact with each other under normal physiological conditions, except when they are overexpressed. However, they were found to be localized on the same mitochondria in a close proximity of 40 nanometers, as evidenced by the Proximity Ligation Assay (PLA) results, suggesting that they might be part of different protein complexes make them specified for different functions related to mitochondrial movement machinery. Based on result of several studies using overexpression and knock-out system we think that endogenous Miro1 and Miro2 proteins bind preferentially to specific protein complex and there are functional differences between Miro1 and Miro2 proteins based on the protein complex they interact with. With this background, I conducted various tests using different immunoprecipitation (IP) conditions to detect the interaction between Miro and the motor-adaptor complex protein. Additional protocol optimization is required to enable the detection of this interaction through mass spectrometry analysis. I also successfully implemented the SH-SY5Y differentiation protocol to differentiate Flag-GFP-Miro1 Knock-in SH-SY5Y cells into neurons. This differentiation process aimed to study the Flag-GFP-Miro1 localization on mitochondria in neuronal like cells. To further improve image resolution and gain a more detailed understanding of Flag-GFP-Miro1 and MYC-mRFP-Miro2 protein localization and distribution on mitochondria, I initiated expansion microscopy, a valuable method for achieving higher resolution images. Looking ahead, the project's future prospects involve three main directions. Firstly, I plan to perform the final optimization of the immunoprecipitation (IP) protocol to identify the optimal conditions that preserve Miro proteins interactions with binding partners, followed by sending the samples for mass spectrometry analysis. Secondly, PLA experiment to detect Flag-GFP-Miro1 and MYC-mRFP-Miro2 interaction with the motor-adaptor complex protein is planned to do. Thirdly, I intend to optimize the imaging protocols to obtain high/super-resolution images, which will facilitate precise localization and distribution studies. Thirdly, there is the exciting opportunity to explore lipidomics and proteomics

studies using these cell lines, which has not yet been addressed at the endogenous level. To achieve this, it will be necessary to develop a protocol for the specific isolation of mitochondria containing each isoform, allowing us to evaluate the potential impact of each isoform on the protein and lipid profiles of these mitochondria. In summary, achieving the objectives of this study could significantly enhance our understanding of endogenous Miro1 and Miro2 functional specificity, if any, within the context of the mitochondrial movement machinery, which is crucial for cellular health and proper function.

## 8 References

- Abraham, Z., Hawley, E., Hayosh, D., Webster-Wood, V. A., & Akkus, O. (2018). Kinesin and Dynein Mechanics: Measurement Methods and Research Applications. *Journal of Biomechanical Engineering*, 140(2). <https://doi.org/10.1115/1.4037886>
- Alberts B., Johnson A., & Lewis J. (2002). Molecular Motors. In *Molecular Biology of the Cell* (4th ed.). Garland Science.
- Ban, T., Ishihara, T., Kohno, H., Saita, S., Ichimura, A., Maenaka, K., Oka, T., Mihara, K., & Ishihara, N. (2017). Molecular basis of selective mitochondrial fusion by heterotypic action between OPA1 and cardiolipin. *Nature Cell Biology*, 19(7), 856–863. <https://doi.org/10.1038/ncb3560>
- Beljan, S., Herak Bosnar, M., & Četković, H. (2020). Rho Family of Ras-Like GTPases in Early-Branching Animals. In *Cells* (Vol. 9, Issue 10). NLM (Medline). <https://doi.org/10.3390/cells9102279>
- Biedler, J. L., Helson, L., & Spengler, B. A. (n.d.). *Morphology and Growth, Tumorigenicity, and Cytogenetics of Human Neuroblastoma Cells in Continuous Culture*1. <http://aacrjournals.org/cancerres/article-pdf/33/11/2643/2390476/cr0330112643.pdf>
- Bocanegra, J. L., Fujita, B. M., Melton, N. R., Cowan, J. M., Schinski, E. L., Tamir, T. Y., Major, M. B., & Quintero, O. A. (2020). The MyMOMA domain of MYO19 encodes for distinct Miro-dependent and Miro-independent mechanisms of interaction with mitochondrial membranes. *Cytoskeleton*, 77(3–4), 149–166. <https://doi.org/10.1002/cm.21560>
- Boureau, A., Vignal, E., Faure, S., & Fort, P. (2007). Evolution of the Rho family of Ras-like GTPases in eukaryotes. *Molecular Biology and Evolution*, 24(1), 203–216. <https://doi.org/10.1093/molbev/msl145>
- Brickley, K., & Stephenson, F. A. (2011). Trafficking kinesin protein (TRAK)-mediated transport of mitochondria in axons of hippocampal neurons. *Journal of Biological Chemistry*, 286(20), 18079–18092. <https://doi.org/10.1074/jbc.M111.236018>
- Campbell, B. C., Nabel, E. M., Murdock, M. H., Lao-Peregrin, C., Tsoulfas, P., Blackmore, M. G., Lee, F. S., Liston, C., Morishita, H., Petsko, G. A., & Appel Alzheimer, R. (2020). *mGreenLantern: a bright monomeric fluorescent protein with rapid expression and cell filling properties for neuronal imaging*. 117(48), 30710–30721. <https://doi.org/10.1073/pnas.2000942117/-DCSupplemental>
- Canty, J. T., Hensley, A., Aslan, M., Jack, A., & Yildiz, A. (2023). TRAK adaptors regulate the recruitment and activation of dynein and kinesin in mitochondrial transport. *Nature Communications*, 14(1), 1376. <https://doi.org/10.1038/s41467-023-36945-8>
- Çelen, E. (2018). The Role of Mitochondrial Dysfunction in the Mechanism of Neurodegenerative Diseases. *Archives in Neurology & Neuroscience*, 1(4). <https://doi.org/10.33552/ann.2018.01.000520>
- Chen, B., Gilbert, L. A., Cimini, B. A., Schnitzbauer, J., Zhang, W., Li, G. W., Park, J., Blackburn, E. H., Weissman, J. S., Qi, L. S., & Huang, B. (2013). Dynamic imaging of genomic loci in living human cells by an optimized CRISPR/Cas system. *Cell*, 155(7), 1479–1491. <https://doi.org/10.1016/j.cell.2013.12.001>
- Chen, F., Alphonse, M., & Liu, Q. (2020). Strategies for nonviral nanoparticle-based delivery of CRISPR/Cas9 therapeutics. In *Wiley Interdisciplinary Reviews: Nanomedicine and Nanobiotechnology* (Vol. 12, Issue 3). Wiley-Blackwell.

- <https://doi.org/10.1002/wnan.1609>
- Chen, F., Tillberg, P. W., & Boyden, E. S. (2015). Expansion microscopy. *Science*, 347(6221), 543–548. <https://doi.org/10.1126/science.1260088>
- Chen, Y., & Sheng, Z. H. (2013). Kinesin-1-syntrophin coupling mediates activity-dependent regulation of axonal mitochondrial transport. *Journal of Cell Biology*, 202(2), 351–364. <https://doi.org/10.1083/jcb.201302040>
- Cheng, A., Hou, Y., & Mattson, M. P. (2010). Mitochondria and neuroplasticity. In *ASN Neuro* (Vol. 2, Issue 5, pp. 243–256). Portland Press Ltd. <https://doi.org/10.1042/AN20100019>
- Chozinski, T. J., Halpern, A. R., Okawa, H., Kim, H. J., Tremel, G. J., Wong, R. O. L., & Vaughan, J. C. (2016). Expansion microscopy with conventional antibodies and fluorescent proteins. *Nature Methods*, 13(6), 485–488. <https://doi.org/10.1038/nmeth.3833>
- Cooper GM. (2000a). Microtubule Motors and Movements. In *The Cell: A Molecular Approach* (2nd ed.). Sinauer Associates.
- Cooper GM. (2000b). The Development and Causes of Cancer. In *The Cell: A Molecular Approach*. (2nd ed.). Sinauer Associates.
- Cooper GM., & Adams K. (2022). Microtubule Motors and Movements. In *The Cell: A Molecular Approach* (9th ed.). Sinauer Associates.
- Cunniff, B., McKenzie, A. J., Heintz, N. H., & Howe, A. K. (2016). AMPK activity regulates trafficking of Mitochondria to the leading-edge during cell migration and matrix invasion. *Molecular Biology of the Cell*, 27(17), 2662–2674. <https://doi.org/10.1091/mbc.E16-05-0286>
- Cytoplasmic dynein subunit heterogeneity: implications for axonal transport. (2000). In *Journal of Neurocytology* (Vol. 29).
- Davis, K., Basu, H., Izquierdo-Villalba, I., Shurberg, E., & Schwarz, T. L. (2023). Miro GTPase domains regulate the assembly of the mitochondrial motor-adaptor complex. *Life Science Alliance*, 6(1). <https://doi.org/10.26508/lsa.202201406>
- Davis, K. J. (2020). *Functional analysis of Miro GTPase domains in the mitochondrial motor adaptor complex A dissertation presented*.
- Detmer, S. A., & Chan, D. C. (2007a). Complementation between mouse Mfn1 and Mfn2 protects mitochondrial fusion defects caused by CMT2A disease mutations. *Journal of Cell Biology*, 176(4), 405–414. <https://doi.org/10.1083/jcb.200611080>
- Detmer, S. A., & Chan, D. C. (2007b). Functions and dysfunctions of mitochondrial dynamics. In *Nature Reviews Molecular Cell Biology* (Vol. 8, Issue 11, pp. 870–879). <https://doi.org/10.1038/nrm2275>
- Ding, L., Lei, Y., Han, Y., Li, Y., Ji, X., & Liu, L. (2016). Vimar Is a Novel Regulator of Mitochondrial Fission through Miro. *PLoS Genetics*, 12(10). <https://doi.org/10.1371/journal.pgen.1006359>
- Drerup, C. M., Herbert, A. L., Monk, K. R., & Nechiporuk, A. V. (2017). *Regulation of mitochondria-dynactin interaction and mitochondrial retrograde transport in axons*. <https://doi.org/10.7554/eLife.22234.001>
- Eberhardt, E. L., Ludlam, A. V., Tan, Z., & Cianfrocco, M. A. (2020). Miro: A molecular switch at the center of mitochondrial regulation. In *Protein Science* (Vol. 29, Issue 6, pp. 1269–1284). Blackwell Publishing Ltd. <https://doi.org/10.1002/pro.3839>
- Emptage, N. J., Reid, C. A., & Fine, A. (n.d.). Calcium Stores in Hippocampal Synaptic Boutons Mediate Short-Term Plasticity, Store-Operated Ca<sup>2+</sup> Entry, and Spontaneous Transmitter Release sidered to function mainly in calcium

- sequestration and buffering (Blaustein et al., 1978b), although release of Ca<sup>2+</sup> from stores has been implicated in the mediation of afterhyperpolarization following action potentials (Sah and McLachlan, 1991) and in generating glutamate receptor-gated postsynaptic calcium transients (Llano et al. In *Neuron* (Vol. 29).
- Engelhart, E. A., & Hoppins, S. (2019). A catalytic domain variant of mitofusin requiring a wildtype paralog for function uncouples mitochondrial outer membrane tethering and fusion. *Journal of Biological Chemistry*, 294(20), 8001–8014. <https://doi.org/10.1074/jbc.RA118.006347>
- England, C. G., Luo, H., & Cai, W. (2015). HaloTag Technology: A Versatile Platform for Biomedical Applications. *Bioconjugate Chemistry*, 26(6), 975–986. <https://doi.org/10.1021/acs.bioconjchem.5b00191>
- Evinova, A., Cizmarova, B., Hatokova, Z., & Racay, P. (2020). High-Resolution Respirometry in Assessment of Mitochondrial Function in Neuroblastoma SH-SY5Y Intact Cells. *Journal of Membrane Biology*, 253(2), 129–136. <https://doi.org/10.1007/s00232-020-00107-4>
- Fatiga, F. F., Wang, L. jie, Hsu, T., Capuno, J. I., & Fu, C. yu. (2021). Miro1 functions as an inhibitory regulator of MFN at elevated mitochondrial Ca<sup>2+</sup> levels. *Journal of Cellular Biochemistry*, 122(12), 1848–1862. <https://doi.org/10.1002/jcb.30138>
- Fenton, A. R., Jongens, T. A., & Holzbaur, E. L. F. (2021). Mitochondrial adaptor TRAK2 activates and functionally links opposing kinesin and dynein motors. *Nature Communications*, 12(1). <https://doi.org/10.1038/s41467-021-24862-7>
- Fonseca, T. B., Sánchez-Guerrero, Á., Milosevic, I., & Raimundo, N. (2019). Mitochondrial fission requires DRP1 but not dynamins. In *Nature* (Vol. 570, Issue 7761, pp. E34–E42). Nature Publishing Group. <https://doi.org/10.1038/s41586-019-1296-y>
- Frederick, R. L., McCaffery, J. M., Cunningham, K. W., Okamoto, K., & Shaw, J. M. (2004). Yeast Miro GTPase, Gem1p, regulates mitochondrial morphology via a novel pathway. *Journal of Cell Biology*, 167(1), 87–98. <https://doi.org/10.1083/jcb.200405100>
- Genova, M. L., & Lenaz, G. (2014). Functional role of mitochondrial respiratory supercomplexes. *Biochimica et Biophysica Acta (BBA) - Bioenergetics*, 1837(4), 427–443. <https://doi.org/10.1016/J.BBABIO.2013.11.002>
- Ghosh, D., Venkataramani, P., Nandi, S., & Bhattacharjee, S. (2019). CRISPR-Cas9 a boon or bane: The bumpy road ahead to cancer therapeutics 06 Biological Sciences 0604 Genetics. In *Cancer Cell International* (Vol. 19, Issue 1). BioMed Central Ltd. <https://doi.org/10.1186/s12935-019-0726-0>
- Gilbert, L. A., Larson, M. H., Morsut, L., Liu, Z., Brar, G. A., Torres, S. E., Stern-Ginossar, N., Brandman, O., Whitehead, E. H., Doudna, J. A., Lim, W. A., Weissman, J. S., & Qi, L. S. (2013). XCRISPR-mediated modular RNA-guided regulation of transcription in eukaryotes. *Cell*, 154(2), 442. <https://doi.org/10.1016/j.cell.2013.06.044>
- Glater, E. E., Megeath, L. J., Stowers, R. S., & Schwarz, T. L. (2006). Axonal transport of mitochondria requires mlt1 to recruit kinesin heavy chain and is light chain independent. *Journal of Cell Biology*, 173(4), 545–557. <https://doi.org/10.1083/jcb.200601067>
- Gleave, E. S., Schmidt, H., & Carter, A. P. (2014). A structural analysis of the AAA+ domains in *Saccharomyces cerevisiae* cytoplasmic dynein. *Journal of Structural Biology*, 186(3), 367–375. <https://doi.org/10.1016/j.jsb.2014.03.019>
- Guo, X., Macleod, G. T., Wellington, A., Hu, F., Panchumarthi, S., Schoenfield, M.,

- Marin, L., Charlton, M. P., Atwood, H. L., & Zinsmaier, K. E. (2005). The GTPase dMiro is required for axonal transport of mitochondria to drosophila synapses. *Neuron*, *47*(3), 379–393.  
<https://doi.org/10.1016/j.neuron.2005.06.027>
- Gutnick, A., Banghart, M. R., West, E. R., & Schwarz, T. L. (2019). The light-sensitive dimerizer zapalog reveals distinct modes of immobilization for axonal mitochondria. *Nature Cell Biology*, *21*(6), 768–777.  
<https://doi.org/10.1038/s41556-019-0317-2>
- Han, X., Aslanian, A., & Yates, J. R. (2008). Mass spectrometry for proteomics. In *Current Opinion in Chemical Biology* (Vol. 12, Issue 5, pp. 483–490).  
<https://doi.org/10.1016/j.cbpa.2008.07.024>
- Hardy, J. (2010). Genetic analysis of pathways to parkinson disease. In *Neuron* (Vol. 68, Issue 2, pp. 201–206). Cell Press.  
<https://doi.org/10.1016/j.neuron.2010.10.014>
- Harris, J. J., Jolivet, R., & Attwell, D. (2012). Synaptic Energy Use and Supply. In *Neuron* (Vol. 75, Issue 5, pp. 762–777).  
<https://doi.org/10.1016/j.neuron.2012.08.019>
- Henrichs, V., Grycova, L., Barinka, C., Nahacka, Z., Neuzil, J., Diez, S., Rohlena, J., Braun, M., & Lansky, Z. (2020). Mitochondria-adaptor TRAK1 promotes kinesin-1 driven transport in crowded environments. *Nature Communications*, *11*(1).  
<https://doi.org/10.1038/s41467-020-16972-5>
- Hollenbeck, P. J. (1996). THE PATTERN AND MECHANISM OF MITOCHONDRIAL TRANSPORT IN AXONS. In *Frontiers in Bioscience* (Vol. 1).
- Hollenbeck, P. J., & Saxton, W. M. (n.d.). *The axonal transport of mitochondria*.
- Hoppins, S., Edlich, F., Cleland, M. M., Banerjee, S., McCaffery, J. M., Youle, R. J., & Nunnari, J. (2011). The Soluble Form of Bax Regulates Mitochondrial Fusion via MFN2 Homotypic Complexes. *Molecular Cell*, *41*(2), 150–160.  
<https://doi.org/10.1016/j.molcel.2010.11.030>
- Ishihara, N., Nomura, M., Jofuku, A., Kato, H., Suzuki, S. O., Masuda, K., Otera, H., Nakanishi, Y., Nonaka, I., Goto, Y. I., Taguchi, N., Morinaga, H., Maeda, M., Takayanagi, R., Yokota, S., & Mihara, K. (2009). Mitochondrial fission factor Drp1 is essential for embryonic development and synapse formation in mice. *Nature Cell Biology*, *11*(8), 958–966. <https://doi.org/10.1038/ncb1907>
- J Ford, M. G., Chappie, J. S., & Marijn J Ford, C. G. (2019). *The structural biology of the dynamin-related proteins: New insights into a diverse, multitalented family*.  
<https://doi.org/10.1111/tra.12676/Abstract>
- Jacquemet, G., Carisey, A. F., Hamidi, H., Henriques, R., & Leterrier, C. (2020). The cell biologist's guide to super-resolution microscopy. *Journal of Cell Science*, *133*(11). <https://doi.org/10.1242/jcs.240713>
- Kang, J.-S., Tian, J.-H., Pan, P.-Y., Zald, P., Li, C., Deng, C., & Sheng, Z.-H. (n.d.). *Docking of Axonal Mitochondria by Syntaphilin Controls their Mobility and Affects Short-term Facilitation*.
- Klosowiak, J. L., Focia, P. J., Chakravarthy, S., Landahl, E. C., Freymann, D. M., & Rice, S. E. (2013). Structural coupling of the EF hand and C-terminal GTPase domains in the mitochondrial protein Miro. *EMBO Reports*, *14*(11), 968–974.  
<https://doi.org/10.1038/embor.2013.151>
- Köfeler, H. C., Fauland, A., Rechberger, G. N., & Trötz Müller, M. (2012). Mass spectrometry based lipidomics: An overview of technological platforms. In *Metabolites* (Vol. 2, Issue 1, pp. 19–38). MDPI AG.  
<https://doi.org/10.3390/metabo2010019>

- Kovalevich, J., & Langford, D. (2013). Considerations for the use of SH-SY5Y neuroblastoma cells in neurobiology. *Methods in Molecular Biology*, 1078, 9–21. [https://doi.org/10.1007/978-1-62703-640-5\\_2](https://doi.org/10.1007/978-1-62703-640-5_2)
- Kruppa, A. J., & Buss, F. (2021). Motor proteins at the mitochondria–cytoskeleton interface. In *Journal of Cell Science* (Vol. 134, Issue 7). Company of Biologists Ltd. <https://doi.org/10.1242/jcs.226084>
- Lee, C. (n.d.). *Coimmunoprecipitation Assay*.
- Levi, T., Sloutskin, A., Kalifa, R., Juven-Gershon, T., & Gerlitz, O. (2020). Efficient in Vivo Introduction of Point Mutations Using ssODN and a Co-CRISPR Approach. *Biological Procedures Online*, 22(1). <https://doi.org/10.1186/s12575-020-00123-7>
- Li, X. F., Zhou, Y. W., Cai, P. F., Fu, W. C., Wang, J. H., Chen, J. Y., & Yang, Q. N. (2019). CRISPR/Cas9 facilitates genomic editing for large-scale functional studies in pluripotent stem cell cultures. In *Human Genetics* (Vol. 138, Issues 11–12, pp. 1217–1225). Springer. <https://doi.org/10.1007/s00439-019-02071-z>
- Li, X., Wang, R., Xun, X., Jiao, W., Zhang, M., Wang, S., Wang, S., Zhang, L., Huang, X., Hu, X., & Bao, Z. (2015). The Rho GTPase family genes in Bivalvia genomes: Sequence, evolution and expression analysis. *PLoS ONE*, 10(12). <https://doi.org/10.1371/journal.pone.0143932>
- Ligon, L. A., & Steward, O. (2000). Role of Microtubules and Actin Filaments in the Movement of Mitochondria in the Axons and Dendrites of Cultured Hippocampal Neurons Indexing terms: organelle transport; axonal transport; dendritic transport. In *J. Comp. Neurol* (Vol. 427).
- Liu, S., Sawada, T., Lee, S., Yu, W., Silverio, G., Alapatt, P., Millan, I., Shen, A., Saxton, W., Kanao, T., Takahashi, R., Hattori, N., Imai, Y., & Lu, B. (2012). Parkinson's disease-associated kinase PINK1 regulates miro protein level and axonal transport of mitochondria. *PLoS Genetics*, 8(3). <https://doi.org/10.1371/journal.pgen.1002537>
- Liu, Y., Wan, X., & Wang, B. (2019). Engineered CRISPRa enables programmable eukaryote-like gene activation in bacteria. *Nature Communications*, 10(1). <https://doi.org/10.1038/s41467-019-11479-0>
- Lopes, F. M., da Motta, L. L., De Bastiani, M. A., Pfaffenseller, B., Aguiar, B. W., de Souza, L. F., Zanatta, G., Vargas, D. M., Schönhofen, P., Londero, G. F., de Medeiros, L. M., Freire, V. N., Dafre, A. L., Castro, M. A. A., Parsons, R. B., & Klamt, F. (2017). RA Differentiation Enhances Dopaminergic Features, Changes Redox Parameters, and Increases Dopamine Transporter Dependency in 6-Hydroxydopamine-Induced Neurotoxicity in SH-SY5Y Cells. *Neurotoxicity Research*, 31(4), 545–559. <https://doi.org/10.1007/s12640-016-9699-0>
- López-Doménech, G., Covill-Cooke, C., Ivankovic, D., Halff, E. F., Sheehan, D. F., Norkett, R., Birsa, N., & Kittler, J. T. (2018). Miro proteins coordinate microtubule- and actin-dependent mitochondrial transport and distribution. *The EMBO Journal*, 37(3), 321–336. <https://doi.org/10.15252/embj.201696380>
- López-Doménech, G., Higgs, N. F., Vaccaro, V., Roš, H., Arancibia-Cárcamo, I. L., MacAskill, A. F., & Kittler, J. T. (2016). Loss of Dendritic Complexity Precedes Neurodegeneration in a Mouse Model with Disrupted Mitochondrial Distribution in Mature Dendrites. *Cell Reports*, 17(2), 317–327. <https://doi.org/10.1016/j.celrep.2016.09.004>
- Lumsden, A. L., Young, R. L., Pezos, N., & Keating, D. J. (2016). Huntingtin-associated protein 1: Eutherian adaptation from a TRAK-like protein, conserved gene promoter elements, and localization in the human intestine. *BMC*

- Evolutionary Biology*, 16(1). <https://doi.org/10.1186/s12862-016-0780-3>
- MacAskill, A. F., Rinholm, J. E., Twelvetrees, A. E., Arancibia-Carcamo, I. L., Muir, J., Fransson, A., Aspenstrom, P., Attwell, D., & Kittler, J. T. (2009). Miro1 Is a Calcium Sensor for Glutamate Receptor-Dependent Localization of Mitochondria at Synapses. *Neuron*, 61(4), 541–555. <https://doi.org/10.1016/j.neuron.2009.01.030>
- Matsuda, T., & Oinuma, I. (2019a). Optimized CRISPR/Cas9-mediated in vivo genome engineering applicable to monitoring dynamics of endogenous proteins in the mouse neural tissues. *Scientific Reports*, 9(1), 11309. <https://doi.org/10.1038/s41598-019-47721-4>
- Matsuda, T., & Oinuma, I. (2019b). Optimized CRISPR/Cas9-mediated in vivo genome engineering applicable to monitoring dynamics of endogenous proteins in the mouse neural tissues. *Scientific Reports*, 9(1), 11309. <https://doi.org/10.1038/s41598-019-47721-4>
- Mattson, M. P., Gleichmann, M., & Cheng, A. (2008). Mitochondria in Neuroplasticity and Neurological Disorders. In *Neuron* (Vol. 60, Issue 5, pp. 748–766). <https://doi.org/10.1016/j.neuron.2008.10.010>
- Mochida, S., Few, A. P., Scheuer, T., & Catterall, W. A. (2008). Regulation of Presynaptic CaV2.1 Channels by Ca<sup>2+</sup> Sensor Proteins Mediates Short-Term Synaptic Plasticity. *Neuron*, 57(2), 210–216. <https://doi.org/10.1016/j.neuron.2007.11.036>
- Modi, S., López-Doménech, G., Halff, E. F., Covill-Cooke, C., Ivankovic, D., Melandri, D., Lorena Arancibia-Cárcamo, I., Burden, J. J., Lowe, A. R., & Kittler, J. T. (n.d.). *Miro clusters regulate ER-mitochondria contact sites and link cristae organization to the mitochondrial transport machinery*. <https://doi.org/10.1038/s41467-019-12382-4>
- Molecular Motors - Molecular Biology of the Cell - NCBI Bookshelf*. (n.d.).
- Moriya, H. (2015). Quantitative nature of overexpression experiments. In *Molecular Biology of the Cell* (Vol. 26, Issue 22, pp. 3932–3939). American Society for Cell Biology. <https://doi.org/10.1091/mbc.E15-07-0512>
- Mórotz, G. M., De Vos, K. J., Vagnoni, A., Ackerley, S., Shaw, C. E., & Miller, C. C. J. (2012). Amyotrophic lateral sclerosis-associated mutant VAPBP56s perturbs calcium homeostasis to disrupt axonal transport of mitochondria. *Human Molecular Genetics*, 21(9), 1979–1988. <https://doi.org/10.1093/hmg/dds011>
- Morris, R. L., & Hollenbeck, P. J. (n.d.). *Axonal Transport of Mitochondria along Microtubules and F-Actin in Living Vertebrate Neurons*.
- Nahacka, Z., Novak, J., Zabalova, R., & Neuzil, J. (2022). Miro proteins and their role in mitochondrial transfer in cancer and beyond. In *Frontiers in Cell and Developmental Biology* (Vol. 10). Frontiers Media S.A. <https://doi.org/10.3389/fcell.2022.937753>
- Nahacka, Z., Zabalova, R., Dubisova, M., Rohlena, J., & Neuzil, J. (2021a). Miro proteins connect mitochondrial function and intercellular transport. In *Critical Reviews in Biochemistry and Molecular Biology* (Vol. 56, Issue 4, pp. 401–425). Taylor and Francis Ltd. <https://doi.org/10.1080/10409238.2021.1925216>
- Nahacka, Z., Zabalova, R., Dubisova, M., Rohlena, J., & Neuzil, J. (2021b). Miro proteins connect mitochondrial function and intercellular transport. In *Critical Reviews in Biochemistry and Molecular Biology* (Vol. 56, Issue 4, pp. 401–425). Taylor and Francis Ltd. <https://doi.org/10.1080/10409238.2021.1925216>
- Nahacka, Z., Zabalova, R., Dubisova, M., Rohlena, J., & Neuzil, J. (2021c). Miro proteins connect mitochondrial function and intercellular transport. In *Critical*

- Reviews in Biochemistry and Molecular Biology* (Vol. 56, Issue 4, pp. 401–425). Taylor and Francis Ltd. <https://doi.org/10.1080/10409238.2021.1925216>
- Nangaku, M., Sato-Yoshitake, R., Okada, Y., Noda, Y., Takemura, R., Yamazaki, H., & Hirokawa, N. (2009). KIF1B, a Novel Microtubule Plus End-Directed Monomeric Motor Protein for Transport of Mitochondria. In *Cell* (Vol. 79).
- Nelles, D. A., Fang, M. Y., O'Connell, M. R., Xu, J. L., Markmiller, S. J., Doudna, J. A., & Yeo, G. W. (2016). Programmable RNA Tracking in Live Cells with CRISPR/Cas9. *Cell*, 165(2), 488–496. <https://doi.org/10.1016/j.cell.2016.02.054>
- Nguyen, T. T., Oh, S. S., Weaver, D., Lewandowska, A., Maxfield, D., Schuler, M. H., Smith, N. K., Macfarlane, J., Saunders, G., Palmer, C. A., Debattisti, V., Koshiba, T., Pulst, S., Feldman, E. L., Hajnóczky, G., & Shaw, J. M. (2014). Loss of Miro1-directed mitochondrial movement results in a novel murine model for neuron disease. *Proceedings of the National Academy of Sciences of the United States of America*, 111(35). <https://doi.org/10.1073/pnas.1402449111>
- Nicholls, D. G., & Budd, S. L. (2000). *Mitochondria and Neuronal Survival*.
- Norkett, R., Lesept, F., & Kittler, J. T. (2018). Miro proteins coordinate microtubule- and actin-dependent mitochondrial transport and distribution. *The EMBO Journal*, 37(3), 321–336. <https://doi.org/10.15252/embj.201696380>
- Nowak, D. E., Tian, B., & Brasier, A. R. (2005). Two-step cross-linking method for identification of NF- $\kappa$ B gene network by chromatin immunoprecipitation. *BioTechniques*, 39(5), 715–724. <https://doi.org/10.2144/000112014>
- Oeding, S. J., Majstrowicz, K., Hu, X. P., Schwarz, V., Freitag, A., Honnert, U., Nikolaus, P., & Bähler, M. (2018). Identification of Miro1 and Miro2 as mitochondrial receptors for myosin XIX. *Journal of Cell Science*, 131(17). <https://doi.org/10.1242/jcs.219469>
- Phhlman, S., Ruusala, A.-I., Abrahamsson, L., Mattsson, M. E. K., & Esscher, T. (1984). Retinoic acid-induced differentiation of cultured human neuroblastoma cells: a comparison with phorbol ester-induced differentiation. In *Cell Differentiation* (Vol. 14).
- Pilling, A. D., Horiuchi, D., Lively, C. M., & Saxton, W. M. (2006). Kinesin-1 and Dynein Are the Primary Motors for Fast Transport of Mitochondria in Drosophila Motor Axons □ D □ V. *Molecular Biology of the Cell*, 17, 2057–2068. <https://doi.org/10.1091/mbc.E05-06>
- P&Iman, S., Hoehner, J. C., Ndnberg, E., Hedborg, F., Fagerstriim, S., Gestblom, C., Johansson, I., Larsson, U., Lavenius, E., Ortoft, E., & Sgderholm, H. (1995). Differentiation and Survival Influences of Growth Fa.ctors in Human Neuroblastoma. In *EurJ Cancer* (Vol. 31, Issue 4).
- Qi, L. S., Larson, M. H., Gilbert, L. A., Doudna, J. A., Weissman, J. S., Arkin, A. P., & Lim, W. A. (2013). Repurposing CRISPR as an RNA-yuided platform for sequence-specific control of gene expression. *Cell*, 152(5), 1173–1183. <https://doi.org/10.1016/j.cell.2013.02.022>
- Rahbari, R., Sheahan, T., Modes, V., Collier, P., Macfarlane, C., & Badge, R. M. (2009). A novel L1 retrotransposon marker for HeLa cell line identification. *BioTechniques*, 46(4), 277–284. <https://doi.org/10.2144/000113089>
- Reis, K., Fransson, Å., & Aspenström, P. (2009). The Miro GTPases: At the heart of the mitochondrial transport machinery. In *FEBS Letters* (Vol. 583, Issue 9, pp. 1391–1398). <https://doi.org/10.1016/j.febslet.2009.04.015>
- Robertson, G. L., Riffle, S., Patel, M., Bodnya, C., Marshall, A., Beasley, H. K., Garza-Lopez, E., Shao, J., Vue, Z., Hinton, A., Stoll, M. S., de Wet, S., Theart, R. P., Chakrabarty, R. P., Loos, B., Chandel, N. S., Mears, J. A., & Gama, V.

- (2023). DRP1 mutations associated with EMPF1 encephalopathy alter mitochondrial membrane potential and metabolic programs. *Journal of Cell Science*, 136(3). <https://doi.org/10.1242/jcs.260370>
- Roger, A. J., Muñoz-Gómez, S. A., & Kamikawa, R. (2017). The Origin and Diversification of Mitochondria. In *Current Biology* (Vol. 27, Issue 21, pp. R1177–R1192). Cell Press. <https://doi.org/10.1016/j.cub.2017.09.015>
- Ryan, C. S., Fine, A. L., Cohen, A. L., Schiltz, B. M., Renaud, D. L., Wirrell, E. C., Patterson, M. C., Boczek, N. J., Liu, R., Babovic-Vuksanovic, D., Chan, D. C., & Payne, E. T. (2018). De Novo DNM1L Variant in a Teenager With Progressive Paroxysmal Dystonia and Lethal Super-refractory Myoclonic Status Epilepticus. *Journal of Child Neurology*, 33(10), 651–658. <https://doi.org/10.1177/0883073818778203>
- Saotome, M., Safiulina, D., Rgy Szabadkai, G., Das, S., Fransson, Å., Aspenstrom, P., Rizzuto, R., Rgy, G., & Czky, H. (2008). *Bidirectional Ca 2-dependent control of mitochondrial dynamics by the Miro GTPase*. [www.pnas.org/cgi/content/full/](http://www.pnas.org/cgi/content/full/)
- Scherer, W. F., Syverton, J. T., & Gey, G. O. (n.d.). *STUDIES ON THE PROPAGATION IN VITRO OF POLIOMYELITIS VIRUSES IV. VIRAL MULTIPLICATION IN A STABLE STRAIN OF HUMAN MALIGNANT J~PITH~LIAL CELLS (STRAIN HELA) DERIVED I~ROM AN EPIDEI~FOID CARCINOMA OF THE CERVIX\**.
- Schwarz, T. L. (2013). Mitochondrial trafficking in neurons. *Cold Spring Harbor Perspectives in Biology*, 5(6). <https://doi.org/10.1101/cshperspect.a011304>
- Schwinn, M. K., Steffen, L. S., Zimmerman, K., Wood, K. V., & Machleidt, T. (2020). A Simple and Scalable Strategy for Analysis of Endogenous Protein Dynamics. *Scientific Reports*, 10(1). <https://doi.org/10.1038/s41598-020-65832-1>
- Scott, I., & Youle, R. J. (2010). Mitochondrial fission and fusion. *Essays in Biochemistry*, 47, 85–98. <https://doi.org/10.1042/BSE0470085>
- Shalem, O., Sanjana, N. E., Hartenian, E., Shi, X., Scott, D. A., Mikkelsen, T. S., Heckl, D., Ebert, B. L., Root, D. E., Doench, J. G., & Zhang, F. (2014). Genome-scale CRISPR-Cas9 knockout screening in human cells. *Science*, 343(6166), 84–87. <https://doi.org/10.1126/science.1247005>
- Shaner, N. C., Steinbach, P. A., & Tsien, R. Y. (2005). A guide to choosing fluorescent proteins. *Nature Methods*, 2(12), 905–909. <https://doi.org/10.1038/nmeth819>
- Shanmughapriya, S., Langford, D., & Natarajaseenivasan, K. (2020). Inter and Intracellular mitochondrial trafficking in health and disease. In *Ageing Research Reviews* (Vol. 62). Elsevier Ireland Ltd. <https://doi.org/10.1016/j.arr.2020.101128>
- Sheng, Z. H. (2014). Mitochondrial trafficking and anchoring in neurons: New insight and implications. In *Journal of Cell Biology* (Vol. 204, Issue 7, pp. 1087–1098). Rockefeller University Press. <https://doi.org/10.1083/jcb.201312123>
- Shipley, M. M., Mangold, C. A., & Szpara, M. L. (2016). Differentiation of the SH-SY5Y human neuroblastoma cell line. *Journal of Visualized Experiments*, 2016(108). <https://doi.org/10.3791/53193>
- Simcox, E. M., & Reeve, A. K. (2016). An introduction to mitochondria, their structure and functions. In *Mitochondrial Dysfunction in Neurodegenerative Disorders: Second Edition* (pp. 3–30). Springer International Publishing. [https://doi.org/10.1007/978-3-319-28637-2\\_1](https://doi.org/10.1007/978-3-319-28637-2_1)
- Stowers, R. S., Megeath, L. J., Gó Rska-Andrzejak, J., Meinertzhagen, I. A., & Schwarz, T. L. (2002). Axonal Transport of Mitochondria to Synapses Depends on Milton, a Novel Drosophila Protein so that the slow diffusion of ATP does not

- limit the function of the cell. To this end, mitochondria can move within the cell, altering their distribution in response to. In *Neuron* (Vol. 36).
- Stuppia, G., Rizzo, F., Riboldi, G., Del Bo, R., Nizzardo, M., Simone, C., Comi, G. P., Bresolin, N., & Corti, S. (2015). MFN2-related neuropathies: Clinical features, molecular pathogenesis and therapeutic perspectives. In *Journal of the Neurological Sciences* (Vol. 356, Issues 1–2, pp. 7–18). Elsevier B.V. <https://doi.org/10.1016/j.jns.2015.05.033>
- Sutherland, B. W., Toews, J., & Kast, J. (2008). Utility of formaldehyde cross-linking and mass spectrometry in the study of protein-protein interactions. In *Journal of Mass Spectrometry* (Vol. 43, Issue 6, pp. 699–715). <https://doi.org/10.1002/jms.1415>
- Tayri-Wilk, T., Slavin, M., Zamel, J., Blass, A., Cohen, S., Motzik, A., Sun, X., Shalev, D. E., Ram, O., & Kalisman, N. (2020). Mass spectrometry reveals the chemistry of formaldehyde cross-linking in structured proteins. *Nature Communications*, 11(1). <https://doi.org/10.1038/s41467-020-16935-w>
- Truckenbrodt, S., Sommer, C., Rizzoli, S. O., & Danzl, J. G. (2019). A practical guide to optimization in X10 expansion microscopy. *Nature Protocols*, 14(3), 832–863. <https://doi.org/10.1038/s41596-018-0117-3>
- Twelvetrees, A. E. E., Pernigo, S., Sanger, A., Guedes-Dias, P., Schiavo, G., Steiner, R. A. A., Dodding, M. P. P., & Holzbaur, E. L. L. F. (2016). The Dynamic Localization of Cytoplasmic Dynein in Neurons Is Driven by Kinesin-1. *Neuron*, 90(5), 1000–1015. <https://doi.org/10.1016/j.neuron.2016.04.046>
- Vakulskas, C. A., Dever, D. P., Rettig, G. R., Turk, R., Jacobi, A. M., Collingwood, M. A., Bode, N. M., McNeill, M. S., Yan, S., Camarena, J., Lee, C. M., Park, S. H., Wiebking, V., Bak, R. O., Gomez-Ospina, N., Pavel-Dinu, M., Sun, W., Bao, G., Porteus, M. H., & Behlke, M. A. (2018). A high-fidelity Cas9 mutant delivered as a ribonucleoprotein complex enables efficient gene editing in human hematopoietic stem and progenitor cells. *Nature Medicine*, 24(8), 1216–1224. <https://doi.org/10.1038/s41591-018-0137-0>
- van Spronsen, M., Mikhaylova, M., Lipka, J., Schlager, M. A., van den Heuvel, D. J., Kuijpers, M., Wulf, P. S., Keijzer, N., Demmers, J., Kapitein, L. C., Jaarsma, D., Gerritsen, H. C., Akhmanova, A., & Hoogenraad, C. C. (2013). TRAK/Milton Motor-Adaptor Proteins Steer Mitochondrial Trafficking to Axons and Dendrites. *Neuron*, 77(3), 485–502. <https://doi.org/10.1016/j.neuron.2012.11.027>
- Vasilescu, J., Guo, X., & Kast, J. (2004). Identification of protein-protein interactions using in vivo cross-linking and mass spectrometry. *Proteomics*, 4(12), 3845–3854. <https://doi.org/10.1002/pmic.200400856>
- Vlahou, G., Eliáš, M., von Kleist-Retzow, J. C., Wiesner, R. J., & Rivero, F. (2011). The Ras related GTPase Miro is not required for mitochondrial transport in *Dictyostelium discoideum*. *European Journal of Cell Biology*, 90(4), 342–355. <https://doi.org/10.1016/j.ejcb.2010.10.012>
- Wakabayashi, J., Zhang, Z., Wakabayashi, N., Tamura, Y., Fukaya, M., Kensler, T. W., Iijima, M., & Sesaki, H. (2009). The dynamin-related GTPase Drp1 is required for embryonic and brain development in mice. *Journal of Cell Biology*, 186(6), 805–816. <https://doi.org/10.1083/jcb.200903065>
- Wang, X., & Schwarz, T. L. (2009). The Mechanism of Ca<sup>2+</sup>-Dependent Regulation of Kinesin-Mediated Mitochondrial Motility. *Cell*, 136(1), 163–174. <https://doi.org/10.1016/j.cell.2008.11.046>
- Wang, X., Winter, D., Ashrafi, G., Schlehe, J., Wong, Y. L., Selkoe, D., Rice, S., Steen, J., Lavoie, M. J., & Schwarz, T. L. (2011). PINK1 and Parkin target miro

- for phosphorylation and degradation to arrest mitochondrial motility. *Cell*, 147(4), 893–906. <https://doi.org/10.1016/j.cell.2011.10.018>
- Wennerberg, K., & Der, C. J. (2004). Rho-family GTPases: It's not only Rac and Rho (and i like it). In *Journal of Cell Science* (Vol. 117, Issue 8, pp. 1301–1312). <https://doi.org/10.1242/jcs.01118>
- Wiedenheft, B., Sternberg, S. H., & Doudna, J. A. (2012). RNA-guided genetic silencing systems in bacteria and archaea. In *Nature* (Vol. 482, Issue 7385, pp. 331–338). <https://doi.org/10.1038/nature10886>
- Willems, J., de Jong, A. P. H., Scheefhals, N., Mertens, E., Catsburg, L. A. E., Poorthuis, R. B., de Winter, F., Verhaagen, J., Meye, F. J., & MacGillavry, H. D. (2020). Orange: A CRISPR/Cas9-based genome editing toolbox for epitope tagging of endogenous proteins in neurons. *PLoS Biology*, 18(4). <https://doi.org/10.1371/journal.pbio.3000665>
- Xie, H. R., Hu, L. Sen, & Li, G. Y. (2010). SH-SY5Y human neuroblastoma cell line: In vitro cell model of dopaminergic neurons in Parkinson's disease. In *Chinese Medical Journal* (Vol. 123, Issue 8, pp. 1086–1092). <https://doi.org/10.3760/cma.j.issn.0366-6999.2010.08.021>
- Zhang, F., Wang, W., Siedlak, S. L., Liu, Y., Liu, J., Jiang, K., Perry, G., Zhu, X., & Wang, X. (2015). Miro1 deficiency in amyotrophic lateral sclerosis. *Frontiers in Aging Neuroscience*, 7(MAY). <https://doi.org/10.3389/fnagi.2015.00100>
- Zhang, Z., Zhang, Y., Gao, F., Han, S., Cheah, K. S., Tse, H. F., & Lian, Q. (2017). CRISPR/Cas9 Genome-Editing System in Human Stem Cells: Current Status and Future Prospects. In *Molecular Therapy - Nucleic Acids* (Vol. 9, pp. 230–241). Cell Press. <https://doi.org/10.1016/j.omtn.2017.09.009>
- Zinsmaier, K. E. (2021). Mitochondrial Miro GTPases coordinate mitochondrial and peroxisomal dynamics. In *Small GTPases* (Vol. 12, Issues 5–6, pp. 372–398). Taylor and Francis Ltd. <https://doi.org/10.1080/21541248.2020.1843957>
- Zinsmaier, K. E., Babic, M., & Russo, G. J. (2009). Mitochondrial transport dynamics in axons and dendrites. *Results and Problems in Cell Differentiation*, 48, 107–139. [https://doi.org/10.1007/400\\_2009\\_20](https://doi.org/10.1007/400_2009_20)

## 9 list of figures

Figure 3-1 Schematic of mitochondrial fission and fusion.....	4
Figure 3-2 Schematic of Mitochondrial motor-adaptor complex. ....	6
Figure 3-3 Structural features of Miro. ....	10
Figure 3-4 Miro1 deletion causes depletion of mitochondria in distal dendrites but not the axons. ....	<b>Error! Bookmark not defined.</b>
Figure 3-5 Schematic representation of CRISPR-Cas9-mediated genome editing process. ....	18
Figure 3-6 Exemplary picture of non-differentiated control. ....	20
Figure 4-1 Vector maps of Addgene PX459 backbone.....	25
Figure 4-2 Vector map of RHOT1HDR (A) and RHOT2HDR (B) provided by Invitrogen. ....	28
Figure 4-3 Schematic illustration of Co-immunoprecipitation protocol ( <a href="https://www.ptglab.com/">https://www.ptglab.com/</a> ).....	35
Figure 4-4 Schematic detailing the procedure of Duolink® Proximity Ligation Assay. ....	37
Figure 4-5 illustration of the differentiation process timetable. ....	39
Figure 4-6 Representative picture of expansion microscopy protocol and comparison between the original DNA method and the subsequent post-stain linker-group functionalization methods, referred to as the 'MA-NHS/GA methods' in this study. .	43
Figure 5-1 Schematics illustration of the Miro1 and Miro2 proteins domains in wild-type (WT) and knock-in versions. ....	46
Figure 5-2 The alignment of the PX459 sequence before and after gRNA cloning reveals a mismatch between BbsI cut sites (↓) where the gRNA has been inserted, confirming the successful cloning of the gRNA. ....	47
Figure 5-3 The alignment of HDR templates and Invitrogen HDR vectors confirmed successful ligation of the HDR sequence into the vectors. ....	47
Figure 5-4 Fluorescent imaging was performed using 60X oil objective lens of Nikon ECLIPSE Ti epi-fluorescent microscope on a mixed population of SH-SY5Y cells with the potential Miro1 and Miro2 Knock-in, both before and after puromycin selections. ....	48
Figure 5-5 Although some of the selected FLAG-eGFP-Miro1 SH-SY5Y clones exhibited positive fluorescent signals, neither PCR genotyping nor protein expression analysis could confirm the success of the knock-in experiment. ....	51
Figure 5-6 Despite the promising results obtained from live imaging and PCR genotyping of the selected potential Miro2 Knock-in SH-SY5Y clones derived from the first approach, no active expression of the fusion protein was detected through western blotting analysis. ....	52
Figure 5-7 Application of the PCR screen/enrichment approach as a valuable strategy, significantly increased the probability of identifying positive FLAG-eGFP-Miro1 knock-in cells within the mixed population of SH-SY5Y cells. ....	54
Figure 5-8 The utilization of the enrichment approach raised the chance of identifying positive MYC-mRFP-Miro2 KI cells within the SH-SY5Y mixed population. ....	55
Figure 5-9 Through comprehensive genomic and proteomic analysis, along with a protein localization study, it was confirmed that the GFP-FLAG tags were successfully inserted at the N-terminus of the endogenous Miro1 protein and actively expressed in the selected pu .....	57
Figure 5-10 Despite obtaining a positive result during the enrichment phase, neither PCR genotyping nor western blotting of potential pure single clones could confirm	

the insertion of tags and expression of the MYC-mRFP-Miro2 fusion protein in HeLa cells.....	59
Figure 5-11 The application of an enrichment approach, coupled with low-density cell seeding, led to the successful finding MYC-mRFP-Miro2 Knock-in HeLa pure clones. ....	62
Figure 5-12 The PCR genotyping and protein expression analysis of the selected pure potential MYC-mRFP-Miro2 HeLa clones provided conclusive evidence of the homozygous insertion of MYC-mRFP tags at the N-terminus of the endogenous Miro2 protein.....	64
Figure 5-13 Despite obtaining positive PCR genotyping results for some wells during the enrichment phase, PCR genotyping of selected pure clones derived from those wells failed to confirm the integration of the fusion tags in the N-terminus of the Miro1 gene in HeLa. ....	66
Figure 5-14 Confirmation of GFP-FLAG tags integration into the endogenous Miro1 in MYC-mRFP-Miro2 Knock-in HeLa cells was achieved through PCR genotyping and protein expression analysis. The cells with successful integration were referred to as Double Miro Knock-in .....	68
Figure 5-15 CO-IP of Miro2 overexpressing well-known interactors. ....	73
Figure 5-16 Despite applying different IP protocols and crosslinking techniques, the immunoblotting of the GFP IP samples did not yield any detectable results for Miro2 and TRAK1, in contrast to the successful pull-down of FLAG-eGFP-Miro1.....	76
Figure 5-17 non-specific binding of GFP Miro1 to the MYC beads when MYC IP was performed from FLAG-eGFP-Miro1 KI samples.....	78
Figure 5-18 The analysis of PLA data has confirmed the interaction between Miro1 and Miro2 localized within the mitochondria.....	81
Figure 5-19 Application of expansion microscopy in combination with conventional co-staining verified the mitochondrial localization of Miro2 in DMKI cells. ....	84
Figure 5-20 In differentiated SH-SY5Y cells, the co-staining procedure revealed a partial co-localization pattern between FLAG-eGFP-Miro1 and HSP60 signals specifically within the FLAG-GFP- Miro1 KI cells, while no such co-localization was observed in the WT cells.....	86

## 10 list of tables

Table 4-1 gRNA list designed for Knock-in experiment with a recognition site for BbsI restriction enzyme highlighted in red. ....	25
Table 4-2 List of PCR primers used for knock-in validation. ....	31
Table 4-3 List of PCR primer used for sequencing. ....	32
Table 4-4 Comparative component of Lysis and washing buffers in ChromoTek and Ismael's protocol. ....	35

## 11 Appendices

### Contributions in Research Articles

**LDHA is enriched in human islet alpha cells and upregulated in type 2 diabetes.**

Paulina Karen Mendoza Sanchez, **Mona Khazaei**, Eva Gatineau, Shirin Geravandi, Blaz Lupse, Huan Liu, Ralf Dringen, Anne Wojtusciszyn, Patrick Gilon, Kathrin Maedler and Amin Ardestani.

Published in Biochemical and Biophysical Research Communications. 2021 Jul; 568(2021):158-166

<https://doi.org/10.1016/j.bbrc.2021.06.065>

My contribution: Elisa, western blot and RT-PCR analysis shown in Figure 2A and 2C, Figure 3A and 3B





## LDHA is enriched in human islet alpha cells and upregulated in type 2 diabetes



Paulina Karen Mendoza Sanchez<sup>a</sup>, Mona Khazaei<sup>a</sup>, Eva Gatineau<sup>b</sup>, Shirin Geravandi<sup>a</sup>, Blaz Lupse<sup>a</sup>, Huan Liu<sup>a</sup>, Ralf Dringen<sup>a</sup>, Anne Wojtuszczyz<sup>c</sup>, Patrick Gilon<sup>b</sup>, Kathrin Maedler<sup>a,\*,1</sup>, Amin Ardestani<sup>a,d,\*\*,1</sup>

<sup>a</sup> Centre for Biomolecular Interactions Bremen, University of Bremen, Bremen, Germany

<sup>b</sup> Pole of Endocrinology, Diabetes, and Nutrition (EDIN), Institute of Experimental and Clinical Research (IREC), Université Catholique de Louvain (UCLouvain), 1200, Brussels, Belgium

<sup>c</sup> Department of Endocrinology, Diabetology and Metabolism, Lausanne University Hospital, Lausanne, Switzerland

<sup>d</sup> Department of Molecular Medicine, School of Advanced Technologies in Medicine, Tehran University of Medical Sciences, Tehran, Iran

### ARTICLE INFO

#### Article history:

Received 17 June 2021

Accepted 20 June 2021

Available online 1 July 2021

#### Keywords:

LDH

LDHA

lactate

islets

Beta-cell

Diabetes

### ABSTRACT

The lactate dehydrogenase isoform A (LDHA) is a key metabolic enzyme that preferentially catalyzes the conversion of pyruvate to lactate. Whereas LDHA is highly expressed in many tissues, its expression is turned off in the differentiated adult  $\beta$ -cell within the pancreatic islets. The repression of LDHA under normal physiological condition and its inappropriate upregulation under a diabetogenic environment is well-documented in rodent islets/ $\beta$ -cells but little is known about LDHA expression in human islet cells and whether its abundance is altered under diabetic conditions. Analysis of public single-cell RNA-seq (sc-RNA seq) data as well as cell type-specific immunolabeling of human pancreatic islets showed that LDHA was mainly localized in human  $\alpha$ -cells while it is expressed at a very low level in  $\beta$ -cells. Furthermore, LDHA, both at mRNA and protein, as well as lactate production is upregulated in human pancreatic islets exposed to chronic high glucose treatment. Microscopic analysis of stressed human islets and autopsy pancreases from individuals with type 2 diabetes (T2D) showed LDHA upregulation mainly in human  $\alpha$ -cells. Pharmacological inhibition of LDHA in isolated human islets enhanced insulin secretion under physiological conditions but did not significantly correct the deregulated secretion of insulin or glucagon under diabetic conditions.

© 2021 The Authors. Published by Elsevier Inc. This is an open access article under the CC BY-NC-ND license (<http://creativecommons.org/licenses/by-nc-nd/4.0/>).

### 1. Introduction

Type 2 diabetes (T2D) is a metabolic disorder closely linked to multiple genetic and environmental factors which together evoke the development of multiple pathophysiological metabolic disturbances. T2D is a bi-hormonal disorder manifested by a relative hypoinsulinaemia and hyperglucagonaemia leading eventually to

hyperglycemia and diabetes and its complications [1]. Deregulated secretion of both hormones insulin and glucagon produced by pancreatic  $\beta$ - and  $\alpha$ -cells respectively is a characteristic feature of T2D [1–5]. The interplay between these two hormones and their respective receptors located in the liver, muscle and adipose tissue enables the maintenance of glucose homeostasis, which is achieved via several mechanisms participating in the fine-tuning of insulin secretion [1]. Insulin secretory function of  $\beta$ -cells is defective in T2D with a higher basal release of insulin in fasting periods and insufficient insulin release after a meal [6]; the secretory defect of  $\beta$ -cells is caused by multiple factors, including chronically elevated glucose (“glucotoxicity”) [7].

A key aspect of  $\beta$ -cell biology is the tight coupling between cellular metabolism and insulin secretion in order to maintain systemic energy homeostasis. To achieve this, islet cells and specifically  $\beta$ -cells show selective repression of some key metabolic

\* Corresponding author. Islet Biology Laboratory, Centre for Biomolecular Interactions Bremen, University of Bremen, Leobener Straße NW2, Room B2080, 28359, Bremen, Germany.

\*\* Corresponding author. Islet Biology Laboratory, Centre for Biomolecular Interactions Bremen, University of Bremen, Leobener Straße NW2, Room B2080, 28359, Bremen, Germany.

E-mail addresses: [kmaedler@uni-bremen.de](mailto:kmaedler@uni-bremen.de) (K. Maedler), [ardestani.amin@gmail.com](mailto:ardestani.amin@gmail.com) (A. Ardestani).

<sup>1</sup> Shared senior authors.



## **Inhibition of PHLPP1/2 phosphatases rescues pancreatic $\beta$ -cells in diabetes**

Blaz Lypse, Karthika Annamalai, Hazem Ibrahim, Supreet Kaur, Shirin Geravandi, Bhavishya Sarma, Anasua Pal, Sushil Awal, Arundhati Joshi, Sahar Rafizadeh, Murali Krishna Madduri, **Mona Khazaei**, Huan Liu, Ting Yuan, Wei He, Kanaka Durga Devi Gorrepati, Zahra Azizi, Qi Qi, Keqiang Ye, Jose Oberholzer, Kathrin Maedler, and Amin Ardestani.

Published in Cell Reports 2021 Aug; 36(5):109490.

<https://doi.org/10.1016/j.celrep.2021.109490>

My contribution: Immunohistochemistry (Ki67 staining) analysis shown in Figure S1D



## Article

Inhibition of PHLPP1/2 phosphatases rescues pancreatic  $\beta$ -cells in diabetes

Blaz Lupse,<sup>1</sup> Karthika Annamalai,<sup>1</sup> Hazem Ibrahim,<sup>1</sup> Supreet Kaur,<sup>1</sup> Shirin Geravandi,<sup>1</sup> Bhavishya Sarma,<sup>1</sup> Anasua Pal,<sup>1</sup> Sushil Awal,<sup>1</sup> Arundhati Joshi,<sup>1</sup> Sahar Rafizadeh,<sup>1</sup> Murali Krishna Madduri,<sup>1</sup> Mona Khazaei,<sup>1</sup> Huan Liu,<sup>1</sup> Ting Yuan,<sup>1</sup> Wei He,<sup>1</sup> Kanaka Durga Devi Gorrepati,<sup>1</sup> Zahra Azizi,<sup>1,2</sup> Qi Qi,<sup>3</sup> Keqiang Ye,<sup>3</sup> Jose Oberholzer,<sup>4</sup> Kathrin Maedler,<sup>1,5,6,\*</sup> and Amin Ardestani<sup>1,2,5,\*</sup>

<sup>1</sup>Centre for Biomolecular Interactions Bremen, University of Bremen, 28359 Bremen, Germany

<sup>2</sup>Department of Molecular Medicine, School of Advanced Technologies in Medicine, Tehran University of Medical Sciences, Tehran 1449614535, Iran

<sup>3</sup>Department of Pathology and Laboratory Medicine, Emory University School of Medicine, Atlanta, GA 30322, USA

<sup>4</sup>Charles O. Strickler Transplant Center, University of Virginia Medical Center, Charlottesville, VA 22903, USA

<sup>5</sup>Senior author

<sup>6</sup>Lead contact

\*Correspondence: kmaedler@uni-bremen.de (K.M.), ardestani.amin@gmail.com (A.A.)

<https://doi.org/10.1016/j.celrep.2021.109490>

## SUMMARY

Pancreatic  $\beta$ -cell failure is the key pathogenic element of the complex metabolic deterioration in type 2 diabetes (T2D); its underlying pathomechanism is still elusive. Here, we identify pleckstrin homology domain leucine-rich repeat protein phosphatases 1 and 2 (PHLPP1/2) as phosphatases whose upregulation leads to  $\beta$ -cell failure in diabetes. PHLPP levels are highly elevated in metabolically stressed human and rodent diabetic  $\beta$ -cells. Sustained hyper-activation of mechanistic target of rapamycin complex 1 (mTORC1) is the primary mechanism of the PHLPP upregulation linking chronic metabolic stress to ultimate  $\beta$ -cell death. PHLPPs directly dephosphorylate and regulate activities of  $\beta$ -cell survival-dependent kinases AKT and MST1, constituting a regulatory triangle loop to control  $\beta$ -cell apoptosis. Genetic inhibition of PHLPPs markedly improves  $\beta$ -cell survival and function in experimental models of diabetes *in vitro*, *in vivo*, and in primary human T2D islets. Our study presents PHLPPs as targets for functional regenerative therapy of pancreatic  $\beta$  cells in diabetes.

## INTRODUCTION

Type 2 diabetes (T2D) is a heterogeneous multifactorial metabolic disease, characterized by insulin resistance and progressive loss of functional  $\beta$ -cell mass. Pancreatic  $\beta$ -cell failure finally results from decreased insulin secretory function and/or  $\beta$ -cell death (Alejandro et al., 2015; Ashcroft and Rorsman, 2012; Butler et al., 2003; Weir et al., 2020), hallmarks of T2D; however, underlying molecular mechanisms are still not fully characterized, and there is currently no  $\beta$ -cell-specific therapy for a cure (Donath et al., 2019). In addition to  $\beta$ -cell death and dysfunction, other mechanisms, such as  $\beta$ -cell dedifferentiation (Cinti et al., 2016; Jeffery and Harries, 2016; Talchai et al., 2012) and failure of adaptive expansion because of impaired regeneration (Aguayo-Mazzucato and Bonner-Weir, 2018; Tiwari et al., 2016), have been proposed as possible causes for  $\beta$ -cell failure in T2D.

The coordinated cellular stress response and enormous metabolic adaptation are necessary for normal  $\beta$ -cell insulin-secretory function, glucose homeostasis, and prevention of T2D; these are largely directed by the highly complex dynamics of signal transduction pathways. Perturbations in  $\beta$ -cell signaling

have complex consequences leading to imbalanced and improper transcriptional and post-transcriptional alterations, metabolic deterioration, continuous decline in  $\beta$ -cell function and viability and the cumulative development of diabetic complications. Thus, comprehensive understanding of cell-fate decisions during stress and metabolic overload will provide new targets for the development of therapeutic approaches aiming at prevention and repair of  $\beta$ -cell failure in T2D.

Serine-threonine phosphatases (STPs) are important components of multiple cell signaling nodes and serve as potential targets for drug development. The pleckstrin homology (PH) domain leucine-rich repeat protein phosphatases (PHLPPs) enzymes are members of the protein phosphatase 2C (PP2C) grouped in the protein phosphatase metal-dependent (PPM) family of STP (Brognard and Newton, 2008). The PHLPP family includes two isozymes, PHLPP1 (also referred to as suprachiasmatic nucleus circadian oscillatory protein [SCOP]) and PHLPP2 (Grzechnik and Newton, 2016). PHLPP1/2 are ubiquitously expressed and involved in several cellular processes, such as proliferation, survival, stress response, inflammation, memory formation, and T cell development (Brognard and Newton, 2008; Chen et al., 2013; Cohen Katsenelson et al., 2019; Gao





**Declaration on the contribution of the candidate to multi-author articles which are included in appendix in the submitted doctoral thesis**

**Contribution of the candidate in % of the total work load (up to 100% for each of the following categories):**

**Publication I: LDHA is enriched in human islet alpha cells and upregulated in type 2 diabetes**

Experimental concept and design:	ca. 5%
Experimental work and/or acquisition of (experimental) data:	ca. 5%
Data analysis and interpretation:	ca. 5%
Preparation of Figures and Tables:	ca. 5%
Drafting of the manuscript:	ca. 5%

**Publication II: Inhibition of PHLPP1/2 phosphatases rescues pancreatic  $\beta$ -cells in diabetes**

Experimental concept and design:	ca. 5%
Experimental work and/or acquisition of (experimental) data:	ca. 5%
Data analysis and interpretation:	ca. 5%
Preparation of Figures and Tables:	ca. 5%
Drafting of the manuscript:	ca. 5%

Date:

Signature: